Interplay between α-synuclein expression and 26S proteasome chaperone Rpn14 and Rpn11 deubiquitinase in the budding yeast *Saccharomyces cerevisiae*

Dissertation

For the award of the degree

“Doctor rerum naturalium”

of the Georg-August-Universität Göttingen

within the doctoral program “Microbiology and Biochemistry”

of the Göttingen Graduate School for

Neurosciences and Molecular Biosciences (GGNB)

Submitted by

Dajana Gałka

from

Lwówek Śląski (Poland)

Göttingen 2022

Thesis Committee:

Prof. Dr. Gerhard H. Braus - 1st reviewer

Department of Molecular Microbiology and Genetics

University of Goettingen

Prof. Dr. Stefanie Pöggeler - 2nd reviewer

Department of Genetics of Eukaryotic Microorganisms

University of Goettingen

Prof. Dr. Tiago F. Outeiro

Department Department of Experimental Neurodegeneration

University Medical Center Goettingen

Members of the Examination Board:

Prof. Dr. Kai Heimel

Department of Molecular Microbiology and Genetics

University of Goettingen

Prof. Dr. Heike Krebber

Department of Molecular Genetics

University of Goettingen

PD Dr. Michael Hoppert

Department of General Microbiology

Georg-August-Universität Göttingen

The date of the oral examination: 19th October 2022

Declaration

Herewith I declare that the PhD Thesis entitled **“Interplay between α-synuclein expression and 26S proteasome chaperone Rpn14 and Rpn11 deubiquitinase in the budding yeast *Saccharomyces cerevisiae*”** has been written independently and with no other sources and aids than quoted.

Dajana Gałka

Göttingen, 18.07.2022

This work was accomplished in the group of Prof. Dr. Gerhard H. Braus at the Department of Molecular Microbiology and Genetics at the Institute of Microbiology and Genetics, University of Goettingen.

Publications:

Popova, B., **Galka, D.**, Häffner, N., Wang, D., Schmitt, K., Valerius, O., Knop, M., & Braus, G. H. (2021). α-Synuclein Decreases the Abundance of Proteasome Subunits and Alters Ubiquitin Conjugates in Yeast. *Cells* 10: 2229.

Popova, B., Wang, D., Pätz, C., Akkermann, D., Lázaro, D. F., **Galka, D.**, Kolog Gulko, M., Bohnsack, M. T., Möbius, W., Bohnsack, K. E., Outeiro, T. F., & Braus, G. H. (2021). DEAD-box RNA helicase Dbp4/DDX10 is an enhancer of α-synuclein toxicity and oligomerization. *PLoS Genet* 17: e1009407.

Table of Contents

Abstract

Alpha-synuclein (αSyn) in a misfolded state is the main component of Lewy bodies (LBs). These filamentous cytoplasmic inclusions are the neuropathological hallmark of Parkinson's disease (PD). αSyn aggregates in LBs are prominently phosphorylated at serine 129 (pS129), suggesting that this posttranslational modification is linked to pathogenicity. Increasing amounts of toxic αSyn species indicate significant perturbation of protein homeostasis in PD. The central question of this thesis focuses on the analysis of the interplay of αSyn with two important components of a functional 26S proteasome: (i) the Rpn14 proteasome assembly chaperone and (ii) the Rpn11 deubiquitinase. The budding yeast *Saccharomyces cerevisiae* was used as eukaryotic reference cell to investigate the impact of αSyn on protein homeostasis and the interplay between αSyn and proteins associated with 26S proteasome. Expression of αSyn in yeast results in growth impairment and cytoplasmic protein inclusions resembling the aggregates observed within LBs. A tandem fluorescent protein timer (tFT) was exploited to perform a high-throughput screen for proteins with altered turnover upon expression of αSyn or a phosphorylation-deficient S129A mutant. The impact of αSyn on the changes in protein stability was more significant than that of S129A.

One of the top hits with different stability depending on the phosphorylation state of αSyn was the Rpn14 assembly chaperone of the 26S proteasome. αSyn expression increased the stability of Rpn14, whereas S129A had an opposite effect. High levels of Rpn14 were deleterious to yeast cells and enhanced αSyn-induced growth retardation. Elevated Rpn14 or αSyn levels increased the accumulation of ubiquitin conjugates upon depletion of the proteasome base subunits Rpt2, Rpt4 or Rpt6. Rpn14 overexpression resulted in accumulation of pS129, suggesting that Rpn14 is directly involved in the turnover of phosphorylated αSyn. Bimolecular Fluorescence Complementation assay (BiFC) revealed a physical interaction between Rpn14 and αSyn. Expression of αSyn and an increased Rpn14 level resulted in decreased 26S activity. The effect was specific for pS129 αSyn. These results demonstrate that inhibition of the proteasomal activity by phosphorylated αSyn in yeast is mediated by the proteasome chaperone Rpn14.

Rpn11 is a deubiquitinating enzyme of the 26S proteasome. Downregulation of the corresponding *RPN11* gene in combination with high levels of αSyn resulted in depletion of the pool of cellular ubiquitinated proteins and enhanced αSyn mediated toxicity. Rpn11 deubiquitinase promotes the degradation of phosphorylated αSyn. In absence of the intrinsically disordered Sem1 proteasome subunit that is required for stabilization of Rpn11, stabilization of αSyn was observed. Expression of αSyn upon deletion of *SEM1* resulted in increased accumulation of ubiquitinated conjugates. This indicates a complex crosstalk between αSyn and Rpn11.

This study corroborates a complex mechanistic interplay between proteasome and pS129 αSyn causing a substantial altered protein homeostasis in yeast as model for PD.

Zusammenfassung

Alpha-Synuclein (αSyn) in fehlgefaltetem Zustand ist der Hauptbestandteil der Lewy Bodies (LBs). Diese fadenförmigen zytoplasmatischen Einschlüsse sind das neuropathologische Markenzeichen der Morbus Parkinson. αSyn-Aggregate in LBs sind in hohem Maße an Serin 129 (pS129) phosphoryliert, was darauf hindeutet, dass diese posttranslationale Modifikation mit der Pathogenität verbunden ist. Zunehmende Mengen toxischer αSyn-Spezies weisen auf eine erhebliche Störung der Proteinhomöostase bei Morbus Parkinson hin. Die zentrale Fragestellung dieser Arbeit konzentriert sich auf die Analyse des Zusammenspiels von αSyn mit zwei wichtigen Komponenten eines funktionellen 26S-Proteasoms: (i) dem Rpn14-Chaperon für die Proteasom-Assemblierung und (ii) der Rpn11-Dubiquitinase. Die Knospenhefe *Saccharomyces cerevisiae* wurde als eukaryotische Referenzzelle verwendet, um die Auswirkungen von αSyn auf die Proteinhomöostase und das Zusammenspiel zwischen αSyn und mit dem 26S-Proteasom assoziierten Proteinen zu untersuchen. Die Expression von αSyn in Hefe führt zu Wachstumsstörungen und zytoplasmatischen Proteineinschlüssen, die den in LBs beobachteten Aggregaten ähneln. Mit Hilfe eines Tandem-Fluoreszenzprotein-Timers (tFT) wurde ein Hochdurchsatz-Screening nach Proteinen mit verändertem Umsatz bei Expression von αSyn oder einer phosphorylierungsdefizienten S129A-Mutante durchgeführt. Der Einfluss von αSyn auf die Veränderungen der Proteinstabilität war deutlicher als der von S129A.

Einer der Top-Treffer mit unterschiedlicher Stabilität in Abhängigkeit vom Phosphorylierungszustand von αSyn war das Montagechaperon Rpn14 des 26S-Proteasoms. Die Expression von αSyn erhöhte die Stabilität von Rpn14, während S129A einen gegenteiligen Effekt hatte. Hohe Rpn14-Konzentrationen waren für Hefezellen schädlich und verstärkten die αSyn-induzierte Wachstumsverzögerung. Erhöhte Rpn14- oder αSyn-Konzentrationen verstärkten die Anhäufung von Ubiquitin-Konjugaten nach Ausschaltung der Proteasom-Basisuntereinheiten Rpt2, Rpt4 oder Rpt6. Die Überexpression von Rpn14 führte zu einer Akkumulation von pS129, was darauf hindeutet, dass Rpn14 direkt am Umsatz von phosphoryliertem αSyn beteiligt ist. Der Bimolekulare Fluoreszenz-Komplementations-Assay (BiFC) zeigte eine physikalische Interaktion zwischen Rpn14 und αSyn. Die Expression von αSyn und ein erhöhter Rpn14-Spiegel führten zu einer verringerten 26S-Aktivität. Der Effekt war spezifisch für pS129 αSyn. Diese Ergebnisse zeigen, dass die Hemmung der proteasomalen Aktivität durch phosphoryliertes αSyn in Hefe durch das Proteasom-Chaperon Rpn14 vermittelt wird.

Rpn11 ist ein deubiquitinierendes Enzym des 26S-Proteasoms. Die Herunterregulierung des entsprechenden *RPN11*-Gens in Kombination mit hohen αSyn-Spiegeln führte zu einer Verarmung des Pools an zellulären ubiquitinierten Proteinen und zu einer verstärkten αSyn-vermittelten Toxizität. Die Rpn11-Dubiquitinase fördert den Abbau von phosphoryliertem αSyn. In Abwesenheit der

intrinsisch gestörten Proteasom-Untereinheit Sem1, die für die Stabilisierung von Rpn11 erforderlich ist, wurde eine Stabilisierung von αSyn beobachtet. Die Expression von αSyn nach Deletion von *SEM1* führte zu einer erhöhten Akkumulation von ubiquitinierten Konjugaten. Dies deutet auf eine komplexe Wechselwirkung zwischen αSyn und Rpn11 hin.

Diese Studie bestätigt ein komplexes mechanistisches Zusammenspiel zwischen Proteasom und pS129 αSyn, das eine erheblich veränderte Proteinhomöostase in Hefe als Modell für Morbus Parkinson verursacht.

1. Introduction

1.1. Parkinson's disease

1.1.1. Epidemiology

Parkinson's disease (PD) is the second most common neurodegenerative disorder after Alzheimer's disease and the most common movement disorder (Kalia & Lang, 2015). PD has the fastest increase in incidence and disability among neurological disorders, with the disease becoming one of the major causes of disability worldwide in the recent years (Feigin *et al*, 2017). According to the Global Burden of Disease (GBD) incident cases were 1.02 million in 2017, whereas 6.1 million PD patients were reported globally (Feigin *et al*, 2019; James *et al*, 2018). The cause of PD remains unclear. Several risk factors such as aging, environmental factors and genetic susceptibility were identified to contribute to the disease onset characterized by bradykinesia, rigidity, tremor and also nonmotor characteristics including, among others, fatigue, anxiety, dementia and depression (Kouli *et al*, 2018). Development of PD predominantly begins between the ages of 55 to 65 years and is diagnosed in 1%-2% of people over the age of 60. The number rises to 3.5% of people aged 85-89 years, therefore PD is regarded as an age-related disease (de Lau & Breteler, 2006; Rizek *et al*, 2016; Dextera & Jenner, 2013) (Table 1). Amongst PD patients, 95% are diagnosed with the disease with an idiopathic background. Onset before age 40 occurs in less than 5% of the cases and is observed in genetic variants of the disease (Wijeratne *et al*, 2021). Familial cases of PD are caused by point missense mutations and multiplications of a number of genes, such as *SNCA* encoding the α-synuclein protein, *Parkin*, *PINK1*, *LRRK2*, *DJ-1* and *ATP13A2* (Bonifati *et al*, 2003; di Fonzo *et al*, 2007; Kitada *et al*, 1998; Polymeropoulos *et al*, 1997; Valente *et al*, 2001; Zimprich *et al*, 2004; Kouli *et al*, 2018).

PD is twice more frequent in men than women, but women suffer faster disease progression and a higher mortality rate (Baldereschi *et al*, 2000; Solla *et al*, 2012; Dahodwala *et al*, 2018). In addition, there are intracultural differences, with prevalence being higher in Europe, North America and South America in comparison to Asian, African and Arabic countries (Kalia & Lang, 2015). Studies predict that the burden of

PD will increase significantly in the coming decades (Kowal *et al*, 2013; Wanneveich *et al*, 2018; Wijeratne *et al*, 2021).

Table 1. Global age and sex distribution of Parkinson's disease prevalence (Orozco *et al*, 2020).

Age	Prevalence estimates per 100.000		
	Global	**Male**	**Female**
All ages	157,92	175	141,91
30-39	2,9	3,9	1,9
40-49	19,5	25,7	13,5
50-59	91,6	115,0	70,1
60-69	336,8	408,8	272,9
70-79	1081,9	1303,9	906,5
80-89	1786,1	2236,9	1508,6
90+	1579,7	1747,4	1492,2

1.1.2. Pathophysiology and etiology

A characteristic pathological feature of PD and essential for its diagnosis is the loss of dopaminergic neurons of the *substantia nigra pars compacta* (SNpc) located in midbrain with simultaneous loss of their axons, which project to the striatum along the nigrostriatal pathway. The process can be observed as loss of the typically dark black pigment in the *substantia nigra* and *locus ceruleus*. Pigment loss correlates with loss of dopaminergic neurons in SNpc and noradrenergic neurons in the *locus ceruleus* (Dickson, 2012). This leads to a loss of the neurotransmitter dopamine, resulting in the primary motor manifestations of PD, described for the first time in 1817 by James Parkinson (Parkinson, 2002; Fearnley & Lees, 1991). The symptoms manifest clinically when striatal dopamine levels are reduced by 50-70% and include bradykinesia, tremor, ataxia, rigidity, and postural instability (Fearnley & Lees, 1991). Dopamine loss, in increasing severity of PD, results in further alteration of basal ganglia pathways,

including changes in the function of other basal ganglia neurotransmitters such as glutamate, glutamate or γ-aminobutyric acid (GABA), and serotonin, which leads to mental disorders often observed in PD patients, such as emotional instability and depression (Gasparini *et al*, 2013).

Another pathologic hallmark of PD is the cellular accumulation of Lewy bodies (LBs). LBs are protein depositions clusters in the cytoplasm of neurons in the *substantia nigra* and other brain regions (Braak *et al*, 2003). A major constituent of Lewy bodies is the protein α-synuclein (αSyn) with various post-translational modifications (Spillantini *et al*, 1997).

1.2. α-synuclein in Parkinson's disease

Abnormal accumulation and aggregation of αSyn protein in LB is the neuropathological hallmark of PD (Xu *et al*, 2016). Pathological aggregation of αSyn is a common characteristic of a number of neurodegenerative diseases, which are referred to as synucleinopathies, such as PD, dementia with Lewy bodies (DLB) and multiple system atrophy (MSA) (Goedert *et al*, 2017).

αSyn is a highly soluble small protein of 140 amino acids encoded by the *SNCA* gene in the *PARK1* gene locus. It is highly expressed in the presynaptic terminals of the nervous system. Although the precise role of αSyn remains substantially unknown, it is presumably involved in the regulation of SNARE-complex assembly of presynaptic vesicles and neurotransmitters release (Abeliovich *et al*, 2000; Lourenço Venda *et al*, 2010; Lundblad *et al*, 2012; Burré *et al*, 2018). Physiological release of endogenous αSyn is dynamically regulated by neuronal/synaptic activity, and thus increased neuronal activity increases αSyn release (Yamada & Iwatsubo, 2018).

The pathogenic role of αSyn in PD is indicated by several lines of evidence. Alongside being the major component of LB, polymorphic variants of *SCNA* gene are a significant risk factor for the development of idiopathic PD and duplication or triplication of the *SNCA* gene as well as point mutations (A30P, E46K, H50Q, G51D, A53T, and A53E) result in autosomal dominant forms of PD (Appel-Cresswell *et al*, 2013; Krüger *et al*, 1998; Lesage *et al*, 2013; Singleton *et al*, 2003; Chartier-Harlin *et al*, 2004; Polymeropoulos *et al*, 1997).

αSyn consists of three domains: the N-terminal domain, which is a positively charged α-helical lipid-binding motif, the central non-amyloid-β component (NAC) domain, which is highly hydrophobic and has the ability to form β-helical structures, and the C-terminal domain, which is a negatively charged and disordered (Emamzadeh, 2016; Xu *et al*, 2016) (Figure 1). The native αSyn in physiological conditions is in dynamic balance between unfolded monomers and tetramerically folded α-helices with a low tendency to aggregate (Lashuel *et al*, 2013). An increase in the monomer to tetramer ratio and thus an increase in the amount of unfolded αSyn monomers promotes αSyn aggregation (Nuber *et al*, 2018). The process of αSyn aggregation consists of a conformational transition that adopts a structure rich in β-sheet, which promotes its aggregation into oligomers, protofibrils, and insoluble fibrils that eventually accumulate in LB. It still remains unclear which species of αSyn are cytotoxic. Whereas both, the oligomeric and fibrillar forms of αSyn, have been shown to be toxic, recent studies imply that species formed during the initial stages of the aggregation process, oligomers and protofibrils, are the neurotoxic species that lead to cell death in PD. Contrarily, αSyn fibrils are the species that appear to be most efficient at spreading, consequently promoting the propagation and progression of the disease (Mehra *et al*, 2019).

The propensity of αSyn to aggregate depends on many factors. It is influenced by mutations in the *SCNA* gene, abundant post-translational modifications of αSyn, imbalance between synthesis and degradation of the protein, and environmental factors. The A53T mutation was identified first and is linked to early onset PD (Polymeropoulos *et al*, 1997). The presence of the E46K mutation is a factor leading to the development of severe parkinsonism with dementia and extensively spread large number of LBs (Zarranz *et al*, 2004). Both mutations promote aggregation of αSyn protein by modifying the structure of the αSyn (Tosatto *et al*, 2015; Li *et al*, 2001; Greenbaum *et al*, 2005).

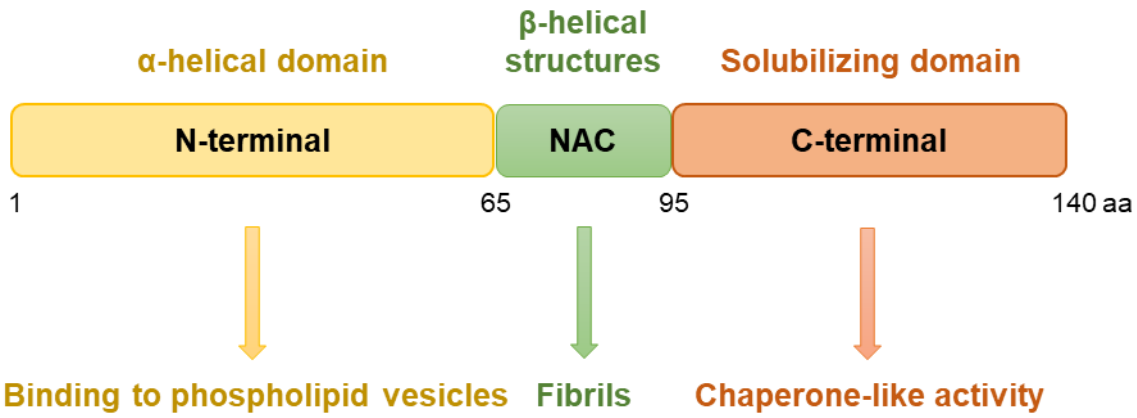

Figure 1. Schematic representation of the three distinct domains of human αSyn. N-terminus (yellow) contains a motif binding the phospholipids, the central NAC domain: non-amyloid-β component (green), is strongly hydrophobic and promotes aggregation, C-terminal domain (orange) is acidic and promotes the protein solubility.

1.3. Phosphorylation of α-synuclein

A large number of posttranslational modifications (PTMs) are present in the relatively small αSyn protein (Figure 2). PTMs are chemical modifications of amino acid residues that can potentially modify the structure of proteins by changes in protein size, structure, or charge and regulate their activity, binding affinity, localization or degradation (Beyer, 2006; Prabakaran *et al*, 2012; Beck-Sickinger & Mörl, 2006; Schmid *et al*, 2013). Major αSyn PTMs include phosphorylation, ubiquitination, nitration, sumoylation, glycosylation, and acetylation (Bartels *et al*, 2014; Dorval & Fraser, 2006; Duda *et al*, 2000; Fujiwara *et al*, 2002; Giasson *et al*, 2000; Guerrero *et al*, 2013; Hasegawa *et al*, 2002; Shimura *et al*, 2001). PTMs modulate the degradation of proteins prone to misfolding and aggregation through various proteolytic pathways. PTMs contribute to maintaining normal αSyn function in the healthy brain, affect αSyn degradation as well as aggregation formation and PD pathology (Pajarillo *et al*, 2019). PTMs such as phosphorylation, ubiquitination or sumoylation have the potential to determine protein fate and their preference for particular protein degradation pathways acting as molecular switches (Pratt *et al*, 2015; Clark *et al*, 2005; Yang *et al*, 2016). Nitration has been observed to promote αSyn oligomerization and act as trigger for αSyn toxicity (Burai *et al*, 2015; Kleinknecht *et al*, 2016), whereas sumoylation tends to have an inhibitory effect on toxicity as it promotes the protein solubility (Shahpasandzadeh *et al*, 2014; Krumova *et al*, 2011).

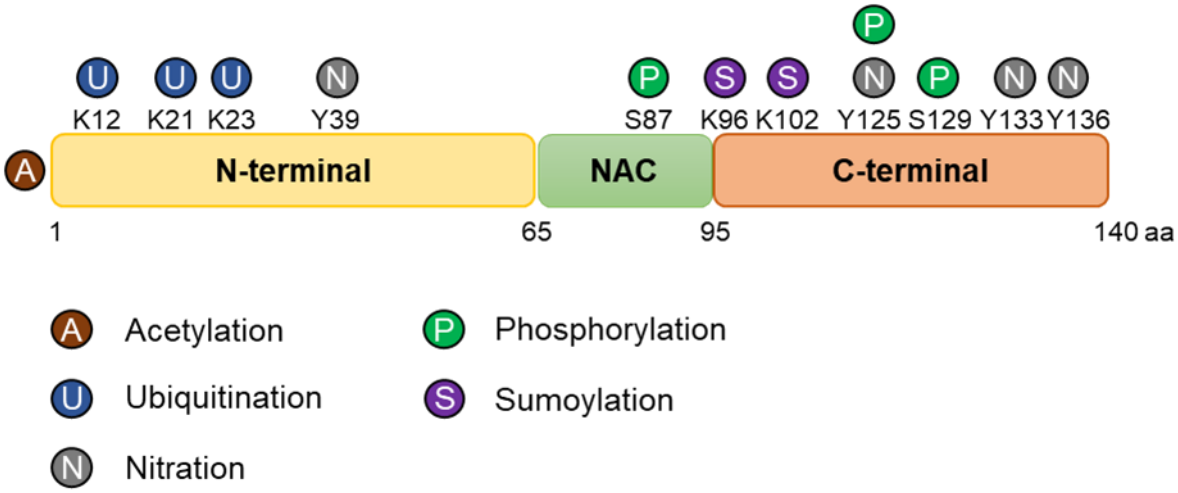

Figure 2. Schematic representation of the major posttranslational modifications (PTMs) of human αSyn at corresponding amino acid residues.
αSyn is abundantly modified by various PTMs including acetylation (at N-terminus), ubiquitination (U), nitration (N), phosphorylation (P) and sumoylation (S).

Protein phosphorylation is one of the most prevalent and potentially the most important posttranslational modification. Phosphorylation is considered to have an important role in the regulation of αSyn susceptibility to aggregation and neurotoxicity (Oueslati, 2016; Paleologou *et al*, 2010). αSyn undergoes phosphorylation at one or more sites, at both serine (S87, S129) and tyrosine residues (Y39, Y125, Y133, Y136) (Fujiwara *et al*, 2002; Okochi *et al*, 2000; Pronin *et al*, 2000). Studies of postmortem human brains have shown that phosphorylation at S129 is the predominant PTMs of αSyn (Anderson *et al*, 2006). Approximately 90% of αSyn found in LBs is phosphorylated at this residue in comparison to 4% of αSyn under physiological conditions (Fujiwara *et al*, 2002). Phosphorylation at S129 has been shown to be an important regulator for αSyn localization, aggregation and toxicity. However, the exact effect of pS129 αSyn and its importance in pathogenicity is still a matter of debate as the results of various studies in different systems are in some respects controversial.

Expression of αSyn phosphorylated at S129 (pS129) has been shown to lead to inclusion formation and enhanced neurotoxicity and in *D. melanogaster*, when compared to αSyn phosphorylation deficient mutant (Chen & Feany, 2005). In contrast, studies in rats and *C. elegans* have shown reduced neurotoxicity and protective effects

of pS129, in comparison to wild type αSyn or S129A mutant expression (Gorbatyuk *et al*, 2008; Kuwahara *et al*, 2012). Studies in mouse and yeast models have also indicated protective role of pS129 as it may play important role in delaying inclusion (Kleinknecht *et al*, 2016; Tenreiro *et al*, 2014b). Expression of pS129 αSyn does not affect zebrafish motility, where phosphorylation at this residue is unlikely to promote αSyn aggregation (Weston *et al*, 2021).

There are several kinases involved in S129 phosphorylation of αSyn in human cells, including polo-like kinases (PLKs) 1-3, G protein-coupled receptor kinases (GRKs), casein kinases (CKs) 1 and 2, and leucine-rich repeat kinase 2 (LRRK2) (Oueslati *et al*, 2013; Qing *et al*, 2009; Waxman & Giasson, 2008; Pronin *et al*, 2000). Phosphorylation of αSyn by GRK5 has a key role in the underlying pathogenesis of PD (Arawaka *et al*, 2006). PLK2 was identified as the most potent polo-like kinase that phosphorylates αSyn at S129 site (Inglis *et al*, 2009; Mbefo *et al*, 2010; Salvi *et al*, 2012). αSyn expressed in yeast is also phosphorylated at the conserved S129 residue by endogenous kinases. PLKs and CKs have orthologs in yeast. Cdc5, yeast PLK2 ortholog, and Yck3, yeast CK-1 ortholog, phosphorylate αSyn at S129 and overexpression of the kinases rescues αSyn toxicity (Gitler *et al*, 2009; Wang *et al*, 2012; Zabrocki *et al*, 2008). Heterologous expression of human kinases PLK2 or GRK5 in yeast and co-expression of αSyn significantly increased phosphorylation of αSyn at S129 residue (Shahpasandzadeh *et al*, 2014). Protective role of S129 phosphorylation in yeast was confirmed in studies where expression of phosphorylation-deficient variants of αSyn, S129A or S129G, was found to promote αSyn-induced toxicity and inclusion formation (Tenreiro *et al*, 2014a).

1.4. Degradation pathways of α-synuclein

αSyn clearance mechanisms play crucial roles in balancing protein levels and represent a key issue for understanding and potentially ultimately treating PD. Ineffective protein clearance caused by impaired degradation pathways is sufficient to cause neurotoxicity (Vilchez *et al*, 2014). Accumulation of misfolded and aggregated αSyn leads to overloading of the proteostasis network and significant perturbation of proteostasis in PD. Cellular αSyn levels are dependent on the equilibrium between the rates of αSyn synthesis, oligomerization, aggregation, and degradation. Degradation

of malfunctioning or potentially toxic proteins in eukaryotic cells involves two pathways: the ubiquitin-proteasome or the autophagy-lysosome/vacuole system (Figure 3; Goldberg, 2003; Klionsky & Emr, 2000). It has been suggested that both of these pathways contribute to degradation of αSyn (Webb *et al*, 2003). αSyn can be degraded by the 26S proteasome complex under physiological conditions *in vivo.* The autophagy system is involved when expression of αSyn is increased (Ebrahimi-Fakhari *et al*, 2011; Petroi *et al*, 2012). The exact factors that distribute αSyn degradation between these specific degradation pathways are still not entirely clear (Stefanis *et al*, 2019).

PTMs act as molecular switches, determining the preference of αSyn for degradation by a specific proteolytic pathway. De-ubiquitinated αSyn has been shown to favour degradation by the autophagy system, whereas monoubiquitinated αSyn is preferentially degraded by the proteasome (Rott *et al*, 2011). αSyn phosphorylated at S129 residue is directed for degradation by the 26S proteasome in a ubiquitin-independent manner (Machiya *et al*, 2010). The increased, PLK2-mediated phosphorylation of αSyn leads to aggregate clearance by the autophagy pathway and suppression of cytotoxicity (Oueslati *et al*, 2013). Studies in yeast have also shown that sumoylated αSyn aggregates are preferentially degraded by the autophagy-vacuole system, and the impairment of αSyn sumoylation leads to enhanced aggregate formation and growth suppression (Shahpasandzadeh *et al*, 2014; Popova *et al*, 2015) (Figure 3). This defect is suppressed by phosphorylation at S129, which by leading to increased ubiquitination shifts the αSyn degradation to the proteasome.

1.4.1. Autophagy

The autophagy system includes the formation of double membraned autophagosomes and degrades long-lived proteins, cytosolic components, and cellular organelles after fusion with lysosomes/vacuoles through various types of proteases, lipases, and nucleases (Reggiori & Klionsky, 2013; Xilouri *et al*, 2013). The impairment of the autophagy lysosomal pathway (ALP) leads to the accumulation of αSyn aggregates and ultimately to cell death (Lee *et al*, 2004). ALP potentially serves as a major pathway for degradation of misfolded and aggregated αSyn under pathological conditions when the ubiquitin-proteasome system (UPS) is compromised and αSyn levels are elevated. Oligomeric αSyn intermediates, but not fibril inclusion bodies, can be removed by ALP

(Ebrahimi-Fakhari *et al*, 2011; Lee *et al*, 2004). Furthermore, it has been shown that the clearance αSyn aggregates in yeast depends more on the autophagy pathway and that αSyn can inhibit this pathway as well (Petroi *et al*, 2012). Since a significant amount of αSyn is presumed to be degraded by ALP, it has been suggested that impairment of this degradation pathway contributes to PD pathology (Xilouri *et al*, 2013). However, the exact contribution of ALP to PD pathology is yet elusive as various studies show contradictory outcomes (Stefanis *et al*, 2019).

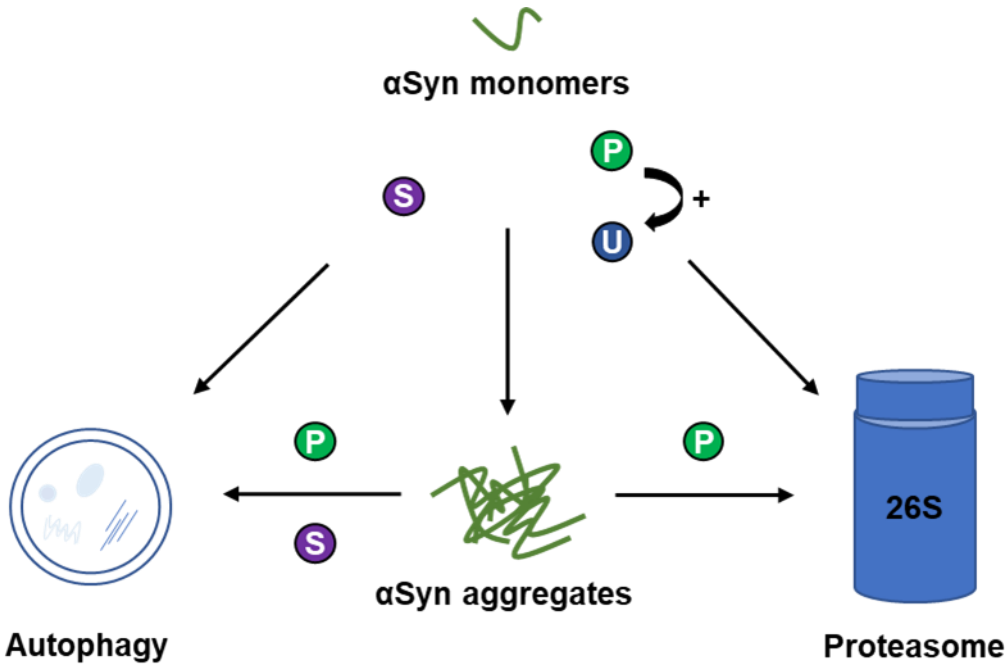

Figure 3. Schematic representation of αSyn protein degradation pathways in yeast.
The autophagy/vacuole and the proteasome represent two major intracellular pathways for protein degradation. Soluble αSyn monomer degradation proceeds via both of these pathways. The inhibition of sumoylation of αSyn prolongs the protein monomers half-life, inhibits degradation through both pathways, and leads to inefficient aggregate clearance through autophagy pathway. Degradation of soluble αSyn is promoted by phosphorylation at serine 129 (S129). Moreover, phosphorylation at this residue enhances ubiquitination and decreased stability of αSyn. Upregulation of S129 phosphorylation by expression of GRK5 or PLK2 rescues aggregate clearance by autophagy and further promotes proteasomal degradation. S = sumoylation; P = phosphorylation; U = ubiquitination.

1.4.2. Proteasome

Numerous studies support a role of proteasome dysfunction in Parkinson's disease pathology (Bentea *et al*, 2017; Chu *et al*, 2009; McNaught & Jenner, 2001; McNaught *et al*, 2002, McNaught *et al,* 2006; Tofaris *et al*, 2003). The finding of αSyn, as well as ubiquitin and proteasomal subunits as components of LBs, has firmly linked αSyn degradation by ubiquitin-proteasome system to PD pathology (Ii *et al*, 1997). Exclusive αSyn degradation by UPS was presumed until studies showed that the autophagy pathway may be more important than previously thought (Wales *et al*, 2013; Petroi *et al*, 2012). The degradation of αSyn by the proteasome has been suggested to occur under endogenous conditions (Ebrahimi-Fakhari *et al*, 2011). Nevertheless, several studies with pharmacological inhibitors have shown that soluble oligomeric intermediate forms of αSyn can be degraded by the 26S proteasome complex (Emmanouilidou *et al*, 2010; Webb *et al*, 2003). However, ubiquitin-proteasome system and autophagy can be modulated differently in response to physiological conditions. Proteasomes themselves can a substrate for autophagy. In this process, called proteaphagy, ALP reduces the abundance of proteasomes and defective particles (Marshall & Vierstra, 2019; Waite *et al*, 2022). A synchronized and complementary interplay between proteasome degradation and synthesis can be critical under proteostatic stress conditions (Marshall & Vierstra, 2018; Cohen-Kaplan *et al*, 2016; Peters *et al*, 2015). Mutated or aggregated forms of αSyn can bind to the proteasome and impair of proteasomal activity (Stefanis *et al*, 2001; Tanaka *et al*, 2001; Emmanouilidou *et al*, 2010; Snyder *et al*, 2003). Thus, proteasomes that attempted αSyn degradation and were damaged by αSyn can be removed by proteaphagy. Therefore, it can be difficult to distinguish whether αSyn has reached the autophagosome directly or with defective proteasomes.

The proteasome complex is composed of a 20S core particle (CP) and a 19S regulatory particle (RP) (Figure 4). The 19S RP binds to one or both ends of the 20S proteasome to form a multicatalytic 26S proteasome that in a multistep process degrades proteins to small peptides. The 20S CP carries the catalytic activity and is formed of two outer α-rings and two inner β-rings, each composed of seven distinct subunits arranged in an α7-β7-β7-α7 arrangement. The 19S RP subunit is required for the recognition and binding of ubiquitinated protein substrates and has the ability for

deubiquitinating and unfolding these substrates for further ATP-dependent translocation into the 20S CP cylinder (Murata *et al*, 2009). Proteins are directed to the proteasome predominantly by attachment of polyubiquitin chains to a lysine side chain. A chain of at least four ubiquitin molecules linked together by isopeptide bonds between the C-terminus of one ubiquitin and lysine 48 (K48) of the next is the standard target signal for the proteasomal degradation (Chau *et al*, 1989; Thrower *et al*, 2000).

The 19S particle can be separated into two subunits: lid and base, which can be subclassified into two groups: Regulatory Particle of Non-ATPase (RPN) subunits and Regulatory Particle of Triple-ATPase (RPT) subunits (Glickman & Ciechanover, 2002; Glickman *et al*, 1998; Hanna & Finley, 2007). The base consists of six related AAA-ATPase unfoldase subunits (Rpt1-6) and four non-ATPase subunits (Rpn1, Rpn2, Rpn10, and Rpn13), whereas the lid contains nine non-ATPase subunits (Rpn3, Rpn5-9, Rpn11, Rpn12, and Rpn15/Sem1) (Glickman *et al*, 1998; Schmidt *et al*, 2005). The 19S base complex has three functions: protein capture through ubiquitin recognition, substrate unfolding, and opening of the channel in the ring. The ATPase subunits (Rpt1-6) of the base are organized into a hexameric ring that promotes gate opening and unfolding, which allows the substrate to reach the catalytic sites in the 20S particle (Förster *et al*, 2005). Three 19S ATPases, Rpt2, Rpt3 and Rpt5, contain a conserved C-terminal hydrophobic-tyrosine-X (HbYX) motif, essential for gate opening (Smith *et al*, 2007; Rabl *et al*, 2008; Saeki & Tanaka, 2007).

The lid is responsible for recognition and deubiquitylation of captured substrates. The metalloisopeptidase Rpn11 cleaves as deubiquitinase (DUB) as prerequisite for recycling of the ubiquitin moieties (Verma *et al*, 2002; Hu *et al*, 2005; Hamazaki *et al*, 2006; Yao *et al*, 2006). Rpn11 is stabilized by another proteasome subunit, Sem1 (Kolog Gulko *et al*, 2018).

Assembly of the 26S proteasome is assisted by molecular chaperones. The 19S RP assembly in yeast is controlled by four proteasome-interacting proteins Nas2, Nas6, Rpn14 and Hsm3, which correspond in mammals to p27, gankyrin, PAAF1 and S5b, respectively. These proteins bind to C-terminal ends of specific Rpt proteins and mediate the interaction between the Rpt subunits and the α-subunits of 20S CP. The chaperons also interact genetically with each other (Saeki *et al*, 2009; Park *et al*, 2009; Madura, 2009; Funakoshi *et al*, 2009; Roelofs *et al*, 2009).

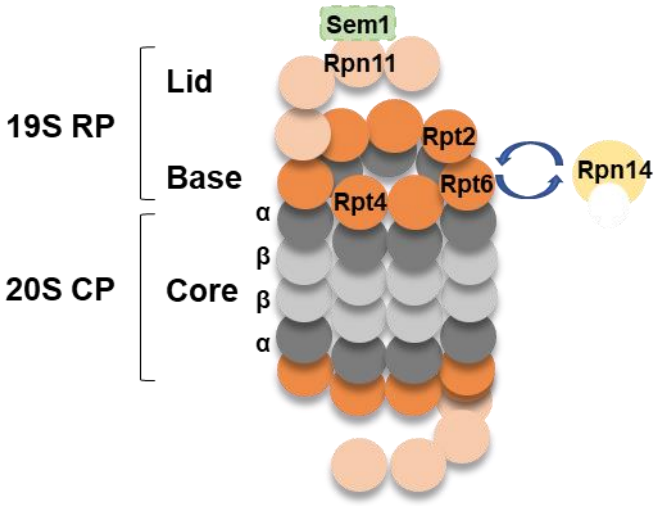

Figure 4. Schematic representation of the yeast 26S proteasome.
The 26S proteasome consists of the 20S catalytic core complex, which includes α- and β-subunits, and two 19S regulatory particles. The regulatory particle is subdivided into base and lid subcomplexes, which consist of subunits of the regulatory particle triple A (RPT) and the regulatory particle non-ATPase (RPN). 26S assembly requires chaperones as the indicated Rpn14. Cellular protein degradation is an essential step in the coordination of diverse signal transduction pathways. Peptides are formed in the degradation process, which are further degraded to amino acids and used in the synthesis of new proteins. Proteasome subunits indicated in the figure are important for this work.

1.5. *Saccharomyces cerevisiae* as reference cell for the study of α-synuclein aggregate formation

The eukaryotic budding yeast *Saccharomyces cerevisiae* represents an established and valuable reference cell for studying fundamental questions regarding the pathogenetic role of human proteins in neurodegenerative diseases such as PD. Using a simple and single-celled organism such as budding yeast to study a complex brain disorder such as PD may not seem apparent. It has its limitations as yeast cannot recreate the complex cellular interactions ongoing in the human brain. However, yeast cells share numerous cellular pathways that control crucial aspects of eukaryotic cell biology. Among these are the mechanisms of protein folding, degradation pathways, mitochondrial function and oxidative stress, as well as the mechanisms of cell death (Bonifacino & Glick, 2004; Botstein *et al*, 1997; Brodsky & Skach, 2011; Hartwell, 2002; Munoz *et al*, 2012). The yeast genome is well characterized. It is composed of 16 chromosomes with 6217 genes and 44% of yeast genes show significantly similar sequences to human genes (Goffeau *et al*, 1996; Hughes, 2002). Thus, many of the

key processes that are most relevant to PD pathology can be effectively studied in a well-established yeast model. Furthermore, yeast model has several distinct benefits over higher model organisms due to its high susceptibility to genetic manipulations and its rapid growth with generation time of approximately 90 minutes. This allows for rapid and simple upscaling, which is advantageous for high-throughput genetic and small molecule studies (Sherman, 2002; Mager & Winderickx, 2005).

Although there is no yeast homologue of the human *SNCA* gene encoding αSyn, it can be expressed in yeast cells resulting in so called humanized yeast. Expression of this human protein in *Saccharomyces cerevisiae* mimics PD by recapitulating processes leading to aggregation and molecular mechanisms causing cellular toxicity. The yeast model of PD was established for the first time by Outeiro and Lindquist in 2003 (Outeiro & Lindquist, 2003). They showed that αSyn expression is toxic to yeast cells and the level of its toxicity is dependent on the gene dose. The threshold for αSyn cytotoxicity which is recognized as growth retardation in yeast has been established (Petroi *et al*, 2012). Three integrated copies of wild type αSyn represent the causative level of αSyn that leads to cell death. Low expression level leads to plasma membrane localization without growth retardation in yeast, whereas high expression level leads to formation of cytoplasmic aggregates and to reduced growth.

1.6. Aim of the study

Proteostasis safeguards cells from misfolded and damaged proteins. Accumulation of misfolded and aggregated αSyn species in PD indicates a significant failure of the proteostasis network. The level of αSyn in the cells depends on the balance between αSyn synthesis, aggregation and clearance. Various posttranslational modifications (PTM) affect this equilibrium and modulate the clearance of the protein by the ubiquitin-proteasome system (UPS) or autophagy. One of the most important PTMs of αSyn is phosphorylation at serine 129 (pS129).

In this study, budding yeast was used as a reference eukaryotic cell to study the impact of αSyn expression and its phosphorylation at S129 on protein homeostasis, and it turn how those changes affect stability and toxicity of αSyn. The emphasis was on changes

in stability of the proteins involved in proteasomal degradation pathway to bring light to how αSyn interacts with the proteasome and thereby impairs proteasome function.
In the first part of the thesis, a high-throughput screen was applied to study the overall impact of αSyn expression on protein stability and to examine which biological pathways are affected by its expression. Additionally, the non-phosphorylatable αSyn variant (S129A) was compared to study the impact of αSyn phosphorylation at S129 on protein homeostasis. The goal was the identification of candidate genes and their respective proteins whose stability is affected by the heterologous expression of αSyn. This part of the thesis focuses on the Rpn14 chaperon of the 26S proteasome, which was identified in the screen as a protein significantly affected in stability by expression of αSyn and less by non-phosphorylatable S129A. As expression of αSyn was found to stabilize Rpn14, the study focused on elucidation of the consequences of its increased stability on 26S proteasomal activity and αSyn turnover.
The second part of the thesis focuses on the deubiquitinating enzyme Rpn11, which we had identified as a modulator of αSyn toxicity (Popova *et al*, 2021a). Rpn11 is an important protein for ubiquitin recycling, because it removes ubiquitin from the proteasome substrates. The interplay between the proteasome subunit Rpn11 and αSyn was investigated. The impact of downregulation of *RPN11* on αSyn turnover was examined, depending on its phosphorylation state, and how in turn these changes affect the overall proteasomal degradation. Furthermore, it was studied if the interplay between Rpn11 and αSyn is mediated by intrinsically disordered Rpn15/Sem1 as 26S proteasome subunit required for stabilization of Rpn11 (Kolog Gulko *et al*, 2018).

2. Materials and methods

2.1. Materials

2.1.1. Manufacturers of chemicals, biological material and equipment

Chemicals for buffers, solutions and media were purchased from the companies Carl Roth GmbH & CO. KG (Karlsruhe, Germany), Invitrogen (Carlsbad, USA), Sigma-Aldrich (St. Louis, USA), Roche (Basel, Switzerland), Merck KGaA (Darmstadt, Germany), AppliChem GmbH (Darmstadt, Germany) and Becton Dickinson (Franklin Lakes, USA). Agarose was obtained from Biozyme Scientific GmbH (Hessisch Oldendorf, Germany). "Roti®-Quant", Bradford solution, for the determination of protein concentration, was used from Carl Roth GmbH & CO. KG (Karlsruhe, Germany).

Restriction enzymes and polymerases were acquired from Thermo Fisher Scientific (Waltham, USA). RNase A from Roche (Basel, Switzerland) was used for RNA degradation. Primary antibodies were bought from Santa Cruz Biotechnology Inc (Dallas, USA), AnaSpec Inc (Fremont, USA), Wako Pure Chemical Industries Ltd (Osaka, Japan), Thermo Fisher Scientific (Waltham, USA), ChromoTek (Planegg, Germany) and EMD Milipore Corp (Burlington, USA). Secondary antibodies were obtained from Invitrogen (Carlsbad, USA) and Jackson ImmunoResearch Laboratories (West Grove, USA). Synthetic oligonucleotides were acquired from Sigma-Aldrich (St. Louis, USA). GeneArt® Seamless Cloning and Assembly Enzyme Mix from Invitrogen (Carlsbad, USA) was used for cloning. DNA-size and protein-weight standards the DNA-marker "GeneRuler 1kb DNA ladder" and the protein-marker "PageRuler Prestained Protein Ladder" were purchased from Thermo Fisher Scientific (Waltham, USA). Wild-type and deletion strains of *Saccharomyces cerevisiae* were acquired from EUROSCARF (Frankfurt, Germany).

Solutions were sterilized using Filtropur S 0.2 and S 0.45 filters from Sarstedt AG & Co (Nümbrecht, Germany). Kits "QIAGEN Plasmid Mini Prep Kit" and "QIAquick Gel Extraction Kit" from QIAGEN (Hilden, Germany) were used for plasmid DNA purification from *Escherichia coli* and DNA extraction from agarose gels the. "NanoDrop ND-1000 photospectrometer" from Peqlab Biotechnologie GmbH (Erlangen, Germany) was used for DNA concentrations measurements. PCR reactions

were run in the “MWG Biotech Inc Primus 96 Thermal Cycler” from MWG-Biotech (Ebersberg, Germany). Gel electrophoresis was performed in the “Mini-Sub Cell GT” chamber using the “Powerpac 300” power supply from Bio-Rad Laboratories (Hercules, USA). “Mini-PROTEAN® 3 Cell”, “Mini Trans-Blot® Electrophoretic Cell” and the “Powerpac 300” power supply from Bio-Rad Laboratories (Hercules, USA) were used for SDS-PAGE and protein immunoblotting. Protein transfer was performed using the nitrocellulose membrane “Amersham™ Protran™ 0.45 µm NC” from GE Healthcare (Little Chalfont, UK). “Amersham™ Hyperfilm™ ECL” from GE Healthcare (Little Chalfont, UK) was used for detection of chemiluminescence. Exposure of Hyperfilms™ for immunoblotting techniques was performed using an "Optimax X-ray Film Processor" from PROTEC GmbH & Co. KG (Oberstenfeld, Germany). Measurement of optical density was performed with a T80 UV/VIS spectrometer from PG Instruments Ltd (Lutterworth, UK) or alternatively with an "Infinite® M200" microplate reader from Tecan Group (Männedorf, Switzerland). Centrifugation was performed in a "Biofuge pico" centrifuge from Heraeus (Hanau, Germany), a "Centrifuge 5804R" from Eppendorf AG (Hamburg, Germany), a "Centrifuge 4K15" from Sigma Laborzentrifugen GmbH (Osterode am Harz, Germany) or a "Sorvall RC-3B Plus Refrigerated Centrifuge" from Thermo Fisher Scientific (Waltham, USA). "BD 53/E2" incubator from BINDER GmbH (Tuttlingen, Germany) and "BE 400" incubator from Memmert GmbH + Co. KG (Schwabach, Germany) were used for incubation of the agar plates at 37°C and 30°C respectively. Additional equipment, manufacturers, or other variations are mentioned later in the work.

2.1.2. Strains, plasmids and oligonucleotides

Cloning procedures as well as plasmid purifications were performed using *Escherichia coli* (*E. coli*) DH5α [*Δ80dlacZ ΔM15, recA1, endA1, gyrA96, thi-1, hsdR17 (rK-, mK+), supE44, relA1, deoR, Δ(lacZYA-argF) U169*]. *Saccharomyces cerevisiae* strains and plasmids as well as oligonucleotides which were used in this study are specified in Tables 2-4.

Table 2. *Saccharomyces cerevisiae* strains

Name	Genotype	Source
W303-1A	*MATa; ura3-1; trp1D2; leu2-3_112; his3-11; ade2-1; can1-100*	EUROSCARF
BY4741	*MATa; his3Δ1; leu2Δ0; met15Δ0; ura3Δ0*	EUROSCARF
Δrpn14	BY4741; *MATa; his3Δ1; leu2Δ0; met15Δ0; ura3Δ0; Δrpn14*	EUROSCARF
Δnas6	BY4741; *MATa; his3Δ1; leu2Δ0; met15Δ0; ura3Δ0; Δnas6*	EUROSCARF
Δrpn14 Δnas6	BY4741; *MATa; his3Δ1; leu2Δ0; met15Δ0; ura3Δ0; Δrpn14 Δnas6*	This study
RH3466	W303 containing 1 genomic copy *GAL1::SNCA::GFP* in *URA3* locus (KLID linker)	(Petroi *et al*, 2012)
RH3467	W303 containing 2 genomic copy *GAL1::SNCA::GFP* in *URA3* locus (KLID linker)	(Petroi *et al*, 2012)
RH3468	W303 containing 3 genomic copy *GAL1::SNCA::GFP* in *URA3* locus (KLID linker)	(Petroi *et al*, 2012)
yMaM330	*MATα can1Δ::STE2pr-SpHIS5 lyp1Δ::STE3pr-LEU2 his3Δ1 leu2Δ0*::*GAL1pr-I-SCEI-natNT2 ura3Δ0*	(Khmelinskii & Knop, 2014)
YBP456	*YER103W::mCherry::sfGFP in* yMaM330 (*SSA4*-tfT)	This study
YBP458	*YNR034W-A::mCherry::sfGFP in* yMaM330 (*EGO4*-tfT)	This study
YBP459	*YFL014W::mCherry::sfGFP in* yMaM330 (*HSP12*-tfT)	This study
YBP460	*YPR080W::mCherry::sfGFP in* yMaM330 (*TEF1*-tfT)	This study
YBP462	*YGL076C::mCherry::sfGFP in* yMaM330 (*RPL7A*-tfT)	This study
YBP464	*YGL256W::mCherry::sfGFP in* yMaM330 (*ADH4*-tfT)	This study
YBP465	*YJL167W::mCherry::sfGFP in* yMaM330 (*ERG20*-tfT)	This study
YBP466	*YDL204W::mCherry::sfGFP in* yMaM330 (*RTN2*-tfT)	This study
YBP467	*YPL223C::mCherry::sfGFP in* yMaM330 (*GRE1*-tfT)	This study
YBP468	*YDL022W::mCherry::sfGFP in* yMaM330 (*GPD1*-tfT)	This study
YBP469	*YGR019W::mCherry::sfGFP in* yMaM330 (*UGA1*-tfT)	This study
YBP487	*YBR118W::mCherry::sfGFP in* yMaM330 (*TEF2*-tfT)	This study
YBP488	*YLR327C::mCherry::sfGFP in* yMaM330 (*TMA10*-tfT)	This study
YBP489	*YDR533C::mCherry::sfGFP in* yMaM330 (*HSP31*-tfT)	This study
YBP491	*YBR088C::mCherry::sfGFP in* yMaM330 (*POL30*-tfT)	This study

YBP493	*YPL129W::mCherry::sfGFP in* yMaM330 (*TAF14*-tfT)	This study
YBP494	*YLR340W::mCherry::sfGFP in* yMaM330 (*RPP0*-tfT)	This study
YBP496	*YKL145W::mCherry::sfGFP in* yMaM330 (*RPT1*-tfT)	This study
YBP528	*YDL087C::mCherry::sfGFP in* yMaM330 (*LUC7*-tFT)	This study
YBP530	*YBR193C::mCherry::sfGFP in* yMaM330 (*MED8*-tFT)	This study
YBP539	*YDL048C::mCherry::sfGFP in* yMaM330 (*STP4*-tFT)	This study
YBP541	*YGL065C::mCherry::sfGFP in* yMaM330 (*ALG2*-tFT)	This study
YBP544	*YGL004C::mCherry::sfGFP in* yMaM330 (*RPN14*-tfT)	This study
YBP547	*YLR023C::mCherry::sfGFP in* yMaM330 (*IZH3*-tFT)	This study
YBP576	*YHR171W::mCherry::sfGFP in* yMaM330 (*ATG7*-tFT)	This study
YBP586	*YLR127C::mCherry::sfGFP in* yMaM330 (*APC2*-tFT)	This study
RPN14-GFP	MATa; *his3Δ1; leu2 Δ0; met15 Δ0; ura3Δ0; rpn14Δ::RPN14-GFP (HIS3)*	(Huh *et al*, 2003)
R1158	*MATa URA3::CMV-tTA his3-1 leu2-0 met15-0 (kanMX4:G418R)*	yTHC collection, Horizon Discovery, UK
yTHC-719	*Tet-RPN11* in R1158	yTHC collection, Horizon Discovery, UK
yTHC-76	*Tet-RPT2* in R1158	yTHC collection, Horizon Discovery, UK
yTHC-24	*Tet-RPT4* in R1158	yTHC collection, Horizon Discovery, UK
yTHC-681	*Tet-RPT6* in R1158	yTHC collection, Horizon Discovery, UK

Table 3. Plasmids

Name	Description	Source
pMaM17	*pFA6a with with mCherry::sfGFP:ADH1^{term}::kanMX*	(Khmelinskii *et al*, 2012)
pMaM432	*pFA6a with mCherry::sfGFP(cp8)::ADH1^{term}::kanMX*	(Khmelinskii *et al*, 2012)
pME2790	*pRS415-GAL1^{pr}, CYC1^{term}, LEU2, CEN, pUC origin, AmpR*	(Sikorski & Hieter, 1989)
pME2792	*pRS423-GAL1^{pr}, CYC1^{term}, HIS3, 2µm, pUC origin, AmpR*	(Sikorski & Hieter, 1989)
pME2794	*pRS425-GAL1^{pr}, CYC1^{term}, LEU2, 2µm, pUC origin, AmpR*	(Sikorski & Hieter, 1989)
pME2795	*pRS426-GAL1^{pr}, CYC1^{term}, URA3, 2µm, pUC origin, AmpR*	(Sikorski & Hieter, 1989)
pRS313	*pBluescript, HIS3, CEN6, ARSH4*	(Sikorski & Hieter, 1989)
pME3759	*pME2795 with GAL1^{pr}::GFP*	(Petroi *et al*, 2012)
pME3760	*pME2795 with GAL1^{pr}::SNCA^{WT}*	(Petroi *et al*, 2012)
pME3763	*pME2795 with GAL1^{pr}::SNCA^{WT}::GFP*	(Petroi *et al*, 2012)
pME5033	*pRS423 (2µm, HIS3, CYC1^{term}, AmpR) with GAL1^{pr}::SNCA::VenusC*	(Tenreiro *et al*, 2016)
pME5034	*pRS426 (2µm, URA3, GAL1^{pr}, CYC1^{term}, AmpR) with GAL1::VenusN::SNCA*	(Tenreiro *et al*, 2016)
pME5035	*pRS423 (2µm, HIS3, CYC1^{term}, AmpR) with GAL1^{pr}::VenusC*	(Popova *et al*, 2021b)
pME5039	*pRS425 (2µm, LEU2, CYC1^{term}, AmpR) with GAL1^{pr}::SNCA::GFP*	(Popova *et al*, 2021b)
pME5320	*pME2795 with GAL1^{pr}::SNCA^{S129A}*	(Popova *et al*, 2021a)
pME5321	*pMaM17 with GAL1^{pr}::SNCA^{WT}*	(Popova *et al*, 2021a)
pME5322	*pMaM17 with GAL1^{pr}::SNCA^{S129A}*	(Popova *et al*, 2021a)
pME5323	*pMaM17 with GAL1^{pr}::SNCA^{Y133F}*	(Popova *et al*, 2021a)

pBP476	*pRS415-GPD^{pr} (CEN, LEU2, CYC1^{term}, AmpR)*	This study
pBP477	*pRS415-GPD^{pr}-mCherry-sfGFP (CEN, LEU2, CYC1^{term}, AmpR)*	(Khmelinskii *et al*, 2016)
pBP480	*pRS415-GPD^{pr}-Ubi-R-mCherry-sfGFP (CEN, LEU2, CYC1^{term}, AmpR)*	(Khmelinskii *et al*, 2016)
pBP494	*pRS425-GPD^{pr} (2µm, LEU2, CYC1^{term}, AmpR)*	This study
pBP552	*pME2790 with GAL1^{pr}::SCNA^{WT}::mCherry::sfGFP*	This study
pBP553	*pME2790 with GAL1^{pr}::SCNA^{S129A}::mCherry::sfGFP*	This study
pBP555	*pME2790 with GAL1^{pr}::SCNA^{S129A}::mCherry::sfGFP*	This study
pBP558	*pME2790 with GAL1^{pr}::mCherry::sfGFP*	This study
pBP559	*pRS415 (CEN, LEU2, CYC1^{term}, AmpR) with GPD^{pr}::RPN14::mCherry::sfGFP*	This study
pBP561	*pRS425 (2µm, LEU2, CYC1^{term}, AmpR) with GPD^{pr}::RPN14::mCherry::sfGFP*	This study
pBP583	*pRS415 (CEN, LEU2, GPD^{pr}, CYC1^{term}, AmpR) with RPN14::His6*	This study
pBP591	*pRS313 with GPD^{pr}::CYC1 ^{term} (CEN, HIS3, AmpR)*	This study
pBP592	*pRS313 with GPD^{pr}::RPN14::His6::CYC1^{term} (CEN, HIS3, AmpR)*	This study
pBP594	*pRS426 (2µm, URA3, GAL1^{pr}, CYC1^{term}, AmpR) with GAL1::VenusN::RPN14*	This study
pBP602	*pRS423 (2µm, HIS3, CYC1^{term}, AmpR) with GAL1::SNCA^{S129A}::GFP*	This study
pBP638	*pRS423 (2µm, HIS3, CYC1^{term}, AmpR) with GAL1^{pr}::SNCA^{S129A}::VenusC*	This study
pBP646	*pRS426 (2µm, URA3, GAL1^{pr}, CYC1^{term}, AmpR) with GAL1::VenusN::SNCA^{S129A}*	This study

Table 4. Oligonucleotides

Name	Sequence (5' - 3')	Use
BP20	GTT AGA GCG GAT GTG GGG	*CYC1 reverse primer used for sequencing*
BP142	GCT GCA TAA CCA CTT TAA CTA	*GAL1* forward primer used for sequencing
BP175	ACT AGT GGA TCC CCC ATG GAT GTA TTC ATG AAA G	αSyn-tFT forward primer used for amplification of αSyn-tFT, S129A-tFT and Y133F-tFT for cloning in pME2790
BP414	GAA TTC CTG CAG CCC TTA GGA TCC CTT ATA AAG	αSyn-tFT reverse primer used for amplification of αSyn-tFT, S129A-tFT Y133F-tFT and tFT alone for cloning in pME2790
BP415	ACT AGT GGA TCC CCC ATG GTG AGC AAG G	tFT froward primer used for amplification of tFT for cloning in pME2790
BP418	ACT AGT GGA TCC CCC ATG ACT AAG ACC ATC AC	*RPN14* forward primer used for amplification of *RPN14*
BP416	CCA TGT CGA CAA GCT TAG GAT TAC TTA AGT TAT ACA AAG	*RPN14* reverse primer used for amplification of *RPN14* on template genomic DNA (W303)
BP417	AAG CTT GTC GAC ATG GTG AGC AAG G	tFT forward primer used for amplification of tFT
BP414	GAA TTC CTG CAG CCC TTA GGA TCC CTT ATA AAG	tFT reverse primer used for amplification of tFT
BP458	CAA AAG CTG GGT ACC GTC ATT ATC AAT ACT CG	Forward primer used for amplification of GPD^{pr}-MCS-$CYC1^{term}$
BP459	AGG GCG AAT TGG AGC TGC AAA TTA AAG CCT TCG	Reverse primer used for amplification of GPD^{pr}-MCS-$CYC1^{term}$
BP429	TTA ATG GTG ATG GTG ATG ATG AGG ATT ACT TAA GTT ATA C	Reverse primer used for amplification of Rpn14-His6
BP430	GAA TTC CTG CAG CCC TTA ATG GTG ATG GTG	Reverse primer used for amplification of Rpn14-His6
BP431	CTC GAT CTC GAA CTC GTG	mCherry reverse primer for sequencing
BP462	GAG GTG GTG GGT CCC TTA AGA TGA CTA AGA CCA TCA C	*RPN14* forward primer used for amplification of *RPN14*

BP461	CGA ATT CCT GCA GCC CTT AAG GAT TAC TTA AGT TAT ACA	*RPN14* reverse primer used for amplification of *RPN14*
BP173	ACT AGT GGA TCC CCC ATG GTG AGC AAG GGC GAG	VenusN forward primer used for amplification of VenusN
BP463	GTG ATG GTC TTA GTC ATC TTA AGG GAC CCA CCA CCT C	VenusN reverse primer used for amplification of VenusN
BP464	TAA ATG CTA CAT AAA TGC ATG CCC TTA AAA CTG TAT AAC CGA CAT GGA GGC CCA G	NatMX6 cassette forward primer used for amplification of NatMX6 cassette for knockout of *NAS6*
BP465	AAT ATT GAT ATG TAA AGT TCT GTA ATA TGT AGT TTT GAA ATC CAG TAT AGC GAC CAG CA	NatMX6 cassette reverse primer used for amplification of NatMX6 cassette for knockout of *NAS6*
BP466	GTT GAC GTT GGT GAC CTC	NatMX6 cassette forward primer used for knockout of *NAS6* and *RPN14*
BP467	ATT ACT CAT AGC AAT AGA GGA AG	3’ UTR of *NAS6* reverse primer used for knockout of *NAS6*
BP476	ACA TAT TAC AGG CGT CAG G	5’ UTR of *RPN14* reverse primer used for knockout of *RPN14*
BP59	GCT TAT GAA ATG CCT GCC GAG GAA GGG TAT CAA G	Quick change mutagenesis forward primer used for substitution of serine129 to alanine in SNCA
BP60	CTT GAT ACC CTT CCT CGG CAG GCA TTT CAT AAG C	Quick change mutagenesis reverse primer used for substitution of serine129 to alanine in SNCA
BP474	AGA AAG TAA AAA GAA ATA GCG AAG TAC AAT AGA AAC GAC AGA CAT GGA GGC CCA G	NatMX6 cassette forward primer used for amplification of NatMX6 cassette for knockout of *RPN14*
BP475	AAT ATT GAT ATG TAA AGT TCT GTA ATA TGT AGT TTT GAA ATC CAG TAT AGC GA CCA GCA	NatMX6 cassette reverse primer used for amplification of NatMX6 cassette for knockout of *RPN14*
BP484	AGT TTT CAA CCC TAA GAG CAG AAA GTA AAA AGA AAT AGC	Nested forward primer for longer homology region for deletion of *RPN14*
BP485	CAA GCT CAT GCA GCG AAG TGA ACT TTT TTG A	Nested reverse primer for longer homology region for deletion of *RPN14*
BP525	CTT AAG GGA CCC ACC ACC TCC AGA GC	VenusN forward primer used for amplification of VenusN
BP526	GGT GGG TCC CTT AAG ATG GAT GTA TTC ATG AAA GG	VenusN reverse primer used for amplification of VenusN

2.1.3. Enzymes

Enzymes used in this study are listed in Table 5.

Table 5. Enzymes

Enzyme (buffer)	**Concentration (activity)**	**Company**
RNase A	50U/mg	Roche
Phusion DNA polymerase (5x GC buffer)	2 U/µL (500 U)	Thermo Fisher Scientific
*Pfu*Turbo *Cx* hotstart DNA polymerase (10x *Pfu* Turbo *Cx* reaction buffer)	2.5 U/µl (100 U)	Agilent Technologies
*Bsp*120I (10x Buffer B)	10 U/µL (1500 U)	Thermo Fisher Scientific
*Dpn*I (10x Tango buffer)	10 U/µL (500 U)	Thermo Fisher Scientific
*Sac*I (10x Buffer *Sac*I)	10 U/µL (1200 U)	Thermo Fisher Scientific
*Sma*I (10x Tango buffer)	10 U/µL (1200 U)	Thermo Fisher Scientific

2.1.4. Media

All media were dissolved in H_2O before being autoclaved for 20 minutes at 121°C and 2 bar. For cultivation of yeast strains and *E. coli* the following media were used. Substances that are thermally unstable were dissolved and filtered to sterility using Filtropur S 0.2 filters (Sarstedt AG & Co). The following media were used to culture bacterial and yeast strains.

Table 6. Media

Medium	Ingredients	Agar plates	Liquid medium
LB medium (*E. coli*)	Tryptone	10 g	10 g
	Yeast extract	5 g	5 g
	NaCl	5 g	5 g
	Agar-Agar	15 g	-
	H_2O	1000 ml	1000 ml
SC medium (*S. cerevisiae*)	YNB-aa-as (yeast nitrogen base w/o AA and AS)	0.9 g	0.9 g
	Ammonium sulfate	3 g	3 g
	Inositol (200 mM)	0.6 ml	0.6 ml
	AA-powder mix	1.2 g	1.2 g
	Glucose/Galactose/Raffinose	12 g	12 g
	Agar	9 g	-
	H_2O	600 ml	600 ml
YEPD (*S. cerevisiae*)	Bacto-Peptone	6 g	6 g
	Yeast extract	3 g	3 g
	Glucose/Galactose	6 g	6 g
	Agar	6 g	-
	H_2O	300 ml	300 ml
Amino acids /Nucleobases (2 g/l)	Adenine (Ade) L-Alanine (Ala) L-Argenine (Arg) L-Asparagine (Asn) L-Aspartic acid (Asp) L-Cystein (Cys) L-Glutamine (Gln) L-Glutamic acid (Glu) Glycine (Gly) L-Isoleucine (Ile) L-Lysine (Lys) L-Methionine (Met) L-Phenylalanine (Phe) L-Prolin (Pro) L-Serine (Ser) L-Threonine (Thr) L-Tyrosine (Tyr) L-Valine (Val) para-Aminobenzoic acid (Paba)	2 g 2 g 2 g 2 g 2 g 2 g 2 g 2 g 2 g 2 g 2 g 2 g 2 g 2 g 2 g 2 g 2 g 2 g 0.2 g	2 g 2 g 2 g 2 g 2 g 2 g 2 g 2 g 2 g 2 g 2 g 2 g 2 g 2 g 2 g 2 g 2 g 2 g 0.2 g

2.1.5. Antibiotics

Stock solutions of all antibiotics used in this study were prepared for antibiotic selection. The autoclaved media were required to cool to approximately 50°C before the addition of the antibiotic stock solutions. The final concentrations of all antibiotics are given below.

Table 7. Antibiotics

Name	Stock Solution	Final Concentration	Storage
Doxycycline	10 mg/ml	10 µg/ml and 2 µg/ml	-20°C
Ampicillin	100 mg/ml	100 µg/ml	-20°C
Cycloheximide	100 mg/ml	50 µg/ml	-20°C
G418	100 mg/ml	200 µg/ml	-20°C
ClonNAT	200 mg/ml	200 µg/ml	-20°C

2.1.6. Antibodies

Table 8. Primary antibodies

Antibody	Organism	Type	Company	Dilution
Anti-α/β/γSyn	rabbit	polyclonal	Santa Cruz Biotechnology	1:2000
Anti-αSyn	mouse	monoclonal	BD Bioscience	1:2000
Anti-ubiquitin	mouse	monoclonal	EMD Milipore Corp	1:2000
Anti-GAPDH	mouse	monoclonal	Thermo Scientific	1:5000
Anti-pS129	mouse	monoclonal	Wako Chemicals	1:3000
Anti-GFP	rat	monoclonal	ChromoTek	1:1000

Table 9. Secondary antibodies

Antibody	Type	Company	Dilution
Peroxidase-conjugated AffiniPure Goat anti-Mouse IgG (H+L)	polyclonal	Jackson ImmunoResearch Laborato-ries	1:5000
HRP-conjugated Goat anti-Rabbit IgG (H+L)	polyclonal	Invitrogen	1:5000
HRP-conjugated Goat anti-Rat IgG (H+L)	polyclonal	Invitrogen	1:1000

2.2. Methods

2.2.1. Cultivation of cells

2.2.1.1. Cultivation of *Escherichia coli*

Escherichia coli strains were cultured in 5 ml of Luria-Bertani (LB) medium containing 1% (w/v) bacto-tryptone, 0.5% (w/v) yeast extract, 1 % (w/v) NaCl on a rotation shaker (Infors AG) at 37°C overnight (Bertani G, 1951). Agar (2%) (Carl Roth GmbH & CO. KG) was added to obtain a solid medium. *Escherichia coli* DH5α strain was used for general cloning protocols and plasmid DNA purification. Ampicillin (100 µg/ml) (Carl Roth GmbH & CO. KG) was applied to the medium for selection of colonies harboring the plasmid of interest.

2.2.1.2. Cultivation of *Saccharomyces cerevisiae*

Saccharomyces cerevisiae strains were grown in 10 ml of YEPD medium (2% (w/v) bacto-peptone, 1% (w/v) yeast extract, 2% (w/v) glucose, for solid medium: 2% (w/v) agar) at 30°C on a rotation shaker (Fröbel Labortechnik GmbH) overnight. On YEPD solid medium, *Saccharomyces cerevisiae* strains were cultivated at 30°C for two to three days. To culture the *Δrpn14*, *Δnas6* and *Δrpn14Δnas6* strains, 200 µg/ml G418 (Geneticin® Selective Antibiotic, Thermo Fisher Scientific) was added to YEPD medium. To select strains carrying the desired plasmid after transformation, cells were grown on Synthetic Complete (SC) medium (0.15% (w/v) YNB-aa-as (yeast

nitrogenous base without AA and AS), 0.5% (w/v) ammonium sulfate, 0.2 mM inositol, 0. 2% (w/v) amino acid powder mixture, for liquid medium: 2% (w/v) raffinose, for solid medium: 2% (w/v) glucose, 1.5% (w/v) agar) supplemented with the appropriate amino acids (Guthrie & Fink, 1991). SC medium contained either 2% raffinose / 2% glucose for growth without αSyn induction or 2% galactose for induction of the *GAL1* αSyn promoter as a carbon source. αSyn expression was induced for 6 hours by transferring overnight cultures from medium containing 2% raffinose to medium containing 2% galactose at an OD_{600} of 0.1 or 0.3. Alternatively, strains from yTHC collection were grown in galactose containing medium overnight in presence of 10 µg/ml doxycycline for downregulation of *Tet*-promoter. To control cell growth, optical density was measured at 600 nm with a T80 UV/VIS spectrometer (PG Instruments Ltd).

2.2.1.3. Cell storage

To ensure long-term storage, *Escherichia coli* and *Saccharomyces cerevisiae* strains were preserved at -80°C in 1.8 ml CryoPure tubes (Sarstedt AG & Co). To prevent freezing related damage, *Escherichia coli* and *Saccharomyces cerevisiae* cells were mixed with 50% (v/v) and 15% (v/v) glycerol (Carl Roth GmbH & CO. KG) respectively.

2.2.1.4. Generation of tFT-library, expressing αSyn or S129A encoding genes

The tFT library is a collection of 4044 yeast strains each expressing a different tFT-tagged protein (Khmelinskii & Knop, 2014). Strains harboring two genomically integrated copies of *GAL1*-driven $SNCA^{WT}$ or $SNCA^{S129A}$ gene or empty vector (EV) control (query strains) were mated with the tFT library in a 1536-colony format, with four technical replicates that were arranged next to each other on the agar plates. Synthetic genetic assay (SGA) procedure (Tong & Boone, 2007) was used, and each query strain was crossed to an array of tFT clones in a high-throughput scale using robotic manipulation with a RoToR HDA pinning robot (Singer instruments, UK). Through several replica-pinning steps on appropriate selective media, haploid progenies of the desired genotype were obtained that simultaneously carry a tFT-tagged protein and the query allele as described previously (Baryshnikova *et al*, 2010),

followed by seamless marker excision (Khmelinskii *et al*, 2011). The generation of the query strains and SGA procedure is described in detail elsewhere (Niederleithinger, 2018).

Yeast cells were pinned on galactose-containing plates in order to induce *GAL1*-driven αSyn expression and the plates were grown for 24 hours at 30°C. High-throughput fluorescence intensity measurement were conducted using a stacker for automated plate delivery to Infinite M1000 Pro plate reader (Tecan) in a custom temperature control chamber. Intensities were recorded in the mCherry and in the sfGFP channel. All plates were imaged using a PhenoBooth Colony Counter (Singer).

The data set obtained in the high-throughput fluorescence intensity measurement was processed by the group of Prof. Knop. Colony segmentation was performed from plate images in order to determine the location of empty spots and colonies with atypical growth. Quality control was performed that removes plates with a high standard deviation of GFP signal. A total of 2980 tFT-strains successfully passed the quality control and filtering after data acquisition. Recorded fluorescence intensities were background corrected by subtracting the median of the local autofluorescence of EV controls on linear scale. Fluorescence intensity measurements were log-transformed. Screen normalization for spatial effects was performed to correct GFP and mCherry signals as a function of position. Standard deviations were regressed against the absolute fluorescence intensities.

2.2.1.5. Evaluation of the tFT-screen

The normalized and corrected intensities were used to calculate mCherry/sfGFP ratio for each single strain (R=log2(mCherry/GFP)). Changes in the protein stability were estimated by calculating the differences (RatioDiff - delta-score) between fluorescence measurements for each control strain (ORF-tFT with EV) and the corresponding strain, expressing αSyn or S129A ($RatioDiff_{(EV-\alpha Syn)}=log2(R_{EV})-log2(R_{\alpha Syn})$). Negative delta-scores values indicate stabilization of the tFT-fusion protein upon αSyn expression, while positive values show destabilization of the tFT-fusion protein compared to the EV control. *P*-values were calculated using a moderated t-test and adjusted using the

Benjamini-Hochberg method controlling the false discovery rate. Significant differences in protein stability were considered when $p \leq 0,01$.

The GFP-signal intensity which is a measure for protein abundance was compared to the median of the background (bg) GFP intensity, and the fusion proteins were divided into three expression groups depending on the ratio Rb = GFP/bg: (i) low expression level (Rb = 1 to 3); (ii) middle expression level (Rb = 3 to 10); (iii) high expression level (Rb = 10 to 350). Following criteria were applied for selection of hits with significantly changed protein stability: p<0.01; cut-off delta-score: low expression level: -2,3; middle expression level: -1; high expression level: -0,5 (Table S1 to Table S3).

2.2.2. Nucleic acid methods

2.2.2.1. Purification of DNA

Purification of linear DNA fragments was performed with QIAquick Gel Extraction Kit (QIAGEN) according to instructions of the manufacturer. Silica membrane in QIAquick kits binds DNA in a high-salt buffer and allows DNA elution with water. The purification procedure eliminates primers, nucleotides, enzymes, agarose, ethidium bromide, salts, mineral oil and other contaminants from DNA samples. For elution of DNA from the columns, 30 µl of dH_2O was used. The concentration of the purified DNA was measured using a NanoDrop ND-1000 spectrophotometer (Peqlab Biotechnologie GmbH). Purified DNA was kept at -20°C or used directly for follow-up procedures.

2.2.2.2. Isolation of plasmid DNA from *Escherichia coli*

Escherichia coli cells harboring a plasmid with the gene of interest were cultured in 5 ml of LB medium supplemented with 100 µg/ml ampicillin at 37°C overnight**.** Cells were harvested by centrifugation at 13000 rpm for 1 minute in a bench-top centrifuge (Biofuge pico, Heraeus) and plasmid DNA was extracted from the cells using the QIAprep Spin Miniprep Kit (QIAGEN) according to the instructions of the manufacturer. DNA was eluted from the columns using 30 µl dH_2O. Following the purification, DNA concentration was measured using a NanoDrop ND-1000 spectrophotometer (Peqlab Biotechnologie GmbH). Purified plasmid DNA was kept at -20°C or used for follow-up procedures.

2.2.2.3. Isolation of genomic DNA from *Saccharomyces cerevisiae*

Yeast genomic DNA isolation was carried out according to standard procedure (Hoffman & Winston, 1987). *Saccharomyces cerevisiae* cells were cultured in 10 ml of YEPD medium at 30°C overnight. After the cells were collected by centrifugation at 3000 rpm for 3 minutes, the cell pellet was rinsed in 1 ml of TE buffer (10 mM Tris-HCl [pH 8.0], 1 mM EDTA [pH 8.0]). Then, 200 µl of smash buffer (2% (v/v) triton X-100, 1% (w/v) SDS, 100 mM NaCl, 10 mM Tris-HCl [pH 8.0], 1 mM EDTA [pH 8.0]) was added to the cell precipitates along with 200 µl of phenol:chloroform:isoamyl alcohol (25:24:1) and 0.25-0.5 mm glass beads. Cells were disrupted by mechanical stirring at 4°C for 10 minutes with a vortex mixer (Vortex-Genie 2, Scientific Industries Inc) and centrifuged at 13000 rpm at 4°C for 5 minutes. The supernatant was collected and mixed with 1 ml of cold ethanol (96%) to precipitate the DNA. After brief centrifugation, precipitates were then incubated in 400 µl TE buffer and 3 µl RNase (10 mg/ml, Roche) at 37°C for 1 hour. Subsequently, 1 ml of cold ethanol (96% (v/v)) and and 10 µl of 4 M ammonium acetate solution were applied and mixed. This was followed by centrifugation at 13000 rpm for 5 minutes and disposal of the supernatant. Then the cell pellet was incubated at room temperature for 5 minutes to allow the residual ethanol to evaporate. Lastly, the DNA pellet was dissolved in 50 µl of TE buffer and its concentration was determined using a NanoDrop photospectrometer (Peglab Biotechnologie GmbH). Genomic DNA samples were stored at -20°C and subjected agarose gel electrophoresis and PCR for its verification.

2.2.2.4. DNA agarose gel electrophoresis

Analytical and preparative DNA fragment separation was performed by agarose gel electrophoresis. In this procedure, DNA fragments run through the agarose gel under an electric field and are separated according to their size. Lower molecular weight nucleic acids migrate through the gel faster than larger fragments. Dye or radioactive tracers that specifically bind to DNA can be used for visualization of DNA fragments (Lee *et al*, 2012). In this study, a 1% agarose gel (1% (w/v) agarose, 0.001 mg/ml ethidium bromide) in 1x TAE buffer (40 mM Tris base, 20 mM acetic acid, 1 mM EDTA) supplemented with 0.001 mg/ml dye ethidium bromide subsequent visualization of DNA, was prepared in a Mini-Sub Cell GT chamber (Bio-Rad Laboratories GmbH).

Prior to applying DNA samples to the gel, 10x DNA loading dye was added (10% (v/v) ficoll typ 400, 0.25% (w/v) bromphenol blue, 0.25% (w/v) xylene cyanol ff, 200 mM EDTA [pH 8.0]). In addition, a size standard the GeneRuler 1 kb DNA ladder (250 to 10 000 bp, MBI Fermentas) was loaded on the gel. The separation of DNA fragments was conducted in Mini-Sub Cell GT chamber (Bio-Rad Laboratories) filled with TAE buffer using a Bio-Rad Powerpac 300 (Bio-Rad Laboratories) in a 90 V electric field. UV light at 254 nm was then applied to detect DNA and imaging was performed using a gel documentation imager (Gel iX20 Imager Windows version, Intas Science Imaging Instruments GmbH).

2.2.2.5. DNA isolation from agarose gels

To purify the DNA fragments from the DNA mix, agarose gel electrophoresis was used to separate the fragments based on their length. The desired fragment was then cut from the gel and QIAquick Gel Extraction Kit (QIAGEN) was used for the purification. The DNA fragments were eluted with 30 µl dH_2O from the column and stored at -20°C or used for further procedures.

2.2.2.6. Polymerase chain reaction (PCR)

PCR is a technique that allows *in vitro* amplification of DNA fragments with partially known sequences (Saiki *et al*, 1988). This technique allows synthesis of DNA fragments in chain reaction catalysed by a polymerase in the presence of a DNA template, a large molar excess of two oligonucleotide primers, and four deoxyribonucleoside triphosphates. For amplification of fragments from genomic or plasmid DNA templates, a high-fidelity Phusion DNA polymerase (Thermo Fisher Scientific) was used. Primers were purchased from Sigma-Aldrich (Table 4, St. Louis, USA). The annealing temperature varies depending on the melting temperature of the oligonucleotides used. Typically, the annealing temperature is 5°C lower than the melting point. Plasmid DNA or chromosomal DNA was applied as DNA template. The reaction was run in a Thermo Cycler thermal cycler (MWG Biotech Inc Primus 96 Thermal Cycler, MWG-Biotech). In Table 10 and 11, an example of the Phusion reaction mix and PCR program can be found.

Table 10. Reaction mix for *Phusion* DNA polymerase.

Component	50 µl Reaction	Final concentration
5x HF buffer	10 µl	1 x
dNTP mix	1 µl	200 µM each
Primer 1	1 µl	0.2 µM
Primer 2	1 µl	0.2 µM
Template DNA	x µl	300-500 ng
DMSO	1.5 µl	3%
Phusion DNA polymerase	0.5 µl	0.02 U/µl

Table 11. PCR program for *Phusion* DNA polymerase

Cycle step	Temperature	Time	Cycles
Initial denaturation	98°C	3 min	1
Denaturation	98°C	30 sec	30
Annealing	Tm - 5°C	30 sec	30
Elongation	72°C	30 sec/kb	30
Final extension	72°C	10 min	1
Pause	4°C	∞	1

2.2.2.7. Digestion of DNA

To digest the DNA molecules, restriction enzymes purchased from Thermo Fisher Scientific were used following the manufacturer's instructions. DNA fragments amplified with PCR and plasmid DNA were digested with the respective restriction enzymes. Restriction enzymes cleave DNA fragments at precise recognition sequences. Typically, 10 U of enzyme per 2-5 µg of DNA was used. Aliquots of 30 µl of the reaction mixture were incubated in the appropriate reaction buffer at 37°C for 2 to 4 hours. The digested DNA fragments were then purified using the QIAquick Gel extraction kit (QIAGEN).

2.2.2.8. Cloning of DNA

GeneArt® Seamless Cloning and Assembly Enzyme Mix (Invitrogen) was used for cloning of DNA inserts into vectors. In the ligation reaction, 100 ng of linearized vector DNA was mixed with 200 ng of insert DNA in 4 µl of 5x reaction buffer. The reaction mix was incubated at room temperature for 30 minutes after the total volume of 20 µl was adjusted with dH_2O, and 1 µl of 10x enzyme was added. Lastly, *Escherichia coli* DH5α strain was transformed with 10 µl of the ligation mixture and incubated on selective LB solid medium containing 100 µg/ml ampicillin at 37°C overnight. To verify that integration of the insert into the vector was successful, plasmid DNA was isolated with the QIAprep Spin Miniprep Kit (QIAGEN) and sequenced as specified in section 2.2.2.2.

2.2.2.9. Quick change site-directed mutagenesis

The quick-change site-directed mutagenesis system is used for modification of selected amino acids in proteins. Based on PCR amplification, this method allows multiple mutations, deletions and insertions to be introduced into genes *in vitro* (Wang & Malcolm, 1999). For this purpose, one pair of complementary oligonucleotide primers carrying the mutation of interest implements the mutation over the course of the PCR amplification process. They are individually designed depending on the desired mutation. Both 5´-phosphorylated mutagenic primers are supposed to have length between 25 and 45 bases and their melting point should be above or equal to 78°C. The desired mutagenic part should be located in the center of the primer and flanked on both sides by 10 to 20 bases complementary to the DNA used as a template. The thermostable high-fidelity DNA polymerase *Pfu*Turbo Cx hotstart (Agilent Technologies) was used for the amplification of target DNA. The polymerase replicates the DNA without displacing mutagenic primers. A plasmid DNA carrying the gene of interest was used as DNA template in this study. Examples of the reaction mixture for the rapid site-directed mutagenesis and PCR program are shown in Table 12 and 13.

Table 12. Reaction mix for PCR with PfuTurbo Cx hotstart DNA polymerase

Component	Reaction (50 µL)	Final concentration
10x *Pfu*Turbo Cx reaction buffer	5 µL	1 x
mutagenic primer I	1 µL	0.2 µM
mutagenic primer II	1 µL	0.2 µM
dNTP mix	1 µL	200 µM (each)
DMSO	1.5 µL	3%
plasmid DNA	x µL	300-500 ng
*Pfu*Turbo Cx hotstart DNA polymerase	1 µL	0.05 U/µL

Table 13. PCR program with PfuTurbo Cx hotstart DNA polymerase

Cycle step	Temperature	Time	Number of cycles
Denaturation	95°C	5 minutes	1
Denaturation	95°C	30 seconds	20
Annealing	60°C	1 minute	20
Elongation	68°C	60 sec/kb	20
Final extension	68°C	10 min	1
Pause	4°C	∞	1

The PCR product was then purified using the QIAquick Gel extraction kit (QIAGEN). To remove the template DNA and extract the mutation-containing synthesized DNA, 2 µl of *Dpn*I endonuclease (20 U) and 2 µl of Tango buffer (Thermo Fisher Scientific) were applied directly to 16 µl of the mutagenesis reaction and incubated at 37°C for 2 hours. This restriction enzyme digests methylated DNA specifically. Since DNA isolated from *Escherichia coli* strains is extensively methylated, the newly synthesized DNA is readily digestible by *Dpn*I. As a control for the effective eradication of the parental DNA template, an additional reaction mixture was incubated simultaneously

in the absence of the restriction enzyme *Dpn*I. Then 15 µl of the digested reaction mixture was used for transformation into *Escherichia coli* DH5α as described in section 2.2.3.1. The cells were incubated on LB plates containing 100 µg/ml ampicillin at 37°C overnight. To verify mutant genes, the plasmid DNA was then isolated using the QIAprep Spin Miniprep Kit (QIAGEN) and sequenced as described in sections 2.2.2.1 and 2.2.2.10.

In this study, the method was used for introduction of mutation in αSyn-VenusC to create αSyn phosphorylation deficient mutant at serine 129 tagged with VenusC (S129A-VC). Primers used for that purpose are listed in Table 4.

2.2.2.10. Sequencing of DNA

All DNA constructs used in this work were verified by Seqlab-Microsynth GmbH (Göttingen, Germany) with the Sanger Cycle Sequencing Method (Sanger *et al*, 1977). Each DNA sample for sequencing contained 1000 ng of plasmid DNA in a volume of 12 µl mixed with 3 µl of the corresponding sequencing primer (30 pmol). The derived sequences were analyzed with the MultAlin multiple sequence alignment tool (Corpet, 1988). The chromosomal sequences of yeast were accessed from the *Saccharomyces genome* database (SGD) website (www.yeastgenome.org) (Cherry *et al*, 2012).

2.2.3. Transformation of DNA into cells

2.2.3.1. Transformation of plasmid DNA into *Escherichia coli*

Transformation of *Escherichia coli* with plasmid DNA was performed with the heat shock method (Inoue *et al*, 1990). For the procedure, 100 µl of *Escherichia coli* DH5α competent cells were thawed on ice for 15 minutes and 0.5 µg of plasmid DNA or 10 µl of ligation reaction, and the mixture was incubated for 10 minutes on ice. The cells were then heated at 42°C for 90 seconds and kept on ice for 5 minutes to facilitate the entry of DNA into cells. After the cells were transformed, they were supplemented with 1 ml of LB medium and cultivated at 37°C for 45 minutes for recovery. Lastly, 100 µl of the cell suspension was applied on LB plates with appropriate antibiotics for a selection of transformants carrying the desired DNA plasmid. To obtain an adequate transformation efficiency, the remaining cell suspension was centrifuged at 13000 rpm in a benchtop centrifuge (Biofuge pico, Heraeus) for one minute and then most of the

supernatant was discarded, with about 100 µl remaining. The cell pellet was resuspended in the remaining supernatant and distributed on another LB plate. The LB plates were incubated at 37°C overnight. The grown *Escherichia coli* colonies were analyzed with PCR and sequencing as described in sections 2.2.2.6 and 2.2.2.10.

2.2.3.2. Transformation of plasmid DNA into *Saccharomyces cerevisiae*

Plasmid DNA was transformed into *Saccharomyces cerevisiae* cells using the LiAc/SS Carrier DNA/PEG method (Ito *et al*, 1983). This technique involves yeast cells treated with alkaline cations that take up plasmid DNA after a heat pulse in the presence of polyethylene glycol. Prior the transformation, yeast cells were grown overnight in 10 ml YEPD medium and 800 µl of overnight culture was further grown in 10 ml of YEPD medium at 30°C on a rotation shaker (Fröbel Labortechnik GmbH) for 4 hours. The total cell culture was then harvested by centrifugation at 3000 rpm for 3 minutes 4°C using a 5804R centrifuge (Eppendorf AG). The cell pellet was washed three times with 10 ml of LiOAc/TE buffer (100 mM LiOAc, 1 mM Tris-HCL [pH 8.0], 0.1 mM EDTA [pH 8.0]) and resuspended in 400 µl of LiOAc/TE buffer. The yeast cells were competent for transformation by this point. 20 µl of preheated to 65°C for 20 minutes SS carrier DNA (single stranded salmon sperm DNA) was mixed with 200 µl of resuspended cells, 15 µg (integrative) or 1,5 µg (non-integrative) plasmid DNA and 800 µl of 50% polyethylene glycol 4000 (PEG 4000, Carl Roth GmbH & CO. KG) dissolved in LiOAc/TE buffer. For each transformation, a control without plasmid DNA was generated. The mixture was then incubated at 30°C for 30 minutes and exposed to a heat shock for 25 minutes at 42°C. Subsequently, the DNA samples were centrifuged at 8000 rpm for 1 minute, the supernatant was discarded, and the cell pellet was supplemented with 1 ml of YEPD medium and incubated for 2 hours (integrative transformation) or 1 hour (non-integrative transformation) at 30°C for recovery. Then, the medium was removed after 1 minute of centrifugation at 4000 rpm, leaving 150 µl of supernatant to resuspend the pellet, allowing it to be distributed on a SC solid medium lacking the appropriate amino acid for the selection of colonies carrying the plasmid with corresponding auxotrophic marker. The plates were incubated for two to three days at 30°C and individual yeast colonies were streaked on a new solid SC medium to select colonies carrying the desired plasmid. Plates were incubated for two

to three days at 30°C, and individual yeast colonies were streaked onto new solid SC medium to select colonies harboring the required plasmid.

2.2.4. Protein methods

2.2.4.1. Yeast crude extracts preparation

Prior the protein extraction, strains to be analyzed were cultured in 10 ml of SC medium containing selective amino acids and 2% raffinose at 30°C overnight. For F promoter induction, the cell pellet from the overnight culture was collected by centrifugation at 3000 rpm for 3 minutes and resuspended in 10 ml of SC selective medium containing 2% galactose and the cells were grown with rotation at 30°C for 6 hours. The samples were then kept on ice for 10 minutes and centrifuged at 3000 rpm for one minute at 4°C. The cell pellet was then rinsed with 1 ml of TE buffer (10 mM Tris-HCl [pH 8.0], 1 mM EDTA [pH 8.0]) and dissolved in 200 µl of R buffer (50 mM Tris-HCl [pH 7.5], 1 mM EDTA [pH 8. 0], 50 mM DTT, 6 µl/ml protease inhibitor [1 tablet cocktail in 1 ml dH_2O], 100 µl/ml phosphatase inhibitor [1 tablet cocktail in 1 ml dH_2O]). Moreover, an equal amount of glass beads with a diameter of 0.25-0.5 mm was added to each mixture. To break the cells, the samples were vigorously shaken at 4°C using a vortex mixer (Vortex-Genie 2, Scientific Industries Inc) for 10 minutes. The suspension was then centrifuged at 13000 rpm for 15 minutes at 4°C, and the crude cell extract was recovered by collecting the supernatant. Once protein concentration was determined by the Bradford method (Bradford, 1976), protein samples were resuspended in 6x sample buffer (250 mM Tris-HCl [pH 6.8], 15% (v/v) β-mercaptoethanol, 7% (w/v) SDS, 30% (v/v) glycerol, 0.3% (w/v) bromophenol blue) and boiled at 95°C for 10 minutes.

Alternatively, denatured yeast protein extraction was performed by NaOH lysis/TCA precipitation. Yeast cells were cultured in a SC selective medium containing raffinose at 30°C overnight. The yeast cells were then harvested and transferred to SC selective medium containing 2% galactose for induction of αSyn expression to final $OD_{600} = 3$ and grown for 6 hours. After the incubation, OD was measured again and the amount of the yeast cells, corresponding to $OD_{600} = 3$ was harvested by centrifugation at 4000 rpm for 3 minutes at 4°C. The cell pellet was then resuspended in 1 ml of ice-cold water and 150 µl NAOH/BME (138.75 µl 1.85M NaOH, 7.5% (11.25 µl) BME (2-mercaptoethanol) was added. The cells were kept on ice for 15 minutes and mixed

occasionally. Afterwards 150 µl 55% TCA (55% (w/v) trichloroacetic acid in H_2O) was added and the cells were incubated on ice for 10 minutes. Following centrifugation at 20000 rpm for 15 minutes at 4°C, the supernatant was removed and the cell pellet was resuspended in 100 µl HU buffer (200 mM Tris buffer, pH 6.8, 8 M urea, 5% w/v SDS, 1 mM EDTA, 100mM DTT (or 1.5% DTT powder) added freshly). Finally, the samples were denatured at 65°C for 10 minutes.

Isolated protein extracts were analyzed by loading on a SDS-polyacrylamide gel and separation by electrophoresis as described in section 2.2.4.5.

2.2.4.2. Cycloheximide chase experiment

Cycloheximide chase assays are performed to determine the degradation rate and protein turnover kinetics over a defined period of time, dependant on a protein half-life. The addition of cycloheximide inhibits ribosomal translocation and thus translation in the cell is arrested (Buchanan *et al*, 2016). Strains used for the procedure were first incubated overnight in a selective SC medium containing 2% raffinose and then switched to galactose containing SC selective medium for 6-hour expression of αSyn. Cells were then treated with 50 µg/ml cycloheximide and samples were collected at indicated time points after addition of cycloheximide. Afterwards, samples were subjected to protein extraction and western blot analysis.

2.2.4.3. Determination of protein concentration

To determine protein concentrations in protein extraction samples, the Bradford protein concentration assay was used, in which an absorption shift from maximum of 465 nm to 595 nm is monitored (Bradford, 1976). For measurement preparation, 0 µl, 1 µl, 4 µl, 10 µl, 15 µl, and 20 µl of bovine serum albumin (BSA, Albumin Fraktion V, Carl Roth GmbH & CO KG) were mixed with 200 µl of 1:5 diluted Bradford reagent (Roti®-Quant, Carl Roth GmbH & CO. KG) to generate a standard curve. 2 µl of protein extracts were mixed with the same amount of diluted Bradford dye and both BSA and protein extracts were applied on a 96-well microtest plate which was then inserted into an Infinite M200 microplate reader (TECAN Group Ltd.) to measure extinction at 595 nm. All samples were prepared in triplicates.

2.2.4.4. Trichloroacetic acid protein precipitation

Treatment with 2,2,2-trichloroacetic acid (TCA) is commonly used to precipitate soluble proteins from aqueous solution. TCA induces protein precipitation by promoting hydrophobic aggregation (Sivaraman *et al*, 1997). For the protein precipitation, 100% TCA solution (500 g TCA in 350 ml dH_2O) was applied to the protein sample at a ratio of 1:4 and incubated at 4°C for 10 minutes. The mixture was then centrifugated at 13000 rpm for 5 minutes at 4°C, the supernatant was removed, and the protein pellet was rinsed with ice-cold acetone. The protein precipitate was then centrifuged at 13000 rpm for 5 minutes at 4°C and washing with acetone was repeated. The precipitate was dried at 95°C for 5 minutes and dissolved in 3x sample buffer. After the protein precipitates were boiled at 95°C for 10 minutes, the samples were stored at -80°C or used for follow-up procedures.

2.2.4.5. SDS-polyacrylamide gel electrophoresis

SDS polyacrylamide gel electrophoresis (SDS-PAGE) is an electrophoretic method that separates proteins according to their molecular weight by denaturing the proteins and consequently coating them with a negative charge (Laemmli, 1970). Protein charge as well as three-dimensional folds are imposed by of SDS. For this reason, proteins are separated on the basis of mass rather than charge. The SDS vertical gel used to separate proteins consists of a stacking gel and a separating gel. The stacking gel contains 5% polyacrylamide and enables proteins to migrate rapidly until they reach the separation gel containing 12% polyacrylamide. These concentrations of polyacrylamide are suitable for the separation of medium sized proteins. In order to prepare the SDS-PAGE gel, the separating gel (2.5 ml of 1.5 M Tris-HCl / 0.4% (w/v) SDS [pH 8.8], 3.5 ml of dH_2O, 4 ml of acrylamide solution [30% acrylamide, 0.8% bisacrylamide], 30 µl of APS [10% (w/v)], 15 µl of TEMED) was first poured and covered with isopropanol. The isopropanol was removed after complete polymerization of the separation gel and the stacking gel (1.5 ml 500 mM Tris-HCl / 0.4% (w/v) SDS [pH 6.8], 3.9 ml dH_2O, 0.6 ml acrylamide solution [30% acrylamide, 0.8% bisacrylamide], 40 µl APS [10% (w/v)], 20 µl TEMED) was poured over the separation gel. Depending on the volume and number of samples, a 1 mm or 1.5 mm 10-well comb or 15-well comb was placed into the stacking gel. Protein samples were mixed with 6x sample buffer and denatured at 95°C for 10 minutes before loading onto the

gel. Electrophoresis was conducted in running buffer (25 mM Tris base, 250 mM glycine, 0.1% (w/v) SDS) using a Mini-PROTEAN® 3 Cell and a Bio-Rad Powerpac 300 (Bio-Rad Laboratories) at 100 V until the samples reached the end of stacking gel. The electrical current was then increased to 200 V and electrophoresis was conducted until the blue band of 6x sample buffer flowed out of the gel. To monitor protein separation, PageRuler Prestained Protein Ladder (10 to 180 kDa, Thermo Fisher Scientific) was applied.

2.2.4.6. Protein immunoblotting

The protein immunoblotting technique is applied for the identification of particular proteins in a protein mixture by specific antigen recognition provided by antibodies on a carrier membrane. Proteins separated in the SDS-PAGE gel were electrophoretically transferred on a nitrocellulose (Amersham™ Protran™ 0.45 µm NC, GE Healthcare) for immunoblotting (Towbin *et al*, 1979). Transfer was carried out in transfer buffer (25 mM Tris base, 192 mM glycine, 0.02% (w/v) SDS) containing 20% methanol with a Mini Trans-Blot® electrophoresis cell (Bio-Rad Laboratories). The proteins have a strong negative charge due to prior treatment with SDS. When 100 V electric current is applied to the blotting device for 1,5 hours, the proteins migrate to the anode, allowing them to be transferred to the membrane. Transfer control was performed with Ponceau S agent immediately after transfer was completed (Gallagher *et al*, 1998). Ponceau S agent was then washed from the membrane, which was subsequently blocked with 5% milk powder in TBST buffer (10 mM Tris-HCl [pH 8.0], 150 mM NaCl, 0.05% (v/v) tween-20) for 1 hour. Proteins from the milk block free binding sites on the membrane which prevents direct binding of an antibody to the membrane. The primary antibody, diluted in TBST buffer with 5% milk powder, was then applied on the membrane and incubated with the membrane overnight at 4°C. After the primary antibody was removed, the membrane was washed with TBST buffer three times for 10 minutes. Subsequently, a secondary antibody diluted in TBST buffer with 5% (w/v) milk powder was applied on the membrane and incubated for 1 hour. Secondary antibodies bind specifically to the primary antibody and are conjugated to horseradish peroxidase. The primary and secondary antibodies that were used in this study are listed in Tables 8 and 9. The unbound antibody was removed by washing the membrane as described above and the proteins were detected by Enhanced

Chemiluminescence (ECL) technique. ECL solution (1 ml 1 M Tris [pH 8.5], 9 ml dH_2O, 45 µl paracoumaric acid [400 mM in DMSO], 100 µl luminol [250 mM in DMSO], 1 ml 1 M Tris [pH 8.5], 9 ml dH_2O, 6.2 µl H_2O_2) was applied on the membrane immediately after preparation and incubated for 2 minutes. This initiated the enzymatic reaction of horseradish peroxidase. This enzyme catalyzes the electron transfer from H_2O_2 to the luminol substrate, which then converts into a light-releasing substrate. Subsequently, the membrane was placed in foil and exposed in the dark on an Amersham™ HyperfilmTM-ECL (GE Healthcare) at intervals of several seconds and several minutes, leading to the imaging of chemiluminescence signals on the film. The detected bands were quantified using image processing software ImageJ (Wayne Rasband, National Institutes of Health). Prior using the membrane for incubation with another antibody, the ECL solution was removed my washing with TBST buffer and the antibodies were removed by incubation of the membrane in 10 ml of stripping solution (50 mM Tris-HCl [pH 7.0], 2% (w/v) SDS, 50 mM DTT) at 60°C for 30 minutes. The membrane was then washed again with TBST buffer, and free binding sites on the membrane were blocked by incubating the membrane in TBST buffer containing 5% (w/v) milk powder for at least 1 hour.

2.2.4.7. Glycerol gradient analysis

Prior to the experiments, yeast cell lysis with glass beads was performed (see section 2.2.4.1.). The cells were lysed in R-buffer (50 mM Tris-HCl [pH 7.5], 1 mM EDTA [pH 8.0], 5 mM DTT) containing 2 mM ATP (Enzo Life Science, Inc.) and 5 mM $MgCl_2$ for preservation of the 26S proteasome complexes. The cells extracts (2 mg) were separated into 20 x 500 ml fractions by centrifugation at 24500 rpm for 22 hours at 4°C (Sorvall™ WX80 Ultracentrifuge with TH-641 rotor; Thermo Fisher Scientific) in 8-32% (v/v) glycerol linear gradient in 25 mM Tris-HCl buffer (pH 7,5) containing 1 mM DTT, 2 mM ATP and 5 mM $MgCl_2$ using Foxy Jr. Fraction Collector, Optical Unit Type 11, Absorbance Detector UA-6, TRIS™ Pump (Teledyne Isco) and Gradient Master 108 (BioComp Instruments). The fractionation was visualized with Peak Track 1 (Teledyne Isco) software. After fractionation, 50 µl of the individual fractions were used for assay of Suc-LLVY-AMC hydrolysis (see section 2.2.4.8).

2.2.4.8. Proteasomal Activity Assay

Peptidase activity was measured using a fluorescent peptide substrate Suc-LLVY-AMC (Enzo Life Science, Inc.) at a final concentration of 100µM. A low concentration of SDS (0,025%) was used as an artificial activator of 20S proteasomes that are usually latent in cells. The degradation of fluorogenic peptide was measured by continuously monitoring the fluorescence of the reaction product, free 7-amino-4-methylcoumarin (AMC). The assay was performed in a protein extraction buffer supplemented with 2 mM ATP (Enzo Life Science, Inc.). The rate of fluorescence increase was measured using a TECAN Infinite 200 microplate reader (Tecan Group Ltd., Männedorf, Switzerland) at 37°C for 30 minutes by the fluorescence excitation at the wavelength 350 nm and the emission at the wavelength 440 nm. The values were expressed in arbitrary units.

2.2.5. Phenotypical characterization

2.2.5.1. Spotting assay

Spotting assays were performed to analyze growth of yeast strains on a solid medium. Cells were cultured in selective SC medium with 2% raffinose at 30°C overnight. After cells were normalized to equal density (OD_{600} equal to 0.1), a series of 10-fold dilutions (10^{-1}, 10^{-2}, 10^{-3}, 10^{-4}) were prepared and spotted in a volume of 10 µl onto selective SC agar plates supplemented with 2% glucose or 2% galactose. Growth of strains derived from the yTHC collection was additionally observed in the presence of doxycycline (10 µg/ml). The growth rate intensity was documented after 2-3 days of incubation at 30°C.

2.2.5.2. Fluorescence microscopy

To perform fluorescence microscopy, cells were pre-cultured in selective SC medium containing 2% raffinose at 30°C overnight and inoculated into SC medium containing 2% galactose to an OD_{600} of 0.1 and grown for another 5 hours. 200 µl of cells were then subjected to fluorescence microscopy. Fluorescence images were acquired using a Zeiss Axio Observer microscope at 63x magnification. Z1 (Zeiss) equipped with a CSU-X1 A1 confocal scanner unit (Yokogawa), a QuantEM:512SC digital camera (Photometrics), and the SlideBook 6.0 software package (Intelligent Imaging

Innovations GmbH) were used. The filter used was s488G, s561R or 405qUV, depending on the fluorescence agent. For quantification of αSyn aggregation, at least 300 cells were counted for each strain, and the number of cells showing αSyn aggregation was referred to the total number of cells counted.

Cell staining with calcofluor white was performed to visualize chitin within the cells of *Tet-RPN11* strain. One drop of white Calcofluor White Stain (Sigma-Aldrich) and one drop of 10% potassium were added to the cells. The mixture was incubated for 1 minute and visualized with microscopy.

Hoechst-staining (Thermo Fisher Scientific) was performed to visualize DNA within *Tet-RPN11* cells. The cells were fixed for 1 hour at 23°C with 37% formaldehyde to a ratio of 1:10. Afterwards, they were centrifuged at 2000 rpm for 2 minutes and washed 2 times with H_2O. The cells were resuspended in 200 µl H_2O and visualized with microscopy.

Time-lapse fluorescence microscopy was performed with a CellASIC® ONIX 2 microfluidic device (Merck, NJ, USA). The cells were precultured in SC selective medium with raffinose, diluted to an OD_{600} of 0.1 in a total volume of 1 ml and loaded into a Y04C-02 microfluidic yeast plate (Merck, NJ, USA). The plate comprised four culture chambers for three-dimensionally trapping yeast cells. This allowed simultaneous observation of individual cells from different strains over time. The system was operated by the connected CellASIC® ONIX2 software (Merck). Default cell loading sequences applying a pressure of 55.1 kPa for 5 seconds were run until sufficient number of cells were observed within the culture chambers. Images were acquired every hour at preset XY-positions using autofocusing with the Differential Interference Contrast (DIC) channel.

2.2.5.3. Flow cytometry

Yeast cells were pre-cultured in selective SC medium containing 2% raffinose at 30°C until mid-logarithmic phase was reached. Expression of αSyn in tFT-strains was induced for 6 hours in SC medium supplemented with 2% galactose. Prior to flow cytometry measurement, cells were rinsed and resuspended in 50 mM trisodium citrate buffer, pH 7.0. Flow cytometry was performed with a BD FACSCANTO II instrument (Becton Dickinson, Franklin Lakes, NJ, USA). A total of 10000 events were counted in

each experiment. Data was analyzed with BD FACSDIVA software (Becton Dickinson, Franklin Lakes, NJ, USA).

2.2.5.4. Growth analysis in liquid culture

For growth studies in liquid cultures, cells were pre-cultured in selective SC medium containing 2% raffinose at 30°C overnight. Subsequently, the overnight cultures were shift to SC medium containing 2% galactose at the final OD_{600} density of 0.1 for induction of αSyn expression. Measurements of optical density for 200 µl cell cultures were performed in triplicate in 96-well plates for 48 hours using a microplate reader (Infinite® M200, Tecan Group).

2.2.5.5. Whole colony measurement

For whole colony measurement, cells were inoculated in a SC selective medium containing 2% raffinose in a 96-well plate at 30°C overnight. The next day, the cells were pinned on a solid SC selective medium containing 2% galactose plate with and without doxycycline. The cells were further grown at 30°C. The measurement was performed with the Tecan reader "Infinite M200" with wavelengths of sfGFP and mCherry after 48 hours.

2.2.5.6. Promoter shut-off assay

Promoter shut-off analysis was performed to examine the capacity of yeast cells for degradation of αSyn. Yeast cells were pre-cultured in selective SC medium containing 2% raffinose overnight and transferred to selective SC medium containing 2% galactose to induce αSyn expression for 4 hours. The cells were then transferred to selective SC medium containing 2% glucose for the promoter shut-off. The cells were visualized by fluorescence microscopy 4 hours after the promoter was shut-off and a reduction in the number of cells with αSyn inclusions was registered. To impair the proteasomal degradation system, carbobenzoxyl-leucine-leucine (MG132, Selleck Chemicals) dissolved in dimethylsulfoxide (DMSO) at a final concentration of 75 µM was added to the cell suspension. Equal volume of DMSO was administered to the cells in parallel as a control. When MG132 drug was used, galactose-containing

induction medium and glucose-containing shut-off medium were supplemented with 0.003% (w/v) SDS and 0.1% (w/v) proline (Liu *et al*, 2007).

2.2.6. Statistical analysis

All data were analyzed with GraphPad Prism 6 software (San Diego, USA) and presented as means ± SEM from at least three independent experiments. The significance of differences was calculated using Student's *t*-test or one-way ANOVA with Bonferroni's multiple comparisons test. It was considered that a p value < 0.05 indicated a significant difference.

3. Results

3.1. Tandem fluorescent protein timer monitoring reveals that expression of p129 α-synuclein has greater impact on protein stabilization in yeast than its non-phosphorylated variant S129A

Misfolding and aggregation of αSyn disturb cellular proteostasis. The exact molecular mechanisms of these processes are an important current subject of research. Increased amounts of toxic or aggregated αSyn species overload the cellular proteostasis network. These effects depend not only on the levels of αSyn, but also on the impact of αSyn proteins on other constituents of the proteostasis network. Increased αSyn decreases the abundance of 26S proteasomes and alters the levels of ubiquitin conjugates (Popova *et al*, 2021a). This raises the question whether the αSyn-mediated alteration of proteostasis is a consequence of altered protein stability. Consequently, it brings into question, which proteins are altered in their stabilities by αSyn. In addition, the molecular functions of αSyn PTMs in this process have to be addressed with a specific focus to the residue S129, which is essential for αSyn turnover.

A novel type of tandem fluorescent protein timer (tFT) was applied to answer these questions. This timer served as a measure for protein age and stability upon expression αSyn and its phosphorylation deficient variant, S129A.

3.1.1. Tandem fluorescent protein timers enable *in vivo* analysis of protein dynamics

Tandem fluorescence protein timer (tFT) fusion genes were constructed and employed as a tool to monitor stabilities of marked cellular yeast proteins upon expression of either αSyn or its phosphorylation-deficient S129A variant. tFT is a tandem fusion of mCherry and superfolder green fluorescence protein (sfGFP). These two fluorescent proteins possess distinct kinetics of fluorophore maturation. This results in different quantitative read-outs corresponding to the age, abundance and localization of different proteins, which is reflected by traffic-light like color changes from green to

yellow to red over time (Khmelinskii *et al*, 2012) (Figure 5). The fluorophore of sfGFP matures rapidly and becomes green-fluorescent shortly after protein translation is completed (Figure 5A). In contrast, the fluorophore of mCherry matures slowly and the protein takes much longer than sfGFP to become red-fluorescent. The fluorescence intensities of the two proteins can be monitored and quantified independently of each other *in vivo*. The difference in mCherry fluorescence compared to sfGFP fluorescence intensity allows to measure differences in steady-state yeast protein stability: a decrease of the intensity ratio indicates an increase of the degradation rate of the tFT-fusion protein, and *vice versa*.

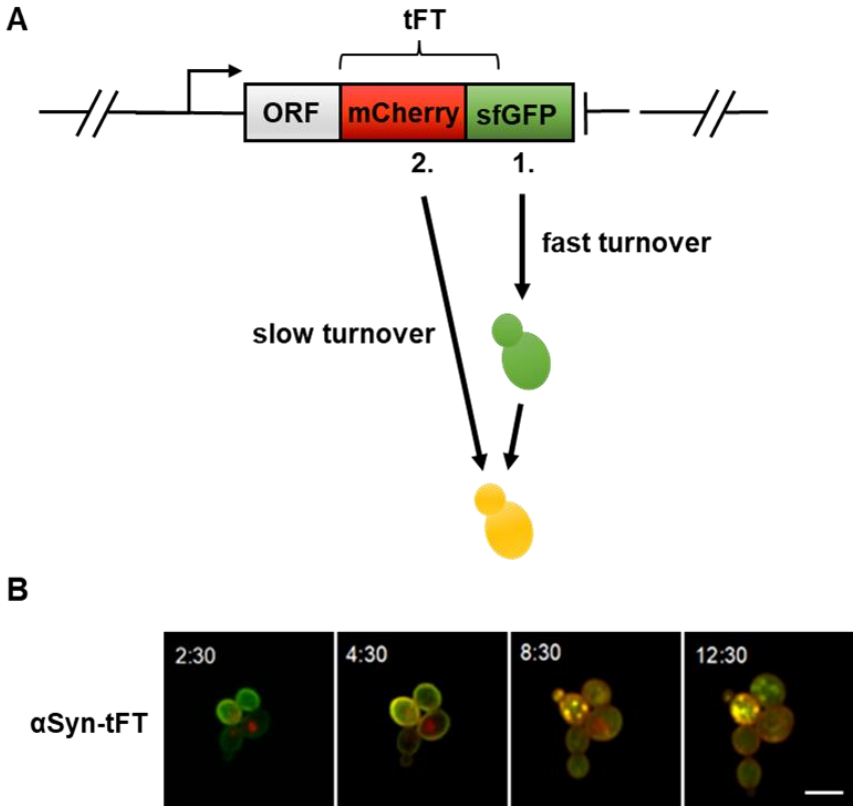

Figure 5. Tandem fluorescence timer labeled proteins report on their turnover kinetics.
(A) Schematic diagram depicting a C-terminally tFT-tagged ORF and maturation steps of tFT. The tFT is composed of a faster-maturing green sfGFP (1) and slower-maturing red fluorophore mCherry (2). The ratio of both fluorescence intensities reports on the stability of the tagged protein. Maturation of both fluorophores leads to yellow fluorescence signal. (B) Fluorescence microscopy time series of yeast cells expressing single copy αSyn-tFT. The cells were trapped in a microfluidic device and the merge images show cells at the indicated time points after *GAL1* promoter-mediated induction of αSyn-tFT expression. Scale bar = 5 µm.

Fluorescence microscopy can be used to visualize the age-dependent subcellular localization and maturation of tFT-fused protein, as exemplified in Figure 5B. Cells, expressing αSyn-tFT were trapped in a microfluidic device and the maturation of the fluorescent timer was followed within single cells with time. The pool of mCherry-sfGFP molecules was mostly green-fluorescent shortly after protein induction and gradually acquired yellow as intermediate color to finally reach red fluorescence over time. This corroborates that the ratio of red to green fluorescence is a function of the age of the corresponding yeast protein pool.

3.1.2. High-throughput screening for proteins with changed turnover upon α-synuclein expression

A high-throughput assay based on tFTs was performed to characterize the impact of αSyn expression on protein dynamics in yeast. The aim was to identify cellular pathways and candidate proteins whose stability is affected by the heterologous expression of αSyn. This was realized by conducting a high-throughput screening using a yeast library based on C-terminal tagging of proteins with this tandem fluorescent protein timer (tFT-library) and simultaneously expressing αSyn. Furthermore, the role of phosphorylation at S129 as the major PTM of αSyn and its contribution to the disturbance of protein homeostasis was investigated by performing a second screening for comparison with the phosphorylation deficient S129A variant.

The employed yeast library consisted of 4044 strains, where each strain harbors a distinct tFT-tagged open reading frame (Khmelinskii *et al*, 2014). Query strains either conditionally expressing the αSyn-encoding gene or the S129A variant, as well as the empty vector as control were generated in the *yMaM1234* background. The query strains harbored two copies of αSyn or S129A encoding genes driven by a regulatable *GAL1* promoter, as expression from two gene copies is under the toxicity threshold, which enables similar growth and allowed to perform the screen under equal conditions. A spotting test of the query strains under inducing (galactose; “αSyn-*ON*”) and non-inducing (glucose; “αSyn-*OFF*”) conditions verified as control that expression of two copies of the genes did not affect yeast growth (Figure 6A). Immunoblotting with crude protein extracts from the two strains confirmed equal protein levels of αSyn and S129A within the corresponding yeasts (Figure 6B).

Each of the three query strains was crossed with the yeast tFT-library. Synthetic genetic array methodology (SGA) was used for generation of haploid double mutant strains (Tong & Boone, 2006). The SGA is an automated procedure, where an ordered array of yeast mutant strains is mated to a query strain using robotic pinning, followed by a series of replica-pinning procedures for selection of haploid double mutant strains. This resulted in generation of yeast strains, simultaneously expressing a single tFT-ORF either with αSyn, S129A or empty vector. Finally, the cells were combined in 1536-colony format with four technical replicates of each clone and pinned on selection plates containing 2% galactose in order to induce *GAL1*-driven αSyn expression.

The plates were grown for 20 hours and 44 hours respectively at 30°C. Fluorescence intensities of mCherry and sfGFP signals of all colonies were measured after the two time points using an Infinite M1000 Pro microplate reader (Tecan). Colony segmentation was performed from previously taken plate images in order to determine the location of empty spots and colonies with atypical growth that were excluded from further evaluation. Subsequently, SGA quality check was conducted using control non-fluorescent strains. A total of 2620 tFT-strains passed the stringent quality control and were further quantified.

The ratios of mCherry/sfGFP fluorescence intensities of αSyn or S129A expressing strains were calculated and compared to the control. A total of 377 unique proteins were identified with significantly changed stability upon αSyn or S129A expression compared to the control strain (Table S1 to Table S3). Among them, there was an overlap of 49 proteins, which were affected in stability by both αSyn as well as the S129A variant. 318 of a total of 367 proteins had specifically changed stability upon αSyn expression. A total of 59 proteins was changed by expression of S129A, including ten proteins, which were exclusively affected by S129A (Figure 6C). These data reveal that the impact of αSyn (with intact S129 phosphorylation site) on the changes of protein stability is by far more significant than that of S129A.

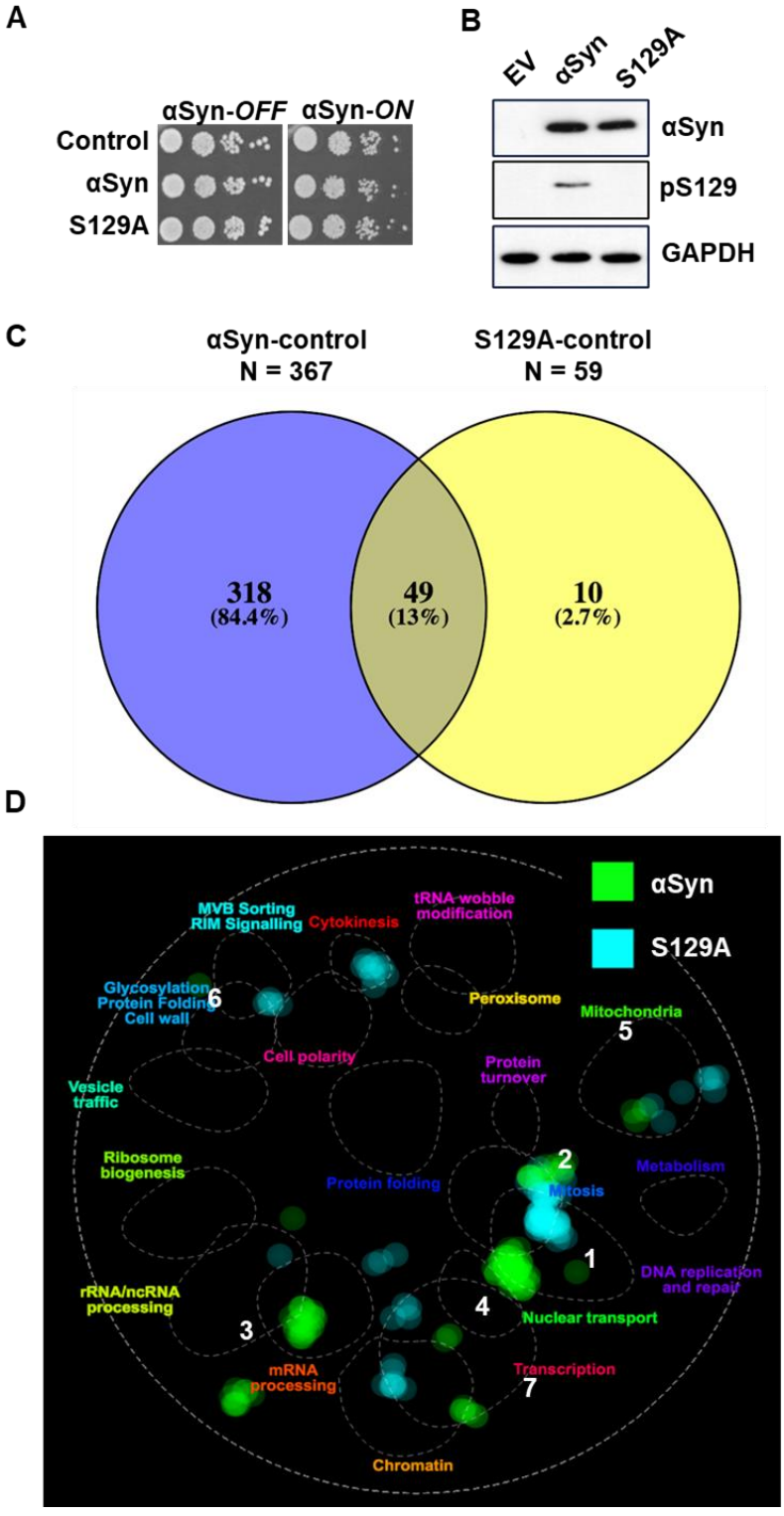

Figure 6. Expression of αSyn has higher impact on yeast protein stabilities than the non-phosphorylated S129A variant.
(A) Growth assays of yeast cells expressing *GAL1*-driven αSyn from two genomically integrated copies in *yMaM1234* background, used as query strain in the tFT collection screen, with empty vector as control. Cells were spotted in 10-fold dilutions on selective plates containing glucose (αSyn-*OFF*) or galactose (αSyn-*ON*). (B) Immunodetection of proteins from (A) using αSyn-specific and pS129-specific antibody. GAPDH antibody

was used as a loading control. (C) Venn diagram depicting unique und shared proteome between pairwise comparisons of αSyn or S129A to the control (empty vector). (D) Spatial Analysis of Functional Enrichment (SAFE) (http://www.thecellmap.org) analysis of hits from (C). Specific biological processes that are enriched upon αSyn expression (green) or S129A expression (blue) are depicted on the network map. 1 - DNA replication and repair; 2 - mitosis; 3 - mRNA processing; 4 - nuclear transport; 5 - mitochondria; 6 - glycosylation and protein folding; 7 - transcription**.**

3.1.3. Analysis of selected yeast proteins with changed stability upon α-synuclein expression

Individual strains from the tFT-collection were chosen and investigated as further proof of concept. Especially, the impacts of αSyn or S129A expression on protein stabilities of proteins from selected candidate genes from the tFT-screen with most significant changes were further examined. Additional selection criteria included corresponding candidate genes, which possess a human homologue, representatives of different functional categories and proteins, which are specifically affected in stability by either αSyn or S129A expression.

The tFT library is based on a yeast strain harboring a conditional expression of a *I-SceI* endonuclease with upstream *CYC1* terminator which prevents expression of sfGFP within the tFT tag. This endonuclease has no endogenous target in *S. cerevisiae* and targets an auxiliar marker encoding orotidine-5'-phosphate decarboxylase (*URA3*) which disrupt mCherry sequence within the tFT tag. The resulting double-strand break caused by *I-SceI* is repaired by homologous recombination between the N-terminal sequence of the first truncated copy of mCherry and the second sequence encoding the N-terminal sequence of full-length mCherry. Consequently, clones that have successfully excised the *URA3* marker exhibit both red and green fluorescence because sfGFP expression is no longer being prevented by upstream $CYC1^{term}$ (Khmelinskii *et al*, 2014, Kmelinskii *et al*, 2011).

After excision of *URA3* from tFT-ORF, the strains were transformed *de novo* with αSyn or S129A encoding plasmids or empty vector as a control. The strains were examined with fluorescence microscopy and immunoblotting analysis as a control to verify the steady-state protein level of tFT fusions and αSyn (Figure S1 and Figure S2).

Several top hits from the screening were verified with flow cytometry (Figure 7). Flow cytometry confirmed the results obtained in tFT-screen and showed that expression of αSyn affects protein stability either by increasing or decreasing it. Furthermore, it was corroborated that the effect of αSyn expression is considerably more profound in comparison to that of the S129A phosphorylation deficient variant.

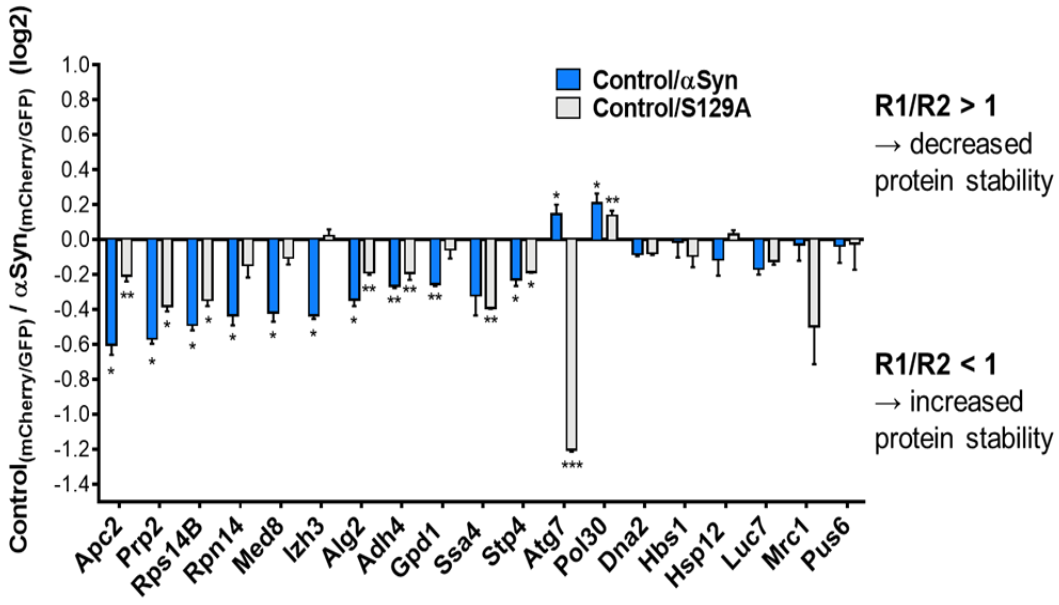

Figure 7. Fluorescence intensity ratios from flow cytometry data confirms results obtained in tFT-screen.
Flow cytometry was conducted with selected tFT-strains expressing αSyn, S129A or empty vector control. Intensity of fluorescence signal derived from mCherry and sfGFP was measured for 10000 single cells. mCherry/GFP ratio was calculated for each of the three replicates. Control/αSyn and Control/S129A ratios were calculated. Significance of differences was calculated with t-test versus control cells (*$p < 0.05$; **$p < 0.01$; ***; $p < 0.001$). R1/R2 indicates ratio mCherry/GFP of control cells (R1) to ratio mCherry/GFP of αSyn or S129A expressing cells (R2) in log2.

3.1.4. Proteasome chaperone Rpn14 is stabilized upon expression of α-synuclein

Two top candidate genes with opposing effects on stabilites of their resulting proteins were examined in more detail to further validate the tFT-screening. The stability of the Pol30 protein was decreased, whereas stability of Rpn14 was increased in presence of either αSyn or S129A in yeast cells (Figure S3 and Figure 7).

Pol30 represents an auxiliary protein of DNA polymerase and is involved in DNA repair. Fluorescence microscopy and cycloheximide chase experiments corroborated the

decreased Pol30 stability observed by the tFT-screening and flow cytometry (Figure S3).

One of the genes identified in the screening for top candidates of a stabilized protein was Rpn14. The proteasome-interacting protein Rpn14 is directly involved in protein homeostasis and acts as chaperone in 26S proteasome assembly. Rpn14 binds to the free 19S RP and helps to dissociate from 20S core by shifting the equilibrium proteasome assembly to disassembly as a negative regulator by interacting with with Rpt6 and Rpt4 base subunits (Park *et al*, 2009; Roelofs *et al*, 2009; Park *et al*, 2005; Shirozu *et al*, 2015) (Figure 4 and Figure 8A).

Live cell fluorescence microscopy of yeast cells expressing Rpn14-tFT and *GAL1*-driven αSyn or S129A confirmed the results obtained in the genomic screening as well as flow cytometry. The ratios of mCherry to sfGFP fluorescence signal indicated stronger effect on Rpn14 stabilization upon expression of αSyn versus expression of S129A (Figure 8B-D).

The effect of αSyn expression on the stability of Rpn14 was assessed using cycloheximide-chase experiments (Figure 8E, F). Rpn14 tagged with GFP was used for this experiment in order to avoid the rather big tFT-tag. Yeast cells were treated with the translational inhibitor cycloheximide to arrest *de novo* protein synthesis after 6 hours αSyn expression. This procedure allows visualization of the degradation kinetics of the steady-state population of cellular proteins. Samples were taken at 0 hours time point, after 2 hours and 4 hours of cycloheximide treatment. The levels of Rpn14-GFP protein were evaluated by immunoblot analysis. Increased stability of Rpn14-GFP was observed upon expression of αSyn, whereas expression of S129A decreased the stability of Rpn14-GFP.

The same results were obtained in live-cell fluorescence microscopy in which yeast cells were trapped in microfluidic device and treated with cycloheximide (Figure 8G, H). αSyn and S129A were expressed from a *GAL1* promoter and abundance and degradation kinetics of Rpn14-tFT were followed *in vivo* by measurement of sfGFP signal for 25 hours. Increased stability of Rpn14 was observed upon expression of αSyn. These data corroborate the results from the screen and flow cytometry and

reveal that expression of αSyn significantly increases Rpn14 stability and that phosphorylation at S129 promotes this effect.

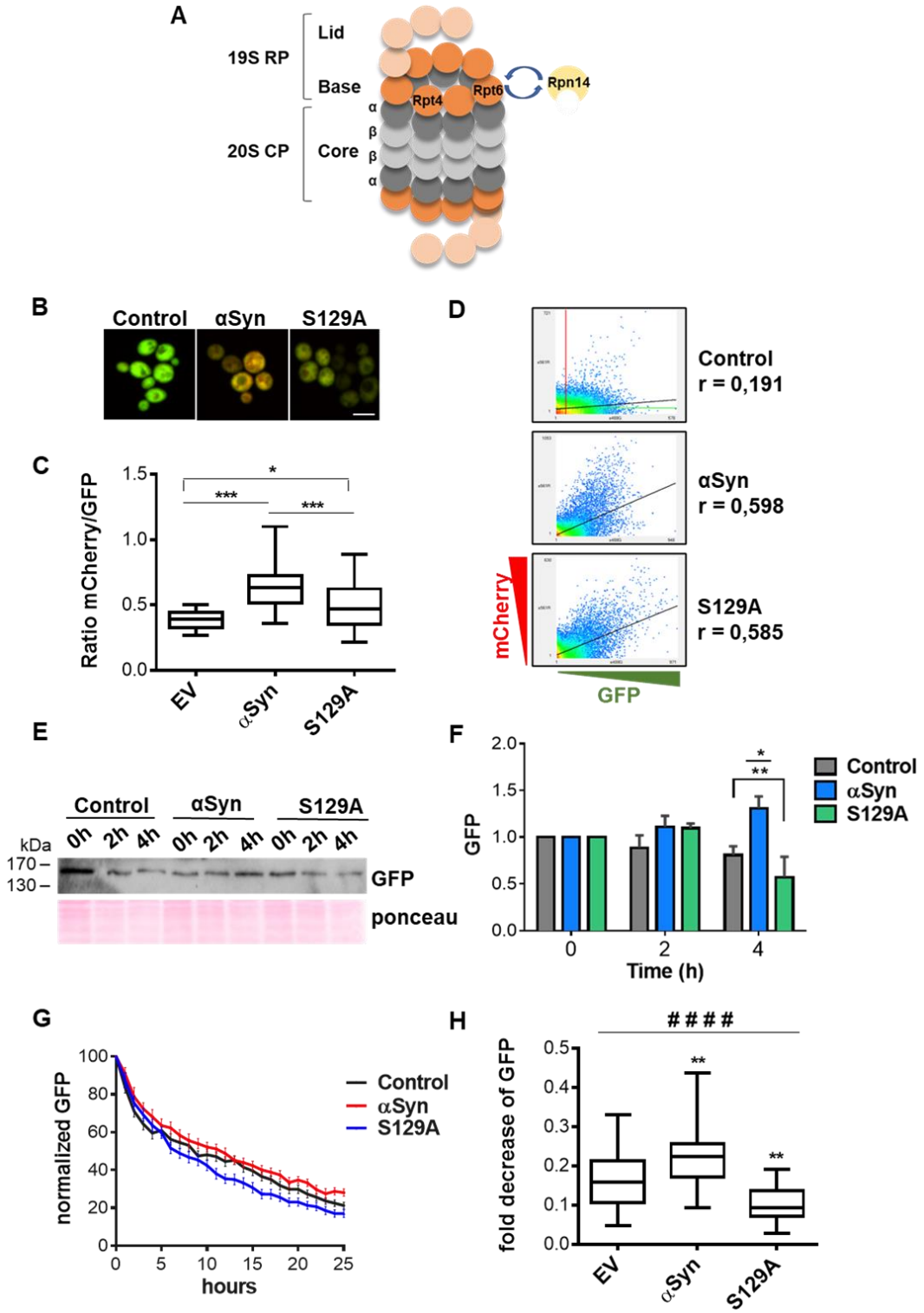

Figure 8. Expression of αSyn increases the stability of Rpn14.
(A) Schematic diagram depicting Rpn14 as 26S proteasome chaperon interacting with base subunits Rpt6 and Rpt4, which directs them to the core particle and interaction

between Rpt and α-subunit leads to displacement of the chaperone. (B) Live cell fluorescence microscopy of yeast cells, expressing Rpn14-tFT and *GAL1*-driven αSyn or S129A from 2 µm plasmid. Protein expression was induced for 6 h in galactose-containing medium prior to microscopy. Control cells are transformed with empty vector. Scale bar: 5 µm. (C) Quantification of the fluorescence signal in cells from A. The GFP and mCherry fluorescence was measured using SlideBook6 software. For each individual cell the ratio mCherry/GFP was calculated. The bars represent mean values ± SD. Significance of differences was calculated with *t*-test versus control cells (***, $p < 0.001$; *, $p < 0.01$; n = 100). (D) Scatterplot of the intensity of all pixels in GFP channel versus the intensity of all pixels in mCherry channel. The points within the scatterplot are colored blue to red, where dark blue represents single pixel events and red represents many pixels with identical intensity values for both channels. The black line in the scatterplot represents a linear regression of the data in the 2D histogram. The slope of the line is related to the correlation of the two signals. r (Pearson's Correlation Coefficient) indicates the extent to which the two variables (green and red fluorescence) are linearly related. A slope of 1 is defined as perfectly correlated signals where the intensity of both is proportionate in each channel at a given pixel. A slope of 0 is defined as random correlation. (E) Immunoblot analysis of Rpn14-GFP treated with cycloheximide. Cells expressing *GAL1*-driven αSyn or S129A or empty vector control from 2 µm plasmid were induced for 6 h in galactose-containing medium prior to treatment with 50 µg/mL cycloheximide to stop *de novo* protein synthesis. Immunoblotting analysis was performed at the indicated time points after addition of cycloheximide with GFP antibody. Ponceau was used as a loading control. (F) Densitometric analysis of the immunodetection of the GFP signal. The GFP signal was normalized to each individual signal at 0 h. The significance of the differences was calculated with *t*-test (*, $p < 0.05$; **, $p < 0.1$). (G) Quantification of sfGFP fluorescence signal of Rpn14-tFT strain from fluorescence microcopy with microfluidic device. Yeast cells were trapped in the microfluidic device and expression of αSyn or S129A from 2 µm plasmid was induced for 6 h in galactose-containing medium prior to treatment with 50 µg/mL cycloheximide. Abundance and degradation kinetics of Rpn14-tFT were recorded *in vivo* by measurement of sfGFP signal for 25 h following cycloheximide treatment. The sfGFP signal was normalized to each individual signal at 0 h (n = 40). (H) Quantification of fold decrease of sfGFP signal from (G) after 14 h of cycloheximide treatment. Significance of differences was calculated with *t*-test versus empty vector (EV) control cells (**, $p < 0.01$; n = 30).

3.2. High level of Rpn14 is deleterious to yeast cells and enhances α-synuclein induced growth retardation

The consequences of the increased stability of Rpn14 for yeast cells were assessed in more detail. We hypothesized that the αSyn-induced toxicity might be connected with the stabilization of the proteasome chaperone. To examine this, different expression levels of *RPN14* were studied in yeast cells: (i) *RPN14* at its native level; (ii) elevated level (from a low copy *CEN* plasmid); (iii) high level (from a high copy 2 µ

plasmid); (iv) or *RPN14* deletion strain. The impact of different *RPN14* expression levels was examined by yeast growth assays. Additionally, simultaneous expression of αSyn, S129A or empty vector control was studied. Expression of *RPN14* at its native level and from a low copy plasmid did not influence yeast cell growth (Figure 9A). Also, deletion of *RPN14* does not affect cell growth, regardless of αSyn or S129A expression (Figure 9B). The same results were obtained when the cells were grown in liquid selective medium (Figure 9C, D).

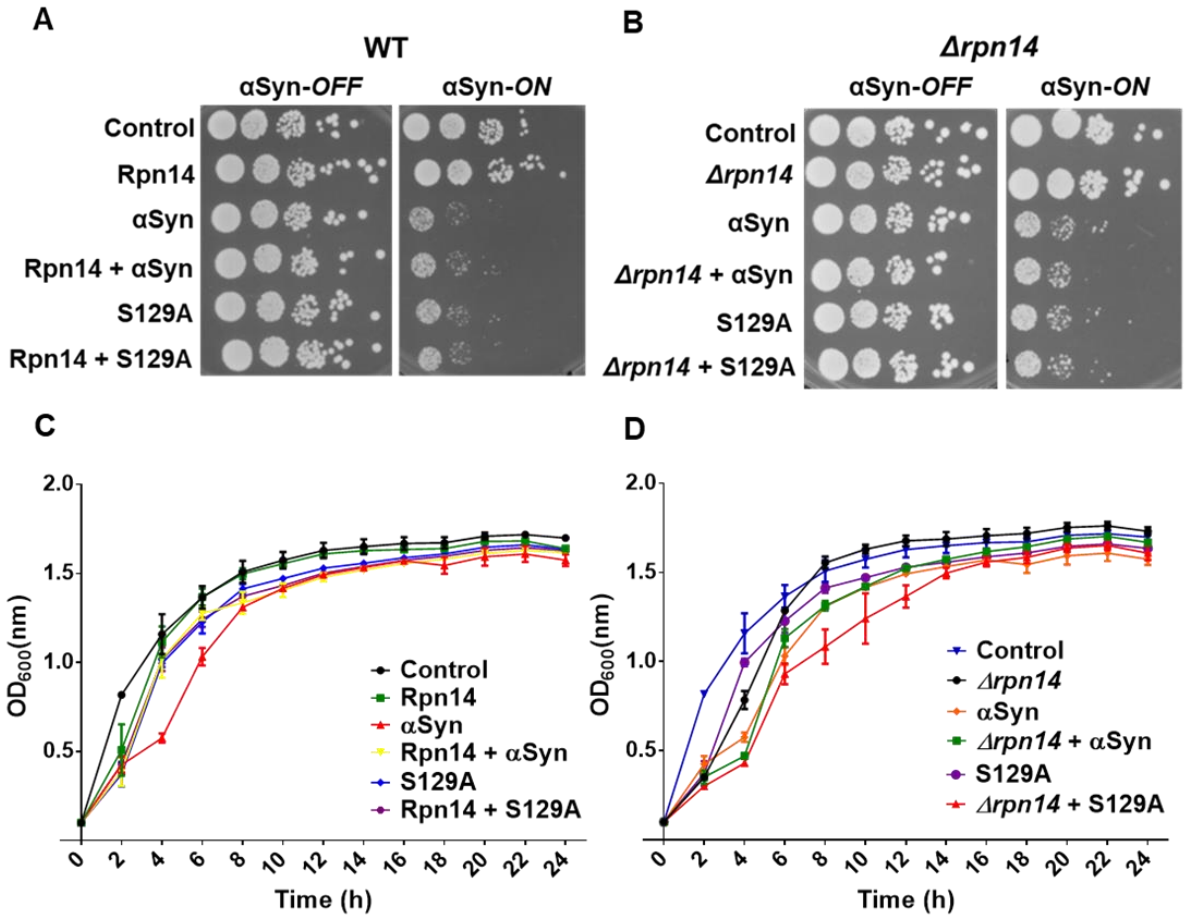

Figure 9. Low Rpn14 protein levels do not affect α-synuclein induced yeast growth retardation.
(A) Growth assay of yeast cells expressing *GAL1*-driven αSyn or S129A from a 2 μm plasmid and *RPN14* from a low copy *CEN* plasmid in wild type (WT) yeast strain. (B) Growth assay of yeast cells expressing *GAL1*-driven αSyn or S129A in *Δrpn14* yeast strain. Cells were spotted in 10-fold dilutions on selective plates containing glucose (αSyn-*OFF*) or galactose (αSyn-*ON*). The plates were incubated at 30°C for 5 days. (C) Cell growth comparison of yeast cells expressing *GAL1*-driven αSyn or S129A and *RPN14* from a low copy plasmid (*CEN*) in wild type (WT) yeast strain in liquid selective medium containing galactose. (D) Cell growth comparison of yeast cells expressing *GAL1*-driven αSyn or S129A in *Δrpn14* yeast strain in liquid selective medium containing galactose. Error bars indicate standard deviations of three independent experiments.

The effect of different *RPN14* expression levels on αSyn toxicity was analyzed in strains with defined copy number of αSyn-encoding gene (Figure 10). Expression of *RPN14* from a low copy *CEN* plasmid did not affect growth of cells, expressing αSyn from one, two or three gene copies, similar to the previous observations. However, when *RPN14* was expressed from a high copy plasmid it enhanced αSyn-induced growth retardation upon expression of two copies of αSyn (Figure 10B). No difference in growth was observed when αSyn was expressed from one gene copy, which does not cause growth retardation. Expression from three copies of αSyn was above the toxicity threshold, as already reported (Petroi *et al*, 2012).

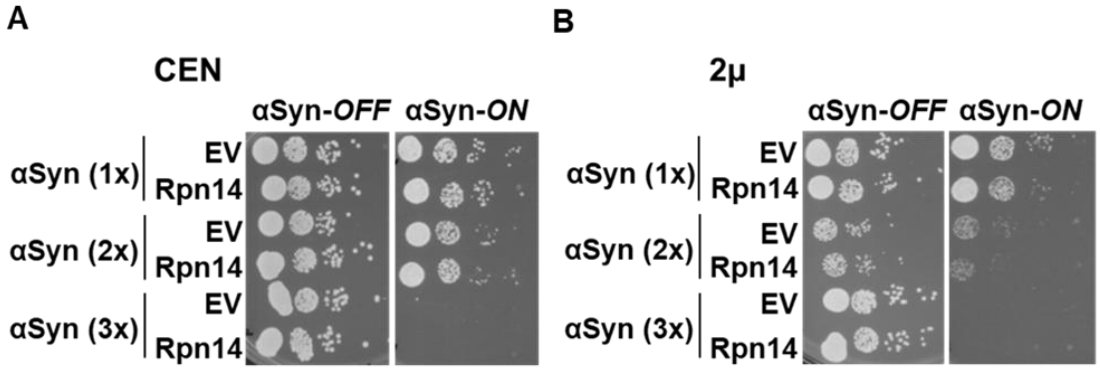

Figure 10. High Rpn14 protein levels are harmful to yeast cells and enhance α-synuclein induced growth retardation.
(A) Growth assay of yeast cells expressing *GAL1*-driven αSyn-GFP from one (1x), two (2x) or three (3x) gene copies and *RPN14* from a low copy plasmid (*CEN*) or a high copy plasmid (2μ) and (B) yeast with empty vector (EV) as a control. Cells were spotted in 10-fold dilutions on selective plates containing glucose (αSyn-*OFF*) or galactose (αSyn-*ON*). The plates were incubated at 30°C for 5 days.

These results reveal that high levels of the proteasomal chaperon Rpn14, which promotes disassembly of the 26S particle enhances αSyn mediated growth retardation. This supports that increased stability of Rpn14 upon αSyn expression mediates toxicity and inhibits cellular growth.

3.3. Rpn14 increases the toxicity of α-synuclein upon stress

Rpn14 has a redundant function with Nas6, another proteasome chaperone. Nas6 binds to the Rpt3 base subunit (Funakoshi *et al*, 2009; Saeki *et al*, 2009). The chaperone Nas6 antagonizes both lid-base association and base-CP association, and

the site-specificity of Nas6 activity depends on the nucleotide state of the base. Upon blocked ATP hydrolysis, Nas6 disrupts base-lid association and does not interfere with base-CP association, and *vice versa*. Nas6 provides a precisely regulated mechanism to organize proteasome assembly events over time (Li *et al*, 2017). Deletion of *RPN14* or *NAS6* alone does not change the accumulation of polyubiquitinated proteins. However, double deletions result in significant accumulation of polyubiquitinated proteins, confirming their redundant function and suggesting that both Nas6 and Rpn14 are important for the degradation of ubiquitinated proteins (Funakoshi *et al*, 2009; Saeki *et al*, 2009). Furthermore, a *Δrpn14Δnas6* double-deletion mutant stain shows a severe growth defect at 37°C (Saeki *et al*, 2009).

The impact of the deletion of *RPN14* or *NAS6* on yeast cell growth was examined at 30°C, 33°C and 37°C in order to elucidate, if the observed enhancement of αSyn toxicity by high protein level of Rpn14 is specific for this chaperon (Figure 11A). In addition, double-deletion mutant *Δrpn14Δnas6* was generated. Single deletion of either chaperon did not affect yeast cells growth, regardless the temperature. Growth retardation was observed upon deletion of both of chaperons at 37°C.

Wild type yeast strain, *Δrpn14* strain, *Δnas6* strain and the double deletion *Δrpn14Δnas6* strain were transformed with plasmids encoding αSyn, S129A or empty vector as a control and used for growth assays. Growth assays were performed at 30°C and 37°C (Figure 11B). No effect on αSyn or S129A-induced toxicity was observed at 30^{o}C in the deletion strains in comparison to the wild type. However, under deletion of *RPN14,* partial rescue of αSyn-induced toxicity at 37^{o}C was observed. Similar growth rescue was not detected in *Δnas6* deletion strain, suggesting that this effect is specific for Rpn14. Importantly, cells expressing S129A revealed similar growth phenotype in presence, as well as in absence of the proteasome chaperones. This is consistent with the previous observations that pS129 contributes to the increased stability of Rpn14, whereas expression of S129A decreases its stability. The results indicate that native expression of Rpn14 increases the toxicity of αSyn but not of S129A upon stress. This αSyn effect correlates with Rpn14 stability.

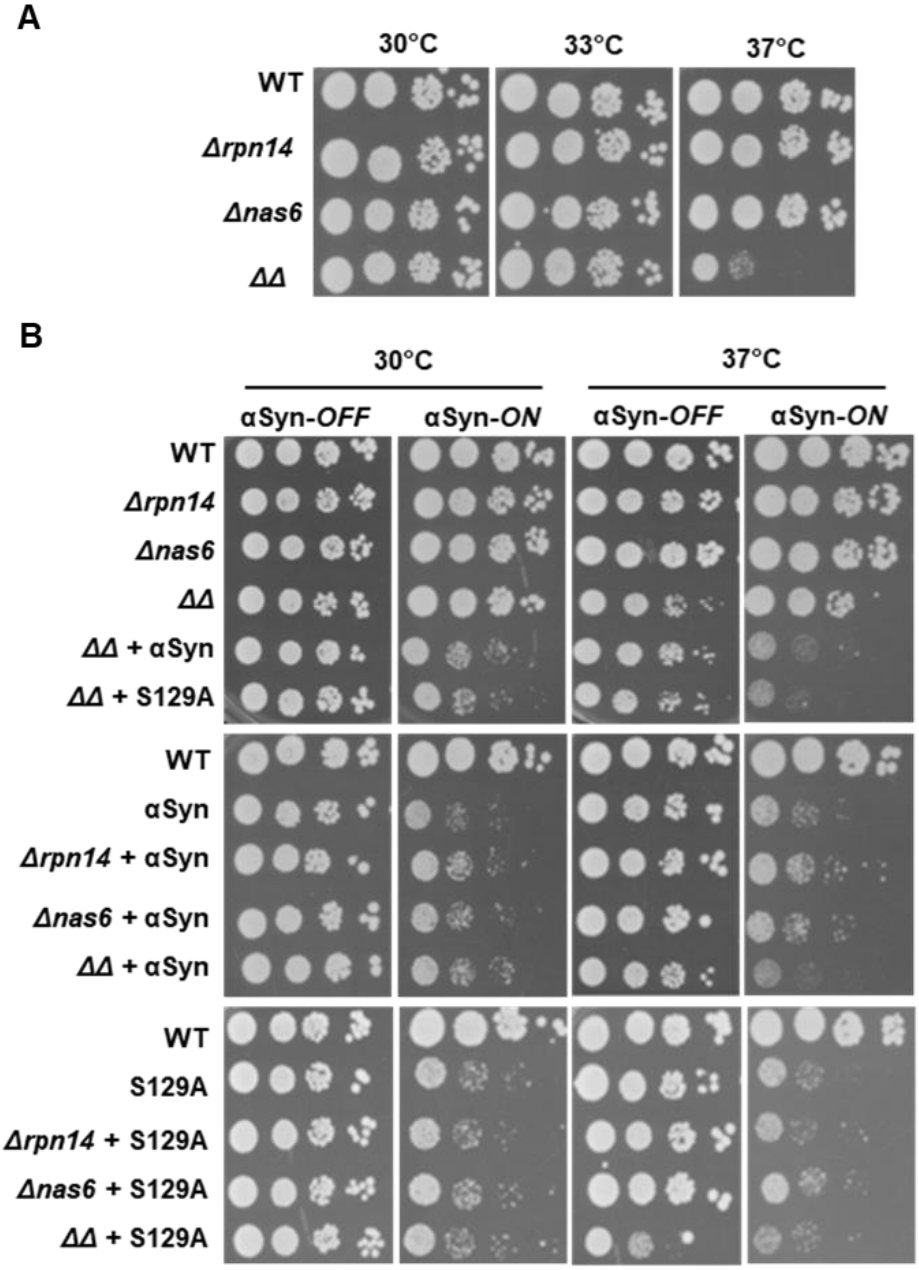

Figure 11. Deletion of *RPN14* but not *NAS6* rescues αSyn-induced toxicity at elevated temperature in yeast cells.
(A) Growth assay of *RPN14*, *NAS6* deletion and double deletion yeast strains, and wild type strain as a control. Cells were spotted in 10-fold dilutions on YEPD medium. The plates were incubated in parallel in 30°C, 33°C and 37°C for 3 days. (B) Growth assay of the strains from (A) expressing *GAL1*-driven αSyn or S129A from 2 μm plasmid. Cells were spotted in 10-fold dilutions on selective plates containing glucose (αSyn-*OFF*) or galactose (αSyn-*ON*). The plates were incubated in parallel at 30°C and 37°C for 5 days.

3.3.5. Rpn14 interacts with α-synuclein

Bimolecular Fluorescence Complementation assay (BiFC) was performed to analyze whether the stabilization of Rpn14 upon αSyn expression was due to their physical interaction (Figure 12).

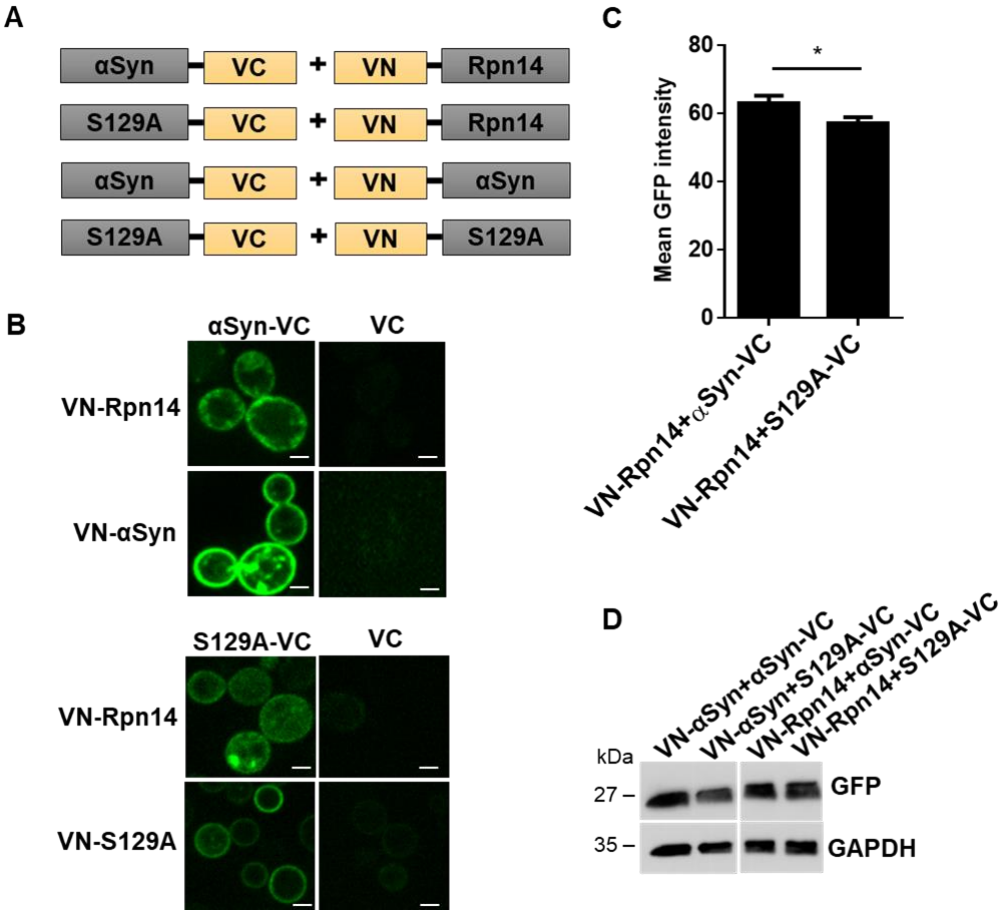

Figure 12. Bimolecular Fluorescence Complementation assay indicates a physical interaction between the 26S proteasome chaperon Rpn14 and αSyn. (A) Schematic representation of Bimolecular Fluorescence Complementation assay (BiFC) constructs. Rpn14, αSyn and S129A were fused to the non-fluorescent complementary N- and C-terminal fragments of fluorescent Venus reporter protein (VN and VC). (B) Fluorescence microscopy of yeast W303 cells expressing different combination of the fusion constructs 6 h post induction. BiFC with VC served as a negative control. The image display is scaled to the minimum and maximum pixel intensity values per image for optimal noise-to signal ratios. Scale bar = 1 µm. (C) Quantification of BIFC signal intensities emerging from VN-Rpn14 interaction with αSyn-VC or S129A-VC. Significance of differences was calculated with t-test (*, $p < 0.05$, n=3). (D) Immunoblotting analysis of cells from A. The GFP antibody detects VC but not VN. GAPDH antibody was used as a loading control.

Rpn14, αSyn and S129A were fused to the non-fluorescent complementary N- and C-terminal fragments of the fluorescent reporter protein Venus (VN and VC) (Figure 12A). Co-expression of αSyn-VC and VN-Rpn14 constructs in yeast yielded green fluorescence indicating reconstitution of the Venus fluorophore by the interaction of Rpn14 with αSyn (Figure 12B). Co-expression of S129A-VC and VN-Rpn14 revealed interaction also between Rpn14 and S129A. The intensity of the BiFC signal was evaluated using SlideBook6 software, revealing that αSyn-VC + VN-Rpn14 pair is more competent to interact in comparison to S129A-VC + VN-Rpn14 pair (Figure 12C). Western blot analysis confirmed the expression of the constructs in yeast cells (Figure 12D). These results reveal that there is a direct interaction between αSyn and Rpn14 and that pS129 promotes this interaction.

3.3.6. Elevated level of Rpn14 has no significant effect on α-synuclein aggregate formation

Fluorescence microscopy was used to study whether the Rpn14-dependant αSyn growth inhibition is accompanied by changes in αSyn inclusion formation. Elevated level of *RPN14* which was expressed from a low copy plasmid in wild type yeast strain, expressing αSyn or S129A variant from the *GAL1* promoter, had no significant effect on αSyn aggregates formation. Similarly, no effect on αSyn aggregates formation was observed in deletion *RPN14* strain in comparison to aggregate formation of S129A variant (Figure 13).

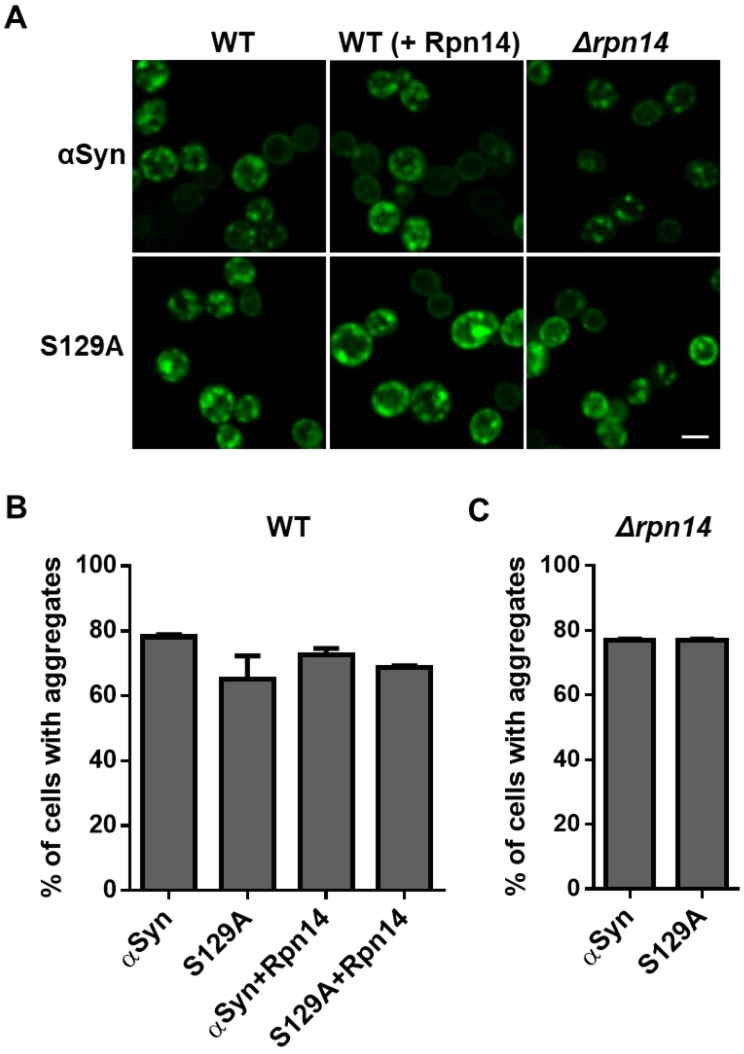

Figure 13. Rpn14 function is independent of αSyn aggregates formation in yeast. (A) Fluorescence microscopy of yeast cells, expressing αSyn-GFP or S129A-GFP after 6 hours of induction in galactose-containing medium at normal (WT) and elevated (WT + Rpn14) level of Rpn14 or by deletion of *RPN14*. Scale bar: 5 µm. (B) Quantification of the percentage of cells displaying αSyn and S129A aggregates in wild type yeast strain expressing elevated level of *RPN14* and *RPN14* deletion strain (B) after 6 hours induction of αSyn expression in galactose-containing medium (n=200).

3.3.7. Increased levels of Rpn14 decrease α-synuclein aggregate clearance upon proteasome inhibition

Inefficient αSyn inclusions clearance may lead to accumulation of toxic protein species resulting in cytotoxicity. Therefore, the impact of the Rpn14 chaperone on clearance of αSyn inclusions was analyzed by applying the proteasome inhibitor MG132 (Figure 14). Promoter shut-off studies were performed by inducing αSyn expression for 4 hours in galactose-containing medium, followed by promoter shut-off in glucose-containing medium that represses the *GAL1* promoter from which αSyn was expressed. Proteasomal degradation pathway was blocked by treating cells with MG132 after αSyn was induced. Clearance of αSyn inclusions was followed for 5 hours in comparison to control with DMSO. Cells expressing αSyn were unable to clear the inclusions, which suggests that the proteasome plays a major role in aggregate clearance of αSyn. Rpn14 increased the accumulation of αSyn aggregates, which indicates that increased levels of Rpn14 decreases αSyn aggregate clearance upon proteasome inhibition.

The inclusions were cleared in cells expressing the S129A variant in a similar manner as control cells without proteasome inhibitor treatment. This suggests that the 26S proteasome does not play a major function in the clearance of unphosphorylated S129A aggregates. Consistently, elevated levels of Rpn14 did not affect S129A aggregate clearance either. Both αSyn as well as S129A aggregates were cleared similarly upon deletion of *RPN14*, further corroborating that Rpn14 has an impact on αSyn inclusion clearance when the proteasome is inhibited.

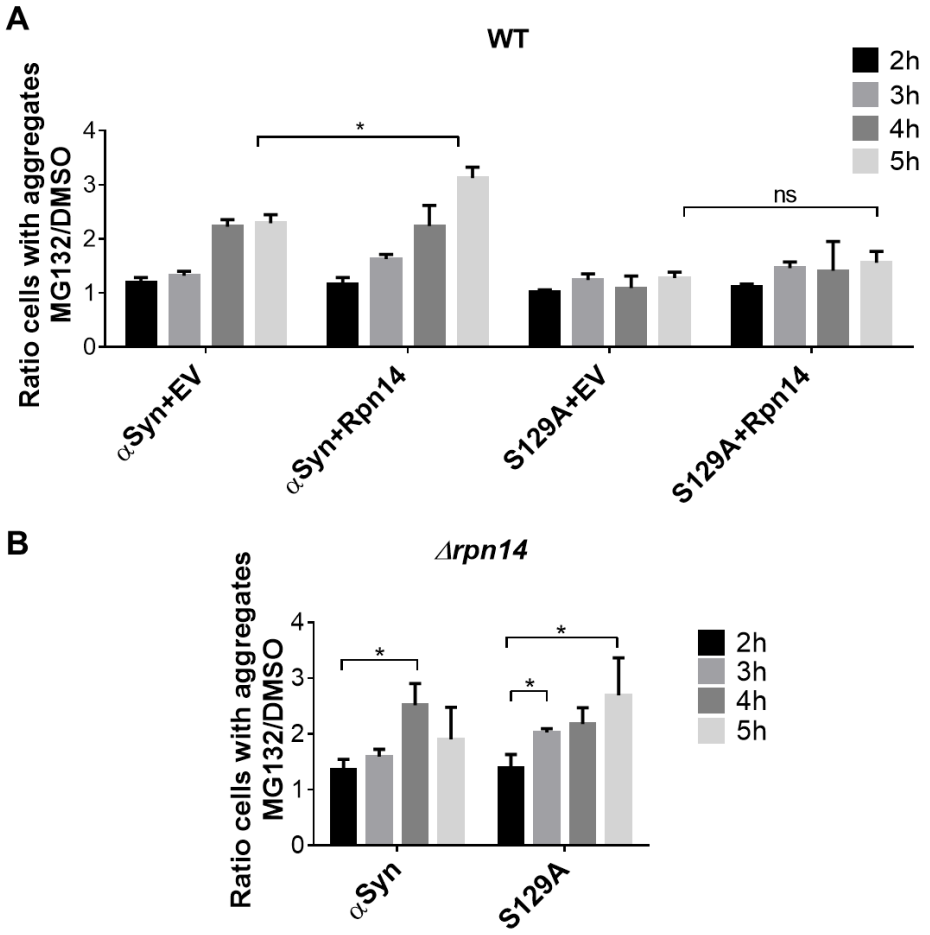

Figure 14. αSyn aggregate clearance in yeast cells after promoter shut-off upon proteasome inhibition.
(A) αSyn aggregate clearance after *GAL1*-pomoter shut-off of yeast cells expressing αSyn and S129A from a high copy plasmid (2 μ) in a wild type yeast strain and in *RPN14* deletion strain (B). After 4 h induction of αSyn and S129A expression in galactose-containing medium, cells were shifted to a glucose medium to repress the *GAL1* promoter. The glucose medium was supplemented with 75 μM MG132 dissolved in DMSO or with DMSO as a control. The cells with inclusions were counted at the time points 2 h, 3 h, 4 h and 5 h after *GAL1*-promoter shut-off and normalized to time point 2 h. The significance of the differences was calculated with *t*-test (*, $p < 0.05$).

3.3.8. Increased Rpn14 or αSyn levels upon proteasome inhibition result in accumulation of ubiquitin conjugates

The proteasome chaperon Rpn14 interacts with the base ATPases Rpt4 and Rpt6 leading to their translocation to the 20S CP (Saeki *et al*, 2009; Roelofs *et al*, 2009). Downregulation of essential proteasome subunits significantly enhances αSyn toxicity which is reflected by yeast cells growth retardation or impairment (Popova *et al*,

2021a). The strongest genetic interactions were observed upon downregulation of the base subunit genes *RPT2*, *RPT4* and *RPT6*, in comparison with downregulation of other proteasome genes. αSyn was found in the proximity of Rpt2 and high levels of αSyn increased the pool of ubiquitinated substrates upon downregulation of *RPT2* (Popova *et al*, 2021a). The present study revealed that αSyn expression increases the stability of Rpn14 proteasome chaperone, which is deleterious to yeast cells. Therefore, it was examined, whether elevated levels of the Rpn14 chaperone disturb the function of the 26S proteasome and the degradation of ubiquitin conjugates. The interplay of Rpn14 and αSyn was examined under proteolytic stress conditions. Changes in the ubiquitin pool by downregulation of *RPT2*, *RPT4* and *RPT6* genes for proteasome base subunits and in presence or absence of Rpn14 and αSyn or S129A were examined. This analysis should clarify whether the impact of αSyn, which significantly alters ubiquitin homeostasis, is influenced by different protein levels of Rpn14. Additionally, the impact of Rpn14 on αSyn turnover was studied in these strains.

Yeast strains from the *Tet*-Promoters Hughes collection (yTHC) were used, in which the endogenous promoter of the gene is replaced with *Tet*-titratable promoter in the genome (Mnaimneh *et al*, 2004). This promoter allows switching off the expression of *Tet-RPT2*, *Tet-RPT4* and *Tet-RPT6* genes encoding base subunits by addition of doxycycline to the yeast growth medium. Double mutant strains were generated in order to elucidate further the role of Rpn14 in proteasomal degradation, where *RPN14* gene was deleted in the background of the three *Tet*-strains. Expression of αSyn was induced overnight in the presence or absence of doxycycline that downregulates *Tet*-promoter. The levels of ubiquitin conjugates were analyzed by immunoblotting (Figures 15-17).

3.3.8.1. Rpn14 is involved in the turnover of phosphorylated α-synuclein

Changes in the ubiquitin pool and αSyn turnover were first examined in *Tet-RPT2* and *Tet-RPT2 Δrpn14* background strains. The Rpt2 subunit of the RP is a part of the base essential for the assembly of the regulatory 19S particle as it is associated with other ATPases promoting their specific localization in the complex (Sakata *et al*, 2021).

Furthermore, it was found in a proximity to the αSyn subpopulation suggesting that αSyn may directly or indirectly physically interact with 19S RP, and thus may interfere with assembly of 26S proteasome (Popova *et al*, 2021a).

Yeast *Tet-RPT2* strain was transformed with 2 μm high copy plasmids, harboring αSyn-GFP, S129A-GFP or an empty vector. Additionally, *RPN14* was expressed from a low-copy *CEN* plasmid. αSyn expression was induced in galactose-containing medium and the cells were incubated in absence or presence of doxycycline for downregulation of *Tet-RPT2* overnight. The levels of ubiquitin conjugates were analyzed by immunoblotting (Figure 15A).

Downregulation of the *Tet-RPT2* had no effect on the level of ubiquitinated conjugates when compared to *Tet-ON* in the empty vector control (Figure 15B). Similarly, expression of αSyn or elevated level of Rpn14 did not alter the accumulation of ubiquitinated proteins upon *Tet-ON.* In contrast, downregulation of *Tet-RPT2* upon expression αSyn, elevated level of Rpn14, or both resulted in a significant increase of the ubiquitin conjugates compared to the empty vector control. A synergistic effect of Rpn14 and αSyn expression was not observed. Significantly less accumulation of ubiquitin conjugates was observed when S129A was expressed in comparison to αSyn.

The consequences of increased levels of Rpn14 on αSyn or S129A turnover were also analyzed by immunoblotting (Figure 15A, C). No changes in the steady-state protein levels of αSyn and S129A were found (Figure 15C). Next, the fraction of phosphorylated αSyn was probed using a specific antibody that recognizes only the phosphorylated form of the protein (pS129). Importantly, significant accumulation of phosphorylated αSyn was observed upon elevated protein level of Rpn14 (Figure 15D). The effect was independent of the expression level of *Tet-RPT2*. This finding indicates that Rpn14 increases the accumulation of pS129 fraction, suggesting that it inhibits the turnover of phosphorylated αSyn.

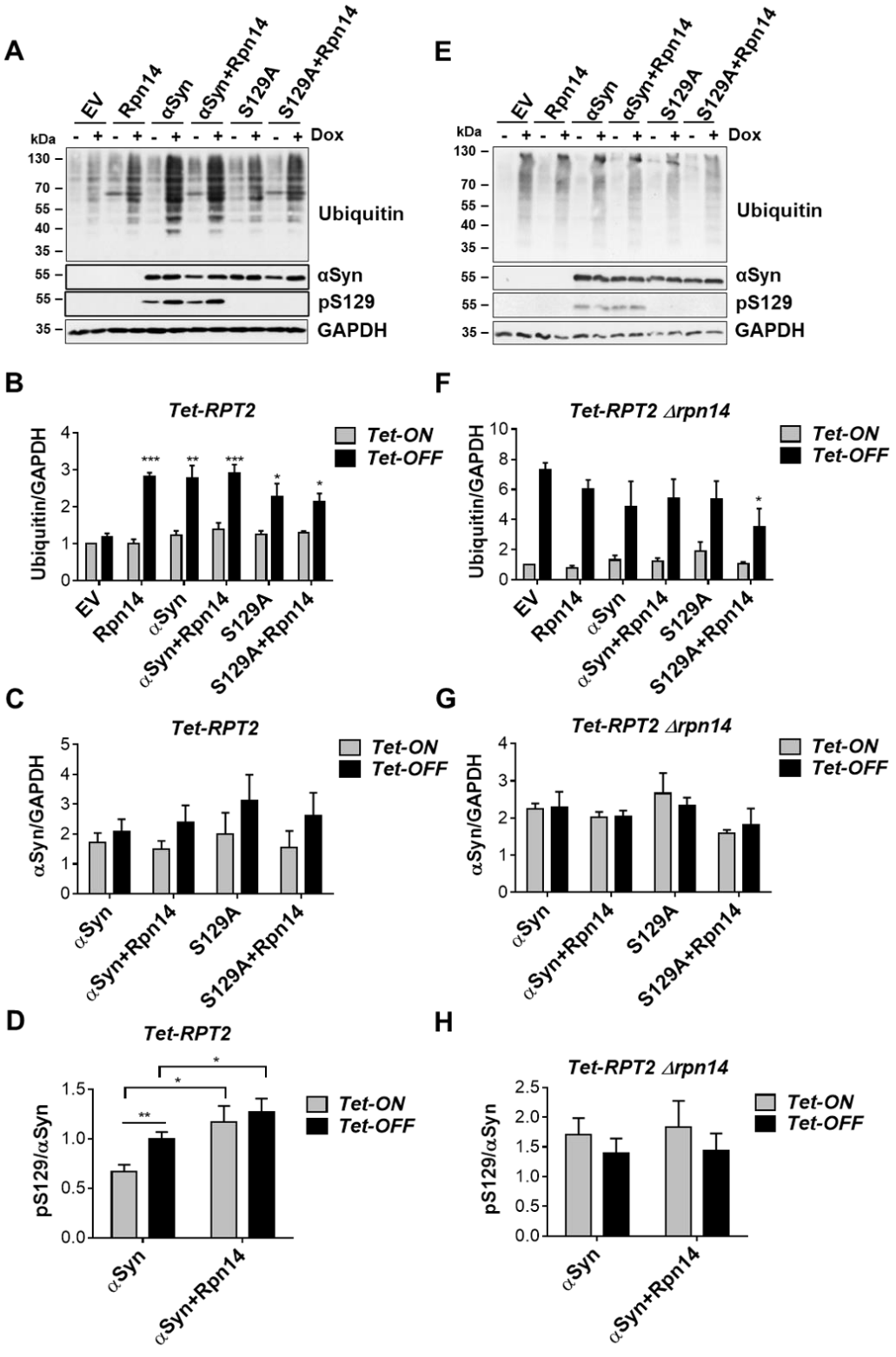

Figure 15. Rpn14 is directly involved in pS129 α-synuclein turnover in yeast cells.

(A) Immunoblot analysis of *Tet-RPT2* strain harbouring *GPD*-driven *RPN14* and *GAL1*-driven αSyn-GFP, S129A-GFP and empty vector (EV) control plasmids. Yeast cells were grown overnight in a galactose-containing medium to induce αSyn expression.

The *Tet* promoter was downregulated by addition of 10 µg/mL doxycycline (Dox) to the growth medium. Immunoblotting analysis was performed with ubiquitin, αSyn and pS129 antibodies. GAPDH was used as a loading control. (B) Densitometric analysis of the immunodetection of the ubiquitin conjugates in *Tet-RPT2* strain relative to the GAPDH control. The significance of differences was calculated with a *t*-test relative to EV control (*, $p < 0.05$**, $p < 0.01$; ***, $p < 0.001$). (C) Densitometric analysis of αSyn protein levels from *Tet-RPT2* (A) relative to the GAPDH loading control. (D) Densitometric analysis of phosphorylated fractions of αSyn protein levels from *Tet-RPT2* strain (A) to αSyn. The level of αSyn, phosphorylated at S129 was probed using a specific antibody that recognizes only the phosphorylated form of the protein (pS129). Significance of differences was calculated with *t*-test (*, $p < 0.05$; **, $p < 0.01$). (E) Immunoblot analysis of *Tet-RPT2 Δrpn14* strain harbouring Rpn14 and *GAL1*-driven αSyn-GFP, S129A-GFP and empty vector (EV) control plasmid performed equally to (A). (F) Densitometric analysis of the immunodetection of the ubiquitin conjugates in *Tet-RPT2 Δrpn14* strain relative to the GAPDH control. The significance of ubiquitin/GAPDH ratio was calculated with a *t*-test relative to EV control (*, $p < 0.05$). (G) Densitometric analysis of αSyn protein levels from *Tet-RPT2 Δrpn14* (E) relative to the GAPDH loading control. (H) Densitometric analysis of phosphorylated fractions of αSyn protein levels from *Tet-RPT2 Δrpn14* strain (E) to αSyn. The level of αSyn, phosphorylated at S129 was probed using a specific antibody that recognizes only the phosphorylated form of the protein (pS129).

The accumulation of ubiquitinated proteins was then analyzed in *Tet-RPT2 Δrpn14* strain (Figure 15E, F). Accumulation of ubiquitin conjugates was observed with empty vector control upon downregulation of *Tet-RPT2.* Low copy *RPN14* expression was exploited as a control to mimic native *RPN14* expression. The accumulation of ubiquitinated proteins when αSyn or *RPN14* were expressed was similar to that of the control cell, in contrast to the same conditions in *Tet-RPT2* strain. These results indicate that the αSyn-induced accumulation of Ubi-conjugates when Rpt2 is depleted is mediated by Rpn14.

The protein abundance of αSyn in *Tet-RPT2 Δrpn14* strain was similar in all examined conditions independently from the *RPT2* expression levels (Figure 15G). Immunoblotting with a pS129 antibody that specifically recognizes αSyn species that are phosphorylated at serine 129 revealed that protein level did not change in *Tet-RPT2 Δrpn14*, in contrast to *Tet-RPT2* strain with intact *RPT14* (Figure 15H). These findings support the results obtained in the *Tet-RPT2* background strain and suggest that Rpn14 is directly involved in the turnover of phosphorylated αSyn.

3.3.8.2. High level of Rpn14 leads to accumulation of ubiquitin conjugates upon downregulation of *RPT4*

Next, changes in ubiquitin pool and αSyn turnover were examined in *Tet-RPT4* and *Tet-RPT4 Δrpn14* background strains. Rpt4 is one of the six distinct AAA-ATPases functioning as unfoldase at the ring base of the 19S regulatory particle. Rpt4 binds the Rpn14 chaperone and connects to the core particle (Roelofs *et al*, 2009). Therefore, the interplay between different levels of the base subunits and Rpn14 was studied.

Yeast *Tet-RPT4* strain was transformed with 2 µm plasmids, harboring αSyn-GFP, S129A-GFP or an empty vector. Rpn14 was expressed from a *CEN* plasmid or a native promoter. αSyn expression was induced in galactose-containing medium and the cells were grown without or with addition of doxycycline for downregulation of *Tet-RPT4* overnight. The levels of ubiquitin conjugates were analyzed by immunoblotting (Figure 16A).

The empty vector control of the *Tet-RPT4* showed no differences in the levels of ubiquitin conjugates between *Tet-ON* and *Tet-OFF*, comparably to *Tet-RPT2* (Figure 16A, B). Similar to *Tet-RPT2,* an increase in the accumulation of ubiquitinated proteins could be observed under downregulation of *Tet-RPT4* when αSyn was expressed and the level of Rpn14 was elevated. However, the differences between *Tet-ON* and *Tet-OFF* were less prominent in comparison to *Tet-RPT2.* Expression of S129A resulted in increased accumulation of ubiquitinated proteins regardless of the protein levels of Rpt4 or Rpn14. No change in the steady-state αSyn protein levels were observed by both expression levels of *Tet-RPT4*. The levels of pS129 αSyn did not change in *Tet-RPT4* with or without downregulation of the *Tet*-promoter or by elevated level of Rpn14.

Similar to *Tet-RPT2,* deletion of *RPN14* in *Tet-RPT4* background strain resulted in increase of ubiquitin conjugates under downregulation of *RPT4* in empty vector control and expression of αSyn and *RPN14* did not increased the level of ubiquitinated proteins in comparison to empty vector (Figure 16E, F). A significant increase in αSyn level in *Tet-RPT4 Δrpn14* was observed when S129A was expressed upon downregulation of *Tet-RPT4.* No changes in pS129 αSyn levels were detected (Figure 16G, H). These results further corroborate that elevated levels of the Rpn14 chaperone contribute to proteasome dysfunction under proteotoxic stress conditions.

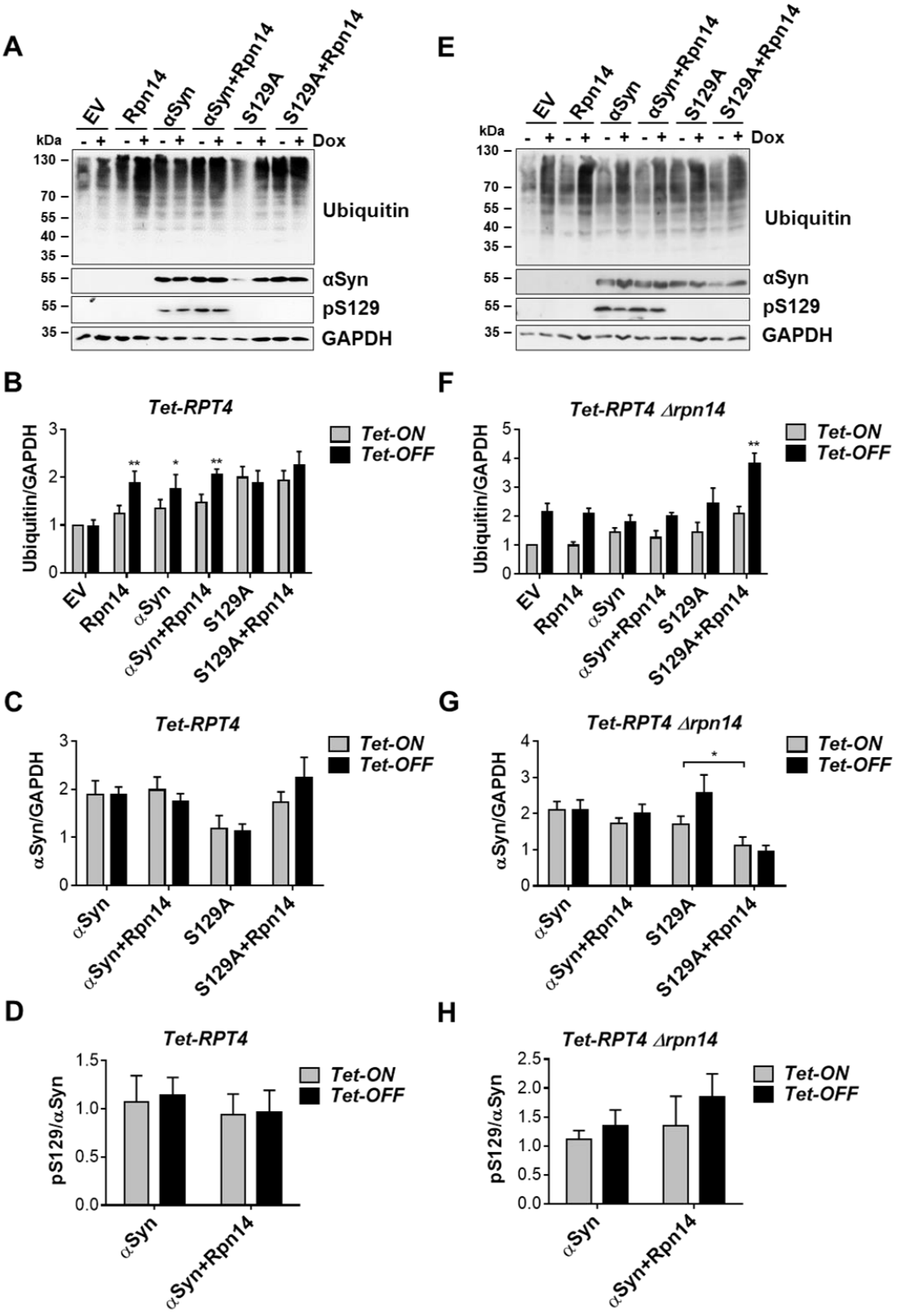

Figure 16. Expression of αSyn and high level of Rpn14 upon downregulation of *Tet-RPT4* leads to accumulation of ubiquitinated proteins in yeast cells.
(A) Immunoblot analysis of *Tet-RPT4* strain harbouring *GPD*-driven *RPN14* from *CEN* plasmid and *GAL1*-driven αSyn-GFP, S129A-GFP or empty vector (EV) control plasmids. Yeast cells were grown overnight in a galactose-containing medium to

induce αSyn expression. The *Tet* promoter was downregulated by addition of 10 µg/mL doxycycline (Dox) to the growth medium. Immunoblotting analysis was performed with ubiquitin, αSyn and pS129 antibodies. GAPDH was used as a loading control. (B) Densitometric analysis of the immunodetection of the ubiquitin conjugates in *Tet-RPT4* strain relative to the GAPDH control. The significance of differences was calculated with a *t*-test relative to EV control (*, $p < 0.05$; **, $p < 0.01$). (C) Densitometric analysis of αSyn protein levels from *Tet-RPT4* (A) relative to the GAPDH loading control. (D) Densitometric analysis of phosphorylated fractions of αSyn protein levels from *Tet-RPT4* strain (A) to αSyn. The level of αSyn, phosphorylated at S129 was probed using a specific antibody that recognizes only the phosphorylated form of the protein (pS129). (E) Immunoblot analysis of *Tet-RPT4 Δrpn14* strain harbouring *RPN14* and *GAL1*-driven αSyn-GFP, S129A-GFP and empty vector (EV) control plasmid, performed as in (A). (F) Densitometric analysis of the immunodetection of the ubiquitin conjugates in *Tet-RPT4 Δrpn14* strain relative to the GAPDH control. The significance of ubiquitin/GAPDH ratio was calculated with a *t*-test relative to EV control (**, $p < 0.01$). (G) Densitometric analysis of αSyn protein levels from *Tet-RPT4 Δrpn14* (E) relative to the GAPDH loading control. The significance of differences was calculated with a *t*-test (*, $p < 0.05$). (H) Densitometric analysis of phosphorylated fractions of αSyn protein levels from *Tet-RPT4 Δrpn14* strain (E) to αSyn. The level of αSyn, phosphorylated at S129 was probed using a specific antibody that recognizes only the phosphorylated form of the protein (pS129).

3.3.8.3. Downregulation of *RPT6* decreases turnover of phosphorylated α-synuclein

Lastly, changes in ubiquitin pool and αSyn turnover were examined in *Tet-RPT6* and *Tet-RPT6 Δrpn14* background strains. Rpn14 binds to the C-terminal basic residues of the Rpt6 base unfoldase subunit with high affinity relocating it to α-subunits of the core particle (Ehlinger *et al*, 2013; Kim *et al*, 2010).

Yeast *Tet-RPT6* strain was transformed with 2 µm plasmids, harboring αSyn-GFP, S129A-GFP or an empty vector. Rpn14 was expressed from a low copy plasmid or a native promoter. αSyn expression was induced in galactose-containing medium and the cells were incubated in absence or presence of doxycycline for downregulation of *Tet-RPT6* overnight. The levels of ubiquitin conjugates were analyzed by immunoblotting (Figure 17A).

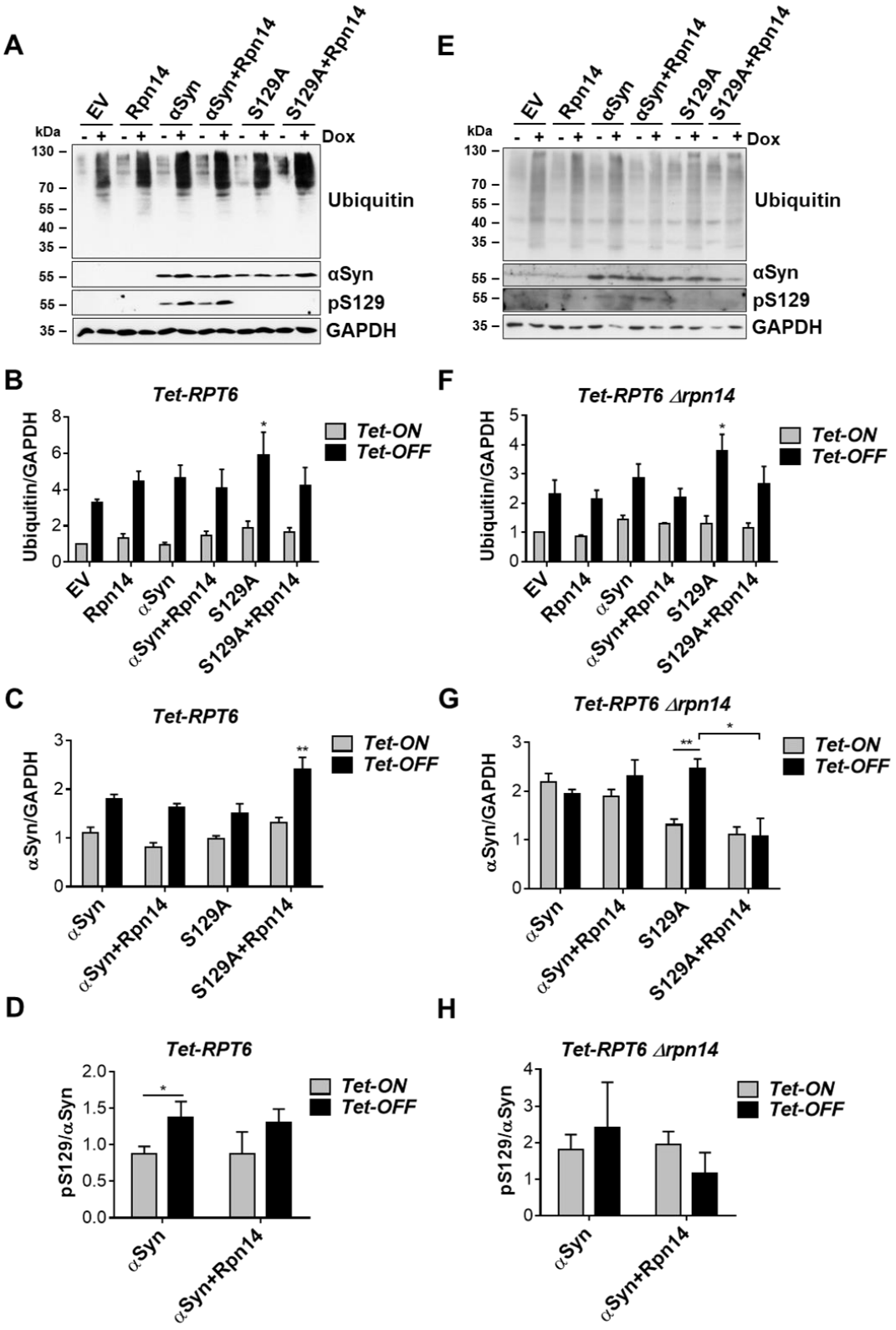

Figure 17. Downregulation of *Tet-RPT6* leads to accumulation of ubiquitin conjugates in yeast cells.

(A) Immunoblot analysis of *Tet-RPT6* strain harbouring Rpn14 and *GAL1*-driven αSyn-GFP, S129A-GFP and empty vector (EV) control plasmids. Yeast cells were grown overnight in a galactose medium to induce αSyn expression. The *Tet* promoter was downregulated by addition of 10 μg/mL doxycycline (Dox) to the growth medium.

Immunoblotting analysis was performed with ubiquitin, αSyn and pS129 antibodies. GAPDH was used as a loading control. (B) Densitometric analysis of the immunodetection of the ubiquitin conjugates in *Tet-RPT6* strain relative to the GAPDH control. The significance of ubiquitin/GAPDH ratio was calculated with a *t*-test relative to EV control (*, $p < 0.05$). (C) Densitometric analysis of αSyn protein levels from *Tet-RPT6* (A) relative to the GAPDH loading control. The significance of αSyn/GAPDH ratio was calculated with a *t*-test relative to EV control (**, $p < 0.01$). (D) Densitometric analysis of phosphorylated fractions of αSyn protein levels from *Tet-RPT6* strain (A) to αSyn. The level of αSyn, phosphorylated at S129 was probed using a specific antibody that recognizes only the phosphorylated form of the protein (pS129). Significance of differences was calculated with *t*-test (*, $p < 0.05$). (E) Immunoblot analysis of *Tet-RPT6 Δrpn14* strain harbouring Rpn14 and *GAL1*-driven αSyn-GFP, S129A-GFP and empty vector (EV) control plasmid performed equally to (A). (F) Densitometric analysis of the immunodetection of the ubiquitin conjugates in *Tet-RPT6 Δrpn14* strain relative to the GAPDH control. The significance of ubiquitin/GAPDH ratio was calculated with a *t*-test relative to EV control (*, $p < 0.05$). (G) Densitometric analysis of αSyn protein levels from *Tet-RPT6 Δrpn14* (E) relative to the GAPDH loading control. The significance of ubiquitin/GAPDH ratio was calculated with a *t*-test (*, $p < 0.05$; **, $p < 0.01$). (H) Densitometric analysis of phosphorylated fractions of αSyn protein levels from *Tet-RPT6 Δrpn14* strain (E) to αSyn. The level of αSyn, phosphorylated at S129 was probed using a specific antibody that recognizes only the phosphorylated form of the protein (pS129).

The levels of ubiquitin conjugates were not changed when *Tet-RPT6* was expressed, both in absence or presence of αSyn, S129A or Rpn14 expression (Figure 17A, B). In contrast to *Tet-RPT2* and *Tet-RPT4,* accumulation of ubiquitinated proteins occurred in the empty vector control, when the proteasome base subunit gene *RPT6* was downregulated. The downregulation of *Tet-RPT6* led to a slight increase in the pool of ubiquitinated proteins when αSyn and S129A were expressed, and under elevated level of Rpn14, but only upon expression of S129A the difference was significant in comparison to empty vector control. A significant increase in αSyn level was observed upon co-expression of S129A and *RPN14* under downregulation of *Tet-RPT6.* Downregulation of *Tet-RPT6* resulted in a significant increase of phosphorylated fraction of αSyn (Figure 17C, D).

The pattern of accumulation of ubiquitin conjugates observed in *Tet-RPT6 Δrpn14* was similar to *Tet-RPT6* (Figure 17E, F). Similar to *Tet-RPT2 Δrpn14* and *Tet-RPT4 Δrpn14,* downregulation of *Tet-RPT6 Δrpn14* resulted in increase of ubiquitin conjugates under downregulation of the base subunit in empty vector control and expression of αSyn and Rpn14 did not increased the levels of ubiquitinated proteins in comparison to empty vector. Observed changes in the levels of αSyn were comparable

to *Tet-Rpt4,* where the level of S129A was increased upon downregulation of *RPT6* and again no changes in pS129 αSyn were detected (Figure 17G, H). These results support the findings that elevated levels of Rpn14 inhibit the turnover of phosphorylated αSyn. Furthermore, the results indicate distinct cellular responses to the expression of Rpn14 and αSyn upon depletion of the three base subunits Rpt2, Rpt4 or Rpt6.

3.3.8.4. Elevated protein levels of Rpn14 upon downregulation of *RPT2* and *RPT4* is deleterious for yeast cells

Immunoblotting analysis revealed that high level of proteasome chaperon Rpn14 as well as expression of αSyn strongly inhibit the degradation of ubiquitin conjugates upon downregulation of *Tet-RPT2,* and to a lesser extend *Tet-RPT4* or *Tet-RPT6.* This deleterious effect on cells was further examined in growth assays employing *Tet*-strains used for the immunoblot analysis (Figure 18).

Yeast cells, expressing αSyn, S129A or *RPN14* were spotted on glucose (αSyn-*OFF*) or galactose (αSyn-*ON*) containing plates, in presence or absence of doxycycline that downregulates the *Tet*-promoter. In all *Tet*-strain backgrounds with intact *RPN14* gene, the observed growth impairment upon expression of αSyn was more severe than upon expression of S129A (Figure 18A). Downregulation of each of the three genes in presence of αSyn or S129A resulted in synthetic-sick phenotype. Furthermore, strong growth impairment was observed due to elevated protein level of Rpn14 upon downregulation of *Tet-RPT2* and *Tet-RPT4*. High level of Rpn14 did not affect yeast growth upon downregulation of *Tet-RPT6.* The results corroborate the immunoblot analysis data where the strongest effect of elevated level of Rpn14 was observed in *Tet-RPT2* background and less in *Tet-RPT4* and *Tet-RPT6* backgrounds.

Growth assays in *Tet-RPT2 Δrpn14*, *Tet-RPT4 Δrpn14* and *Tet-RPT6 Δrpn14* revealed a strong synthetic-sick phenotype upon downregulation of each of the three genes (Figure 18B). Growth on galactose-containing plates resulted in very severe synthetic-lethal phenotype by downregulation of the *Tet*-promoter.

These results further demonstrate that yeast cells are highly sensitive to changed protein levels of Rpn14 and downregulation of the base subunit genes, indicating that

controlled normal protein levels of the Rpn14 chaperone are important for cellular well-being upon proteasome stress conditions.

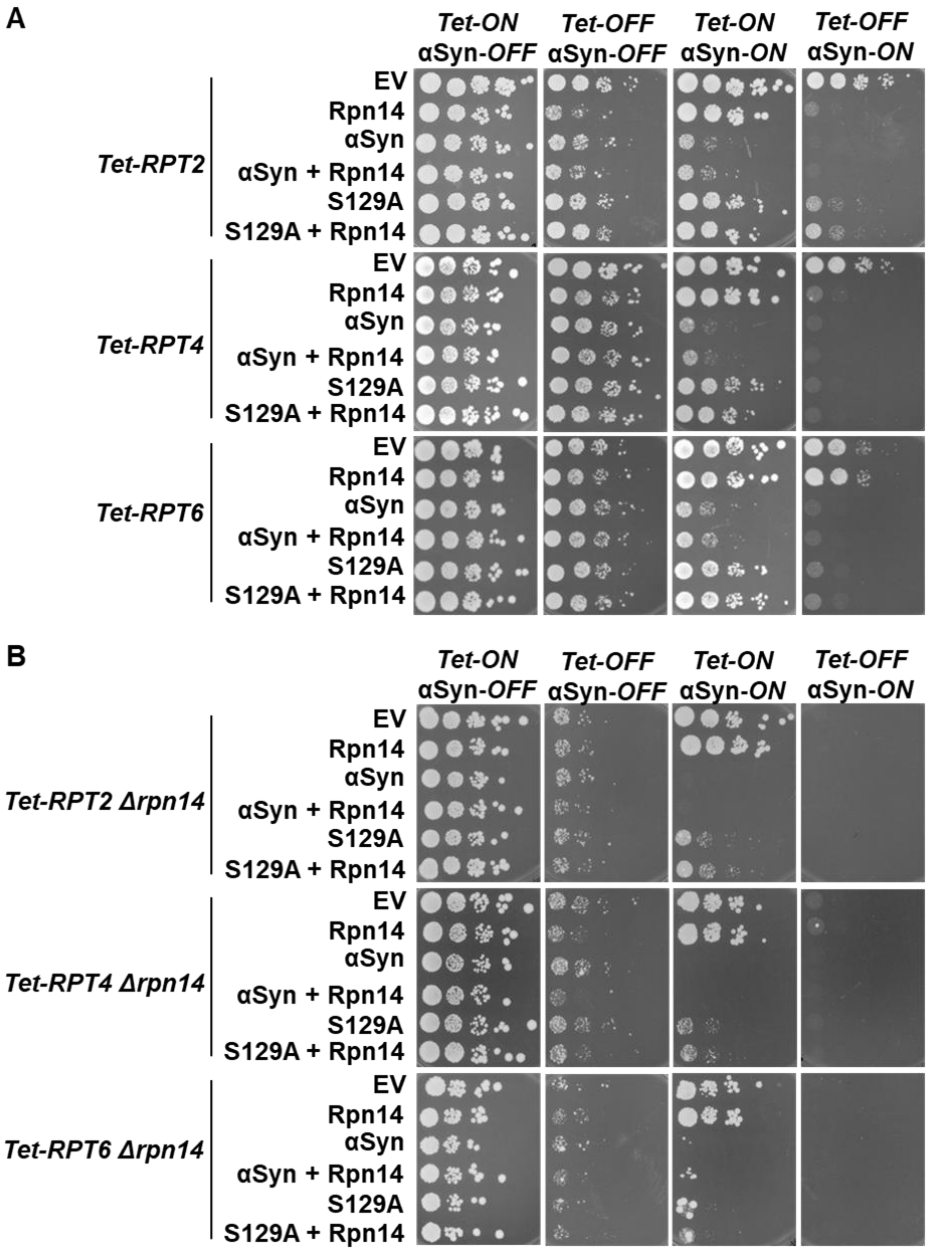

Figure 18. High level of Rpn14 causes growth impairment in *Tet-RPT2* and *Tet-RPT4* yeast strains and upon downregulation of *Tet-RPT4 Δrpn14.*
(A) Growth assays of yeast cells expressing *GPD*-driven *RPN14* from *CEN* plasmid and *GAL1*-driven αSyn or S129A from 2 µ plasmid with an empty vector (EV) as a control in *Tet-RPT2*, *Tet-RPT4* and *Tet-RPT6* yeast strains. (B) Growth assays of yeast cells expressing *GPD*-driven *RPN14* from *CEN* plasmid and *GAL1*-driven αSyn or S129A from 2 µ plasmid with an empty vector (EV) as a control in *Tet-RPT2 Δrpn14*, *Tet-RPT4 Δrpn14* and *Tet-RPT6 Δrpn14* yeast strains. Cells were spotted in 10-fold dilutions on selective plates containing glucose (αSyn-*OFF*) or galactose (αSyn-*ON*), in the presence (*Tet-OFF*) or absence (*Tet-ON*) of 2 µg/mL doxycycline to repress the *Tet*-promoter. The plates were incubated at 30°C for 6 days.

3.3.9. Expression of α-synuclein and increased Rpn14 protein levels result in decreased 26S activity

The 26S proteasomal degradation is an active, ubiquitin-dependent process. This degradation pathway is ATP-dependent, in which substrate proteins are tagged with a ubiquitin chain by a cascade of three different types of enzymes. This enables the proteins recognition and proteolysis by 26S proteasome. The 26S proteasome consist of 19S regulatory particle, which identifies the substrates, and 20S core particle, which has a proteolytic activity. Therefore, the 20S can degrade proteins without the assistance of the 19S regulatory particle in an unspecific, ubiquitin-independent degradation process (Ben-Nissan & Sharon, 2014; Goldberg, 2003; Schmidt *et al*, 2005; Schwartz & Ciechanover, 1999).

Overexpression of *RPN14* or *NAS6* results in a decrease of 26S proteasomal activity and increase of 20S activity presumably because the 26S proteasome is not efficiently assembled (Shirozu *et al*, 2015). This report showed that free 20S CP and free 19S RP levels are increased in yeast cells which suggests that high levels of Rpn14 or Nas6 inhibit the association between CP and RP. Therefore, the effect of elevated levels of Rpn14 on the proteasomal activity and its interplay with αSyn and S129A variant expression was determined. The proteasomal activity was measured using the fluorogenic peptide Succinyl-Leu-Leu-Val-Tyr-7-amido-4-methylcoumarin (Suc-LLVY-AMC). This peptide is a fluorogenic substrate for chymotrypsin-like proteases. Cleavage of the AMC peptide by the 26S proteasome releases the AMC fluorophore and its fluorescence intensity can be measured.

The degradation of the fluorogenic peptide was measured by continuously monitoring the fluorescence of the reaction. The assay was performed in a protein extraction buffer supplemented with 2 mM ATP. ATP is required for stable interaction between the 20S CP and 19S RP. Therefore, the cell extracts were prepared in the presence of 2 mM ATP to keep 26S proteasomes intact. Low concentration of SDS was used as artificial activator of 20S proteasomes that are typically latent in cells (Tanahashi *et al*, 2000).

The impact of Rpn14 and expression of αSyn or S129A on 26S and 20S proteasomal activity was examined in wild type yeast strain as well as *RPN14* deletion strain. First, the proteasomal activities were measured in total protein extracts (Figure 19). The rate

of fluorescence increase was monitored for 25 minutes. The linear slope values represent the proteasomal activity of each sample (Figure 19C, E). Crude protein extracts, treated with the proteasome inhibitor MG132 as a control prior to the measurements revealed that the kinetic assay is specific for proteasome cleavage (Figure 19A, B). Significant decrease of the 26S proteasomal activity was observed upon expression of αSyn as well as upon *RPN14* expression in wild type yeast strain. Both proteins decreased 26S proteasomal activity to similar level and no synergistic effect was observed. In contrast, no significant decrease in 26S proteasomal activity was found upon expression of S129A. Co-expression of *RPN14* and S129A reduced the 26S activity, indicating that the major role for the 26S proteasome inhibition is due to elevated Rpn14 protein levels.

Measurements of the 20S proteasomal activity were performed in presence of 0,025% SDS. No change of the 20S proteasomal activity was observed regardless expression of αSyn, S129A or Rpn14 (Figure 19E, F).

The 26S proteasomal activity was measured in *RPN14* deletion strain, in presence or absence of αSyn, S129A or plasmid-borne *RPN14* expression (Figure 20A, B). Differences in 26S proteasomal activity were not observed. However, increased activity of 20S proteasome was detected upon αSyn expression in this genetic background (Figure 20C, D). These results reveal that αSyn does not affect 26S proteasomal activity, when *RPN14* is absent and support that Rpn14 functions as mediator for αSyn-induced proteasome inhibition.

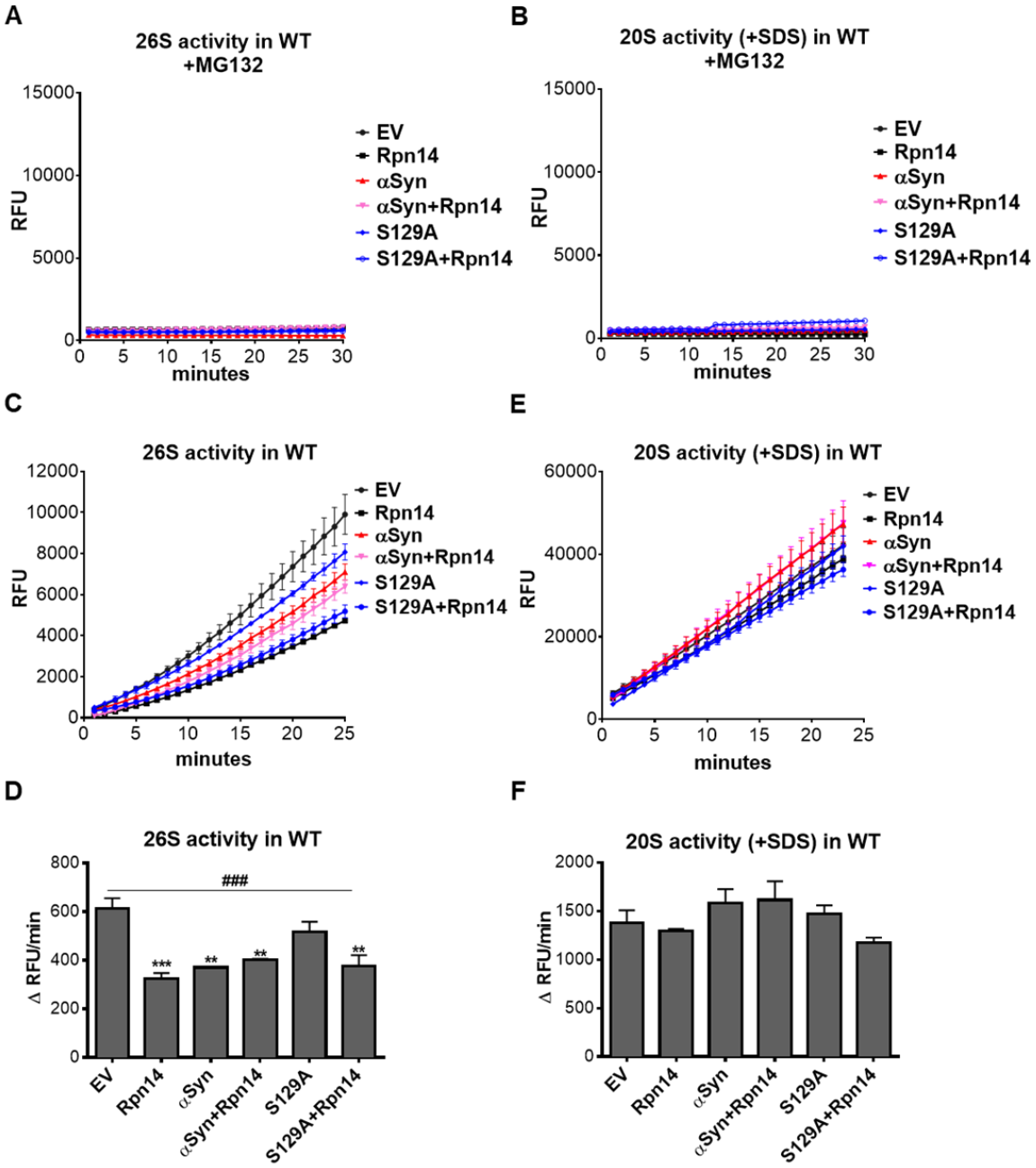

Figure 19. Expression of αSyn and elevated level of Rpn14 decrease 26S proteasomal activity in wild type yeast strain.
(A) Wild type yeast cells (BY4741) expressing *GPD*-driven *RPN14* from *CEN* plasmid and *GAL1*-driven αSyn or S129A from 2 μ plasmid with an empty vector (EV) as a control were collected after 6 hours of αSyn induction. The 26S proteasomal activity in total protein extracts was measured using Suc-LLVY-AMC by detecting relative fluorescence units (RFU). The assay was performed in a protein extraction buffer supplemented with 2 mM ATP. Crude protein extracts were treated with 100μM proteasome inhibitor MG132 as a control. (B) The crude protein extracts from (A) were complemented additionally with 0.025% SDS as artificial activator of 20S proteasomes and again with MG132 as a control. The 20S proteasomal activity in total protein extracts was measured using Suc-LLVY-AMC by detecting relative fluorescence units (RFU). (C) The 26S proteasomal activity in total protein extracts from (A) was

measured using Suc-LLVY-AMC by detecting relative fluorescence units (RFU). The assay was performed in a protein extraction buffer supplemented with 2 mM ATP. (D) Mean slope values of the curves from (C) reflect the relative proteasomal activity. Significance of differences was calculated with t-test versus EV (**, $p < 0.01$; ***, $p < 0.001$; n=4). (E) The yeast cells from (A) were treated additionally with 0.025% SDS as artificial activator of 20S proteasomes. The 20S proteasomal activity in total protein extracts was measured using Suc-LLVY-AMC by detecting relative fluorescence units (RFU). (F) Mean slope values of the curves from (E).

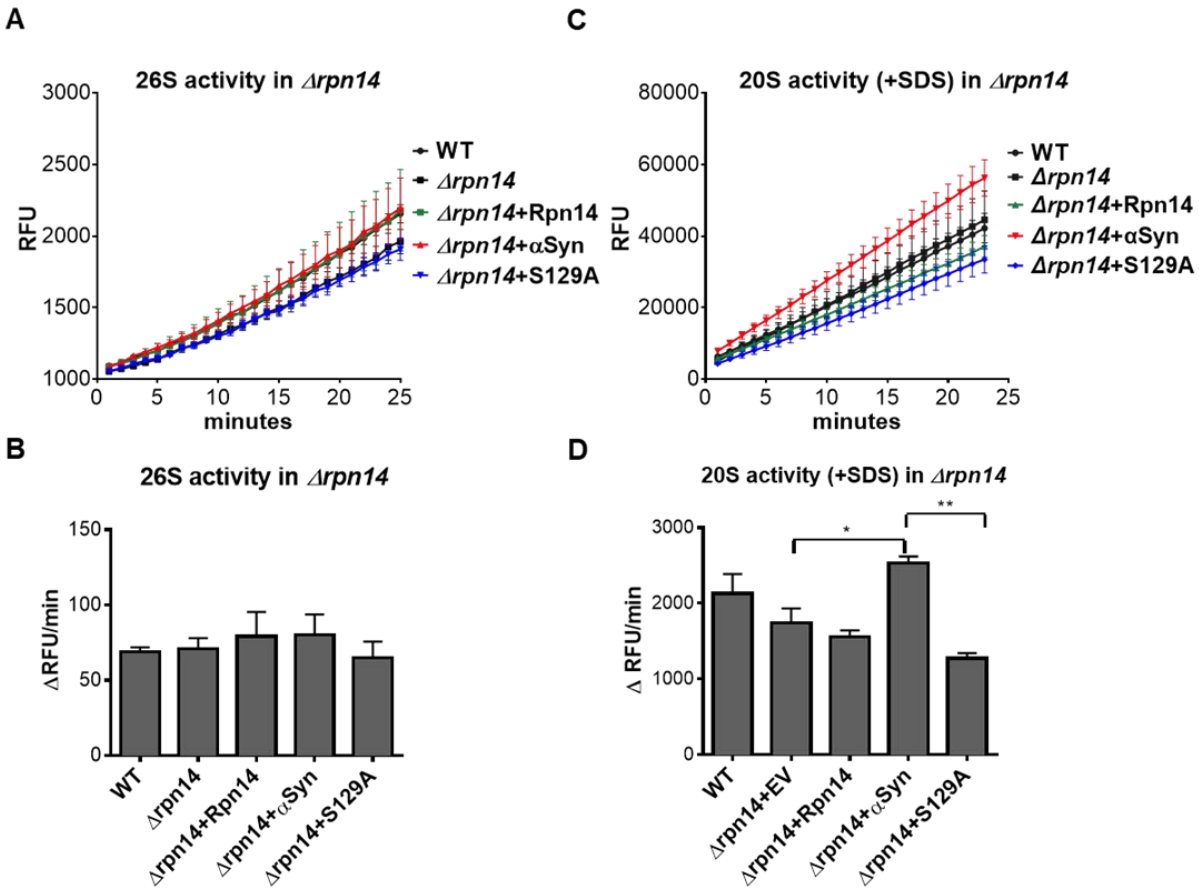

Figure 20. Expression of αSyn increases 20S proteasomal activity in *Δrpn14* yeast strain.
(A) RPN14 deletion strain expressing *GPD*-driven *RPN14* from *CEN* plasmid and *GAL1*-driven αSyn or S129A from 2 µ plasmid with an empty vector (EV) as a control were collected after 6 hours of αSyn induction. The 26S proteasomal activity in total protein extracts was measured using Suc-LLVY-AMC by detecting relative fluorescence units (RFU). The assay was performed in a protein extraction buffer supplemented with 2 mM ATP. (B) Mean slope values of the curves from (A) reflect the relative proteasomal activity. (C) The yeast cells from (A) were complemented additionally with 0.025% of SDS as artificial activator of 20S proteasomes. The 20S proteasomal activity in total protein extracts was measured using Suc-LLVY-AMC by detecting relative fluorescence units (RFU). (D) Mean slope values of the curves from (C). Significance of differences was calculated with t-test (*, $p < 0.05$; **, $p < 0.01$, n=4).

A second experimental approach for proteasomal activity measurements was applied. 26S and 20S proteasomes were separated by glycerol gradient centrifugation of cell extracts from strains expressing αSyn, S129A or control upon different levels of Rpn14 (Figure 21). Equal amounts of crude protein extracts were separated into 20 fractions by 8-32% glycerol gradient centrifugation. Proteasomal activity measurements were performed with the collected fractions from wild type strain with intact *RPN14* and *RPN14* deletion strain. 20S proteasomal activity was detected in fractions 1 - 4, and 26S - in fractions 7 - 12. 20S activity could be monitored after addition of 0,025% SDS. Elevated level of Rpn14 as well as expression of αSyn decreased the 26S proteasomal activity. Increase in 20S proteasomal activity was again observed upon expression of αSyn in *Δrpn14* background. The results suggest that αSyn decreases the proteasomal activity of yeast cells by increasing the stability of Rpn14 chaperone.

3.4. Toxicity of α-synuclein is enhanced in absence of the Rpn11 deubiqitinase

Expression of αSyn has a significant effect on the accumulation of ubiquitinated proteins in yeast. αSyn diminishes the pool of ubiquitin conjugates upon downregulation of *Tet-RPN11.* Rpn11 is a deubiquitinase which detaches K-48 polyubiquitinated substrates of the 26S proteasome which acts as a modulator of αSyn toxicity. Downregulation of *RPN11* enhances αSyn toxicity and aggregation which results in synthetic-sick phenotype (Popova *et al*, 2021a). Therefore, we assessed the impact of downregulation of *RPN11* on αSyn turnover and the role of phosphorylation at S129 on the interplay between αSyn and Rpn11 on proteasomal degradation (Figure 22 and Figure 4).

Growth assays were performed to study if enhanced αSyn toxicity upon downregulation of *Tet-RPN11* is linked to phosphorylation of αSyn at serine 129. Therefore, yeast cell growth was compared when αSyn or S129A were expressed upon depletion of Rpn11. Equal effects of expression of αSyn or S129A on yeast cell growth was observed. Both αSyn and S129A led to enhanced growth retardation when *Tet-RPN11* was downregulated, resulting in synthetic sick phenotype (Figure 22B).

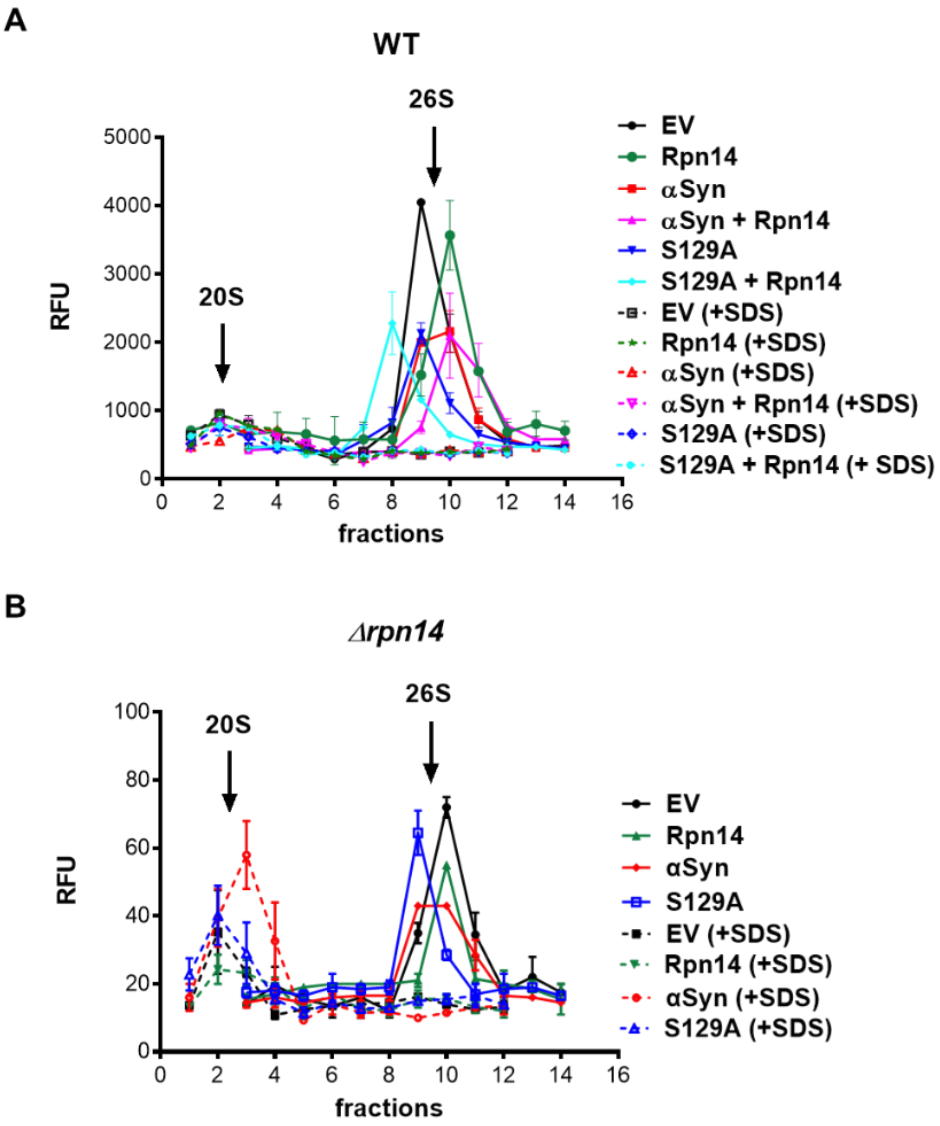

Figure 21. Expression of αSyn and high level of Rpn14 inhibit the 26S activity in yeast.

(A) Crude protein extracts from wild type yeast cells expressing *GPD*-driven *RPN14* from *CEN* plasmid and *GAL1*-driven αSyn or S129A from 2 μ plasmid with an empty vector (EV) as a control were prepared after 6 hours of αSyn induction and 2 μg of the proteins were separated into 20 fractions by 8-32% glycerol gradient centrifugation. The fractions were assayed for Suc-LLVY-MCA hydrolyzing activity simultaneously with and without 0.025% SDS to measure the activities of 26S and 20S proteasomes. Values represent the mean ± SEM of two independent experiments. (B) The procedure from (A) was applied to measure the proteasomal activity of 26S and 20S in *RPN14* deletion strain.

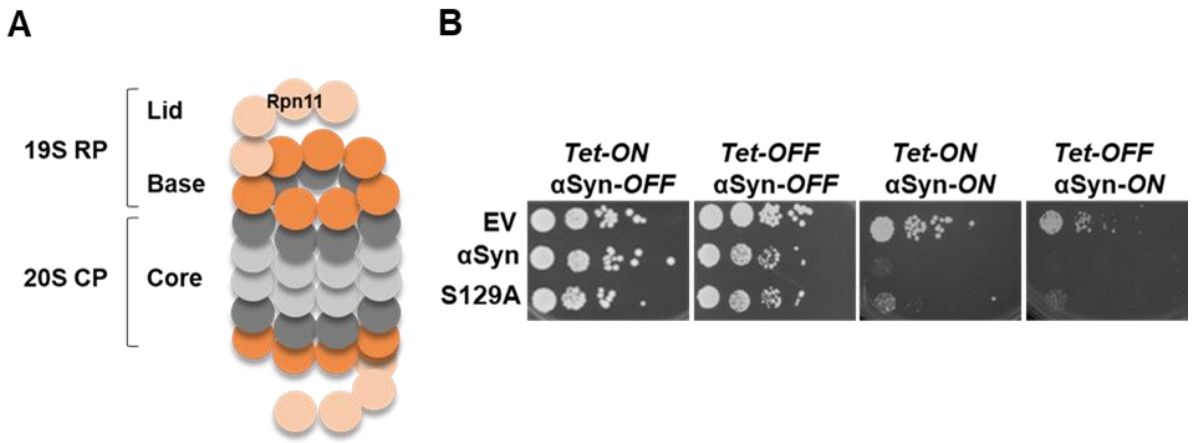

Figure 22. Downregulation of *RPN11* enhances αSyn toxicity in yeast.
(A) Schematic diagram depicting Rpn11 as a part of 19S RP where it acts as metalloisopeptidase of the lid. Rpn11 removes K48 polyubiquitin residues from substrates to be degraded by the 26S proteasome. (B) Growth assay of yeast cells expressing *GAL1*-driven αSyn or S129A and empty vector control (EV) in *Tet-RPN11* yeast strain. Cells were spotted in 10-fold dilutions on selective plates containing glucose (αSyn-*OFF*) or galactose (αSyn-*ON*) in the presence (*Tet-OFF*) or absence (*Tet-ON*) of 10 µg/mL doxycycline to repress the *Tet* promoter. The plates were incubated at 30°C for 5 days.

3.4.1. *RPN11* expression is required for appropriate yeast cell morphology

Downregulation of *RPN11* enhances αSyn toxicity. *Tet-RPN11* strain was used for live cell fluorescence microscopy to visualize expression of αSyn-tFT within single cells in presence and absence of Rpn11. The impact of phosphorylation at S129 was assessed by expression of S129A variant or Y133F variant, which is deficient for phosphorylation or nitration. Modification of the C-terminal Y133 residue is required for S129 phosphorylation (Kleinknecht *et al*, 2016). Aberrant growth phenotypes were observed upon downregulation of *Tet-RPN11* in presence of αSyn or PTM variants (Figure 23A). Unipolar bud chains of 3 to 4 small buds, projecting from the mother cell were observed upon αSyn expression. Cells were stained with calcofluor white (CFW) to visualize chitin in septa of budding yeast cells. Septin rings were identified only by the mother cell. Percentage of the cell displaying the haploid adhesive growth did not differ among the αSyn variants (Figure 23B).

The cells were then stained with Hoechst and fluorescence microscopy was performed to investigate if nuclear division takes place in the yeast cells displaying the haploid adhesive growth after 24 hours induction of αSyn expression and *RPN11*

downregulation. Filaments with one nucleus were observed which indicates repeated rounds of budding without nuclear division (Figure 23C). These results suggest that Rpn11 is required for accurate control of the cell division cycle in presence of αSyn.

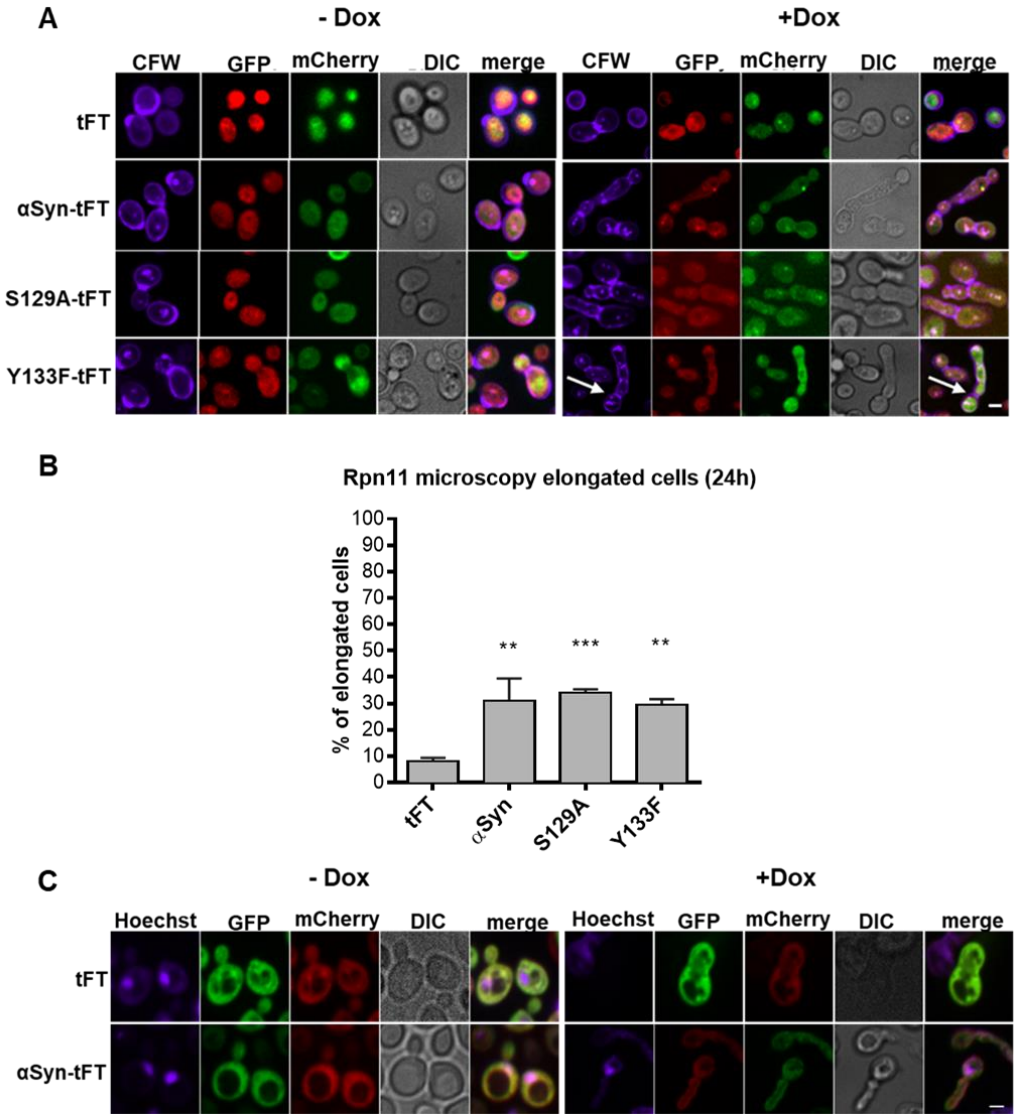

Figure 23. αSyn expression enhances haploid adhesive growth but inhibits nuclear division upon downregulation of *Tet-RPN11.*
(A) Live cell fluorescence microscopy of *Tet-RPN11* strain. Yeast cells expressing αSyn-tFT and its variants from *CEN* plasmids were grown for 24 hours in galactose-containing medium in absence or presence of 10 µg/mL doxycycline. Cells were stained with calcofluor white (CFW) to visualize septa of budding yeast cells. White arrows indicate septin rings. Scale bar: 1 µm. (B) Quantification of the percentage of cells displaying haploid adhesive growth after 24 hours induction in galactose-containing medium and treatment with 10 µg/ml doxycycline. Significance of differences was calculated with *t*-test relative to tFT control (**, p< 0.01; ***, p<0.001; n=100). (C) Fluorescence microscopy of *Tet-RPN11* strain. Yeast cells expressing αSyn-tFT from a *CEN* plasmid were grown for 24 hours in galactose-containing medium in absence or presence of doxycycline. Cells were stained with Hoechst to visualize nuclei of budding yeast cells. Scale bar: 1 µm.

3.4.2. The *RPN11* encoded isopeptidase destabilizes α-synuclein

Turnover of αSyn upon downregulation of *Tet-RPN11* was investigated with whole colony fluorescence measurements and flow cytometry (Figure 24). For both experiments yeast cells were grown in selective SC medium with raffinose overnight. For the whole colony measurements, overnight cultures were pinned on SC selective solid medium with 2% galactose as a carbon source to induce expression of αSyn-tFT, S129A-tFT or Y133F-tFT in *Tet-RPN11*. Additionally, the medium was supplemented with doxycycline for downregulation of *Tet-RPN11.* The cells were grown for 48 hours (Figure 24A). For the flow cytometry, the overnight cultures with raffinose were used for inoculation of the cells into SC selective liquid medium containing galactose for induction of the expression of αSyn-tFT, S129A-tFT or Y133F-tFT in *Tet-RPN11.* The cells were grown in the absence and presence of doxycycline for the downregulation of *Tet-RPN11* for 24 hours (Figure 24B). As control, *Tet-RPN11* yeast strain was transformed with an empty vector plasmid harboring tFT tag itself. Two tFT constructs were used, expressing fusion proteins with N-terminal degrons that have different rate of degradation, depending on the N-terminal amino-acid residue according to the N-end rule - arginine (unstable tFT) or tyrosine (stable tFT) (Khmelinskii *et al*, 2016). Afterwards, mCherry and sfGFP signals were measured for both experiments and ratios mCherry/GFP were calculated as a read-out for the turnover of αSyn-tFT, S129A-tFT and Y133F-tFT.

Increased stability of αSyn upon downregulation of *RPN11* was observed in both, whole colony and flow cytometry approaches. Downregulation of *RPN11* has a higher impact on αSyn stability in comparison to the control (tFT). Downregulation of the gene increased drastically the stability of αSyn, S129A or Y133F variants, whereas the stability of tFT was increased less. No differences in αSyn turnover upon downregulation of *Tet-RPN11* were observed between the αSyn variants. These results indicate that Rpn11 promotes degradation of αSyn and its variants.

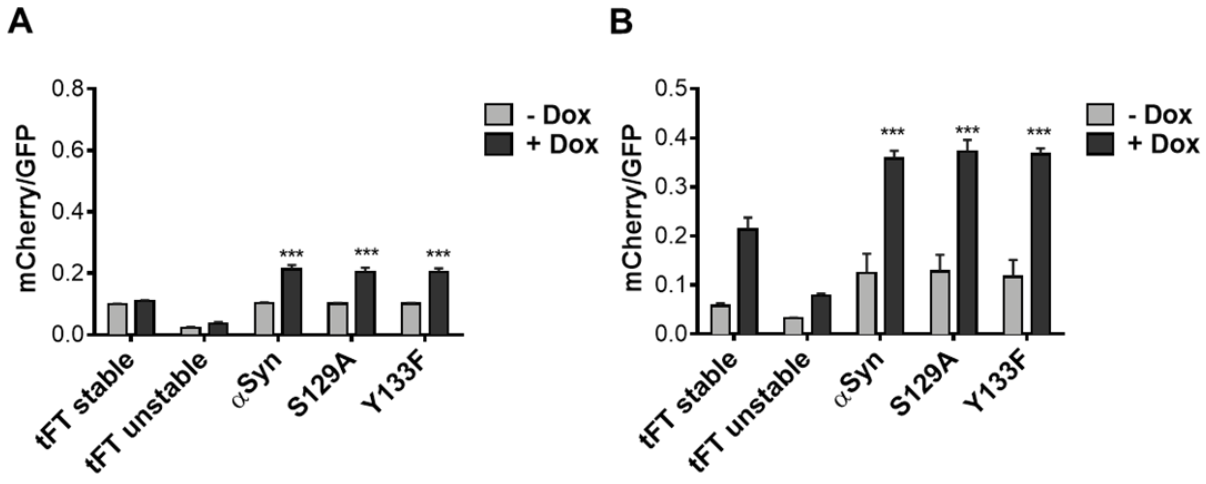

Figure 24. αSyn is stabilized in yeast cells upon downregulation of *Tet-RPN11* lid deubiqitinase.
(A) Whole colony measurements of the mCherry/sfGFP ratio after 48 hours yeast cells growth on a solid SC selective medium without or with 10 µg/ml doxycycline for downregulation of *Tet-RPN11*. Expression of αSyn-tFT, S129A-tFT or Y133F-tFT was induced by 2% galactose in the SC medium. Two tFT variants with different stabilities were used as controls. Significance of differences was calculated with t-test relative to tFT stable (EV-tFT) (***, $p < 0.001$). (B) Flow cytometry measurements of the mCherry/sfGFP ratio after 24 hours yeast cells growth with or without 10 µg/ml doxycycline in SC selective medium containing galactose for expression induction of αSyn-tFT, S129A-tFT or Y133F-tFT. Significance of differences was calculated with t-test relative to tFT stable (EV-tFT) (***, $p < 0.001$).

3.4.3. *RPN11* expression promotes proteasomal degradation of α-synuclein

Tandem fluorescent protein timer (tFT) fusions can be employed as a tool to monitor the contribution of the two major degradation pathways - autophagy and proteasome, to degradation of αSyn-tFT monomers *in vivo*. Processed tFT fragments can be used as a marker because of the incomplete proteasomal degradation sfGFP from the tFT that resists proteasomal degradation due to the stability of the GFP fold (Khmelinskii *et al*, 2016). Presence of 33 kDa band is an indicator of proteasomal degradation of tFT whereas 26 kDa band indicates a vacuolar degradation (Klionsky *et al*, 2021).
We followed the effect of αSyn PTMs on degradation pathways using immunoblotting analysis (Figure 25). Decreased proteasomal and vacuolar degradation of S129A-tFT was observed. Significant increase in 33 kDa band intensity was observed for Y133F-

tFT when compared to αSyn-tFT, which indicates that Y133F is preferentially cleared by the proteasome.

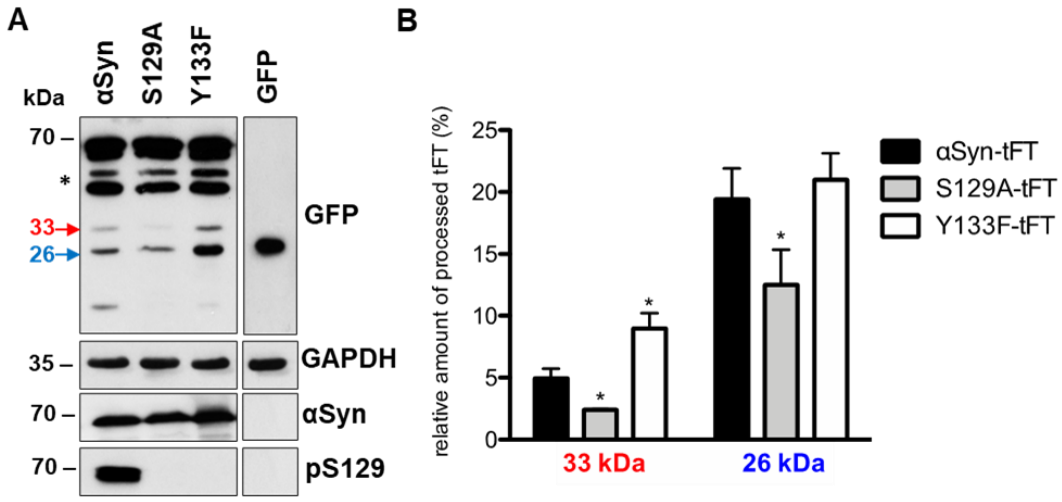

Figure 25. Tandem fluorescence timer monitoring reveals that phosphorylation at S129 promotes α-synuclein turnover in yeast.
(A) Immunoblotting analysis of tFT-tagged αSyn variants and GFP as control, probed with GFP antibody, αSyn antibody or S129 phosphorylation-specific αSyn antibody (pS129) and GAPDH antibody as loading control. Signal at 33 kDa indicates proteasomal and the 26 kDa autophagy/vacuole-mediated degradation products. Asterisks indicates an mCherryΔN product resulting from mCherry hydrolysis during cell extract preparation. (B) Quantification of the specific αSyn-tFT degradation products. The relative amount of tFT degradation fragments to the total amount of loaded protein within one lane was calculated. Significance of the differences was determined with a *t*-test relative to αSyn (*, p< 0.05; n = 3).

The above approach was applied to investigate an effect of *RPN11* expression on αSyn turnover more thoroughly (Figure 26). The expression level of *Tet-RPN11* was downregulated by addition of doxycycline to the growth medium. The yeast strain *Tet-RPN11* was transformed with αSyn-tFT, S129A-tFT or Y133F-tFT encoding plasmids. In a first approach, the degradation pathway of αSyn-tFT and its variants was followed using immunoblotting analysis by measurement of the band intensity of the degradation by-products after 6 hours of doxycycline treatment. A major 20 kDa degradation band was observed, along with faint 33 kDa and 26 kDa bands. The 20 kDa band was attributed to proteasomal activity, since accumulation of the processed tFT fragment in control cells, expressing tFT alone was significantly reduced in cells, where the proteasome processivity is impaired by Rpn11 depletion (Figure 26A, B).

Quantification of the intensity of the 20 kDa band revealed significant decrease upon downregulation of *Tet-RPN11* when αSyn was expressed. Less accumulation of processed tFT fragments upon *RPN11* downregulation was observed for S129A-tFT in comparison to αSyn-tFT. Immunoblot analysis with ubiquitin antibody did not reveal differences in the accumulation of ubiquitinated proteins. These results indicate higher impact of Rpn11 on pS129 αSyn than on S129A degradation.Immunoblot analysis was performed with the same strains as above after 24 hours treatment with doxycycline. No degradation bands 33 kDa, 20 kDa and 26kDa were observed at that time point. Immunoblot analysis with ubiquitin antibody revealed differences in the accumulation of ubiquitinated proteins in comparison to 6 hours treatment (Figure 26C, D). Densitometric analysis of the immunodetection of the ubiquitin conjugates was done. Accumulation of ubiquitinated proteins was observed after 24-hour downregulation of *RPN11*, in contrast to 6 hours of downregulation, which indicates that prolonged downregulation of *RPN11* inhibits protein turnover. These results corroborate previous findings and demonstrate that αSyn phosphorylated at S129 is preferentially degraded by the ubiquitin proteasome system.

3.5. Expression of α-synuclein effects proteasomal degradation in deletion *SEM1* mutant

Degradation of αSyn requires the presence of Rpn11 deubiquitinating enzyme which, in turn, requires another proteasome subunit, Sem1, for its stabilization (Figure 27A and Figure 4). Sem1 maintains the association of the lid and base subcomplexes of the regulatory particle (Funakoshi *et al*, 2004). Sem1 is required for stabilization of the Rpn11 deubiquitinating enzyme, incorporation of the ubiquitin receptor Rpn10 into the 19S regulatory particle and efficient 26S proteasome assembly (Kolog Gulko *et al*, 2018). Yeast deletion *SEM1* mutant accumulates polyubiquitinated proteins and is defective for proteasome mediated degradation (Funakoshi *et al*, 2004).

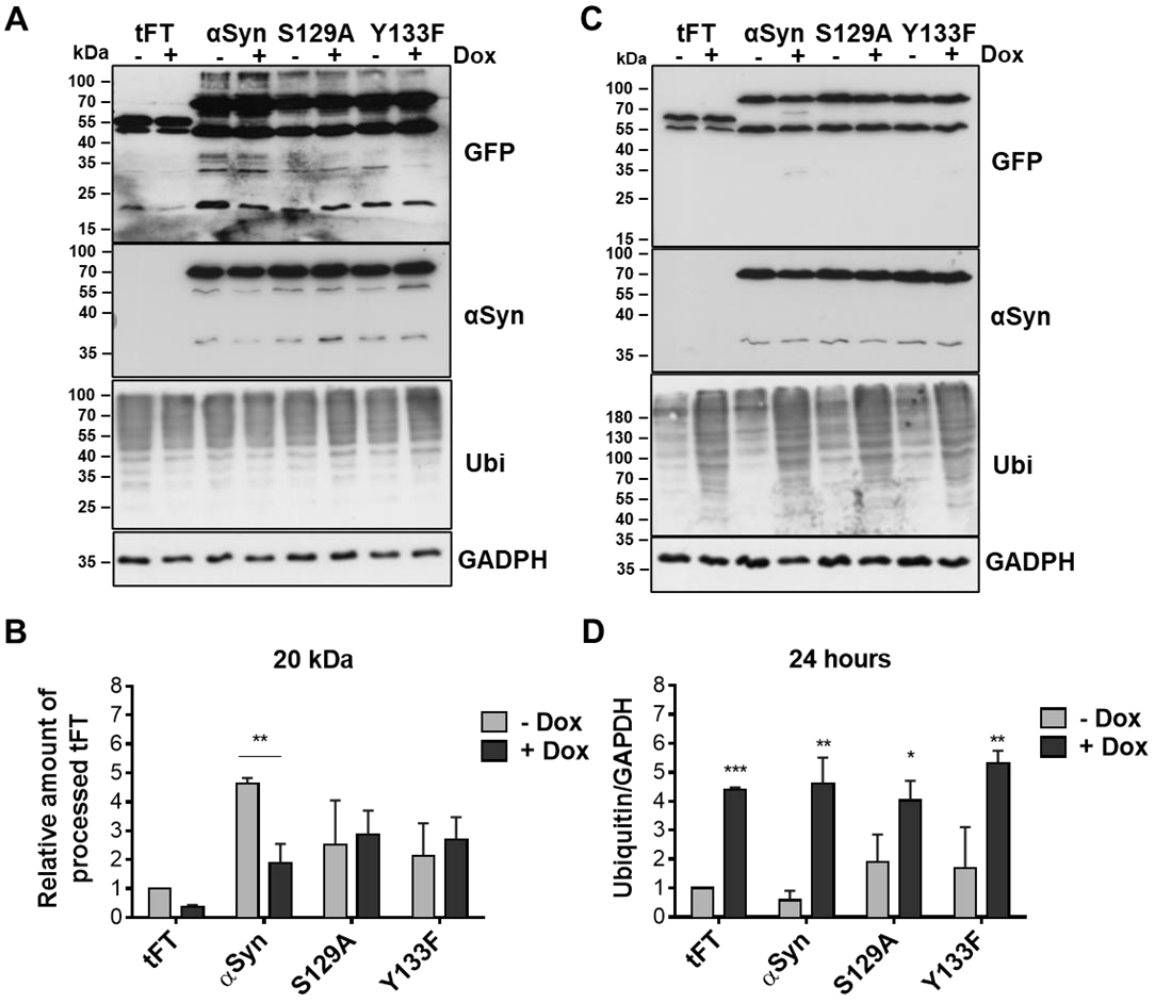

Figure 26. The Rpn11 deubiquitinase promotes degradation of α-synuclein phosphorylated at serine 129 in yeast.

(A) Immunoblotting analysis of yeast cells expressing αSyn-tFT, S129A-tFT and Y133F-tFT in *Tet-RPN11* strain. Expression of tFT alone was used as a control. Prior the analysis the expression of αSyn and its variants was induced in galactose containing medium for 6 hours. Simultaneously, the yeast cells were grown in parallel in presence and absence of 10 µg/ml doxycycline for 6 hours to downregulate *Tet* promoter. Immunoblotting analysis was performed with GFP, αSyn or ubiquitin (Ubi) antibodies. GAPDH antibody was used as a loading control. (B) Quantification of 20 kDa band intensity from the blot probed with GFP antibody. The values were normalized to tFT without doxycycline. Significance of differences was determined with a *t*-test relative to normalized values of corresponding variant without doxycycline (**, $p < 0.01$). (C) Immunoblotting analysis of yeast cells expressing αSyn-tFT, S129A-tFT, Y133F-tFT or tFT control in *Tet-RPN11* strain. The expression of αSyn and its variants was induced in galactose-containing medium for 6 hours. Cells were grown in parallel in presence and absence of 10 µg/ml doxycycline for 24 hours to downregulate the *Tet*-promoter. Immunoblotting analysis was performed with GFP, αSyn or ubiquitin (Ubi) antibodies. GAPDH antibody was used as a loading control. (D) Densitometric analysis of the immunodetection of the ubiquitin conjugates in *Tet-RPN11* strain relative to the GAPDH control. The significance of differences was calculated with a *t*-test (*, $p < 0.05$; **, $p < 0.1$; ***, $p < 0.001$).

Growth assay was performed to study whether deletion of *SEM1* has an impact on αSyn-induced toxicity. Wild type and yeast deletion *SEM1* mutant (*Δsem1*) expressing αSyn, S129A or EV as a control were used (Figure 27B). No effect of *Δsem1* on αSyn-induced growth retardation was observed, regardless αSyn variant, in comparison to wild type control, supporting that Sem1 function is independent of the cellular growth effects caused by αSyn.

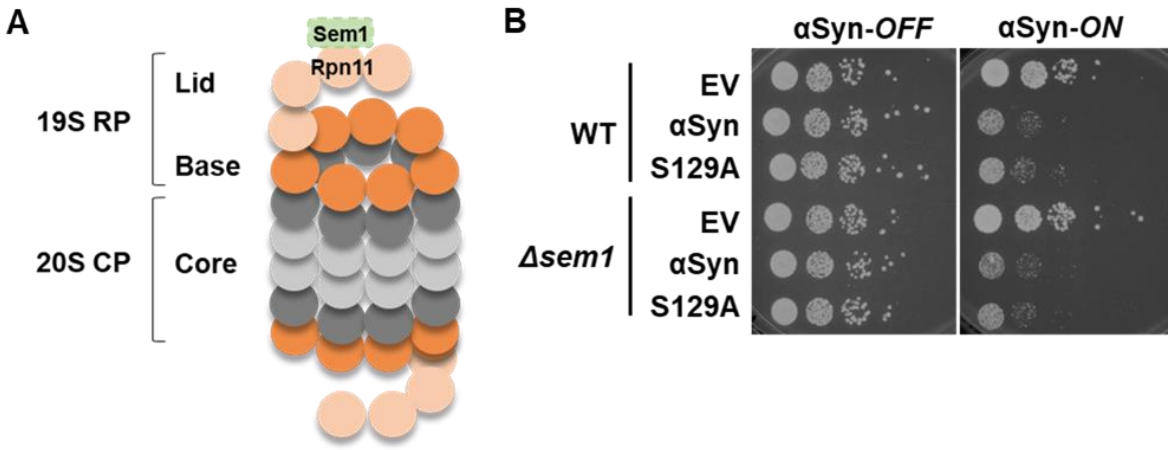

Figure 27. Deletion of *SEM1* does not affect αSyn-induced toxicity in yeast.
(A) Schematic diagram depicting Sem1 as a component of 19S RP where it maintains the association of the lid and the base subcomplexes of the regulatory particle. Sem1 is required for stabilization of Rpn11 deubiquitinase. (B) Growth assay of yeast cells expressing *GAL1*-driven αSyn or S129A and empty vector control (EV) in wild type (WT) and deletion *SEM1* (*Δsem1*) yeast strains. Cells were spotted in 10-fold dilutions on selective plates containing glucose (αSyn-*OFF*) or galactose (αSyn-*ON*). The plates were incubated at 30°C for 5 days.

For better understanding of the interplay between Rpn11 and αSyn turnover, the stability of αSyn-tFT and its variants S129A-tFT and Y133F-tFT was followed in presence and absence of Sem1. Wild type and deletion *SEM1* yeast strains were transformed with αSyn-tFT, S129A-tFT or Y133F-tFT. Expression of αSyn was induced for 6 hours or 24 hours prior to immunoblotting analysis (Figure 28).

Absence of Sem1 led to a different degradation pattern of αSyn-tFT after 6 hours of induction. The steady-state protein levels of αSyn-tFT and S129A-tFT were increased in absence of *SEM1* after 6 hours expression and decreased after 24 hours expression in *Δsem1* in comparison to *SEM1* background. Upon deletion of *SEM1* and 6-hour expression of αSyn-tFT and Y133F-tFT, increased accumulation of ubiquitinated proteins was detected. It was observed that *Δsem1* mutant accumulates ubiquitinated proteins similar to *RPN11* downregulation.

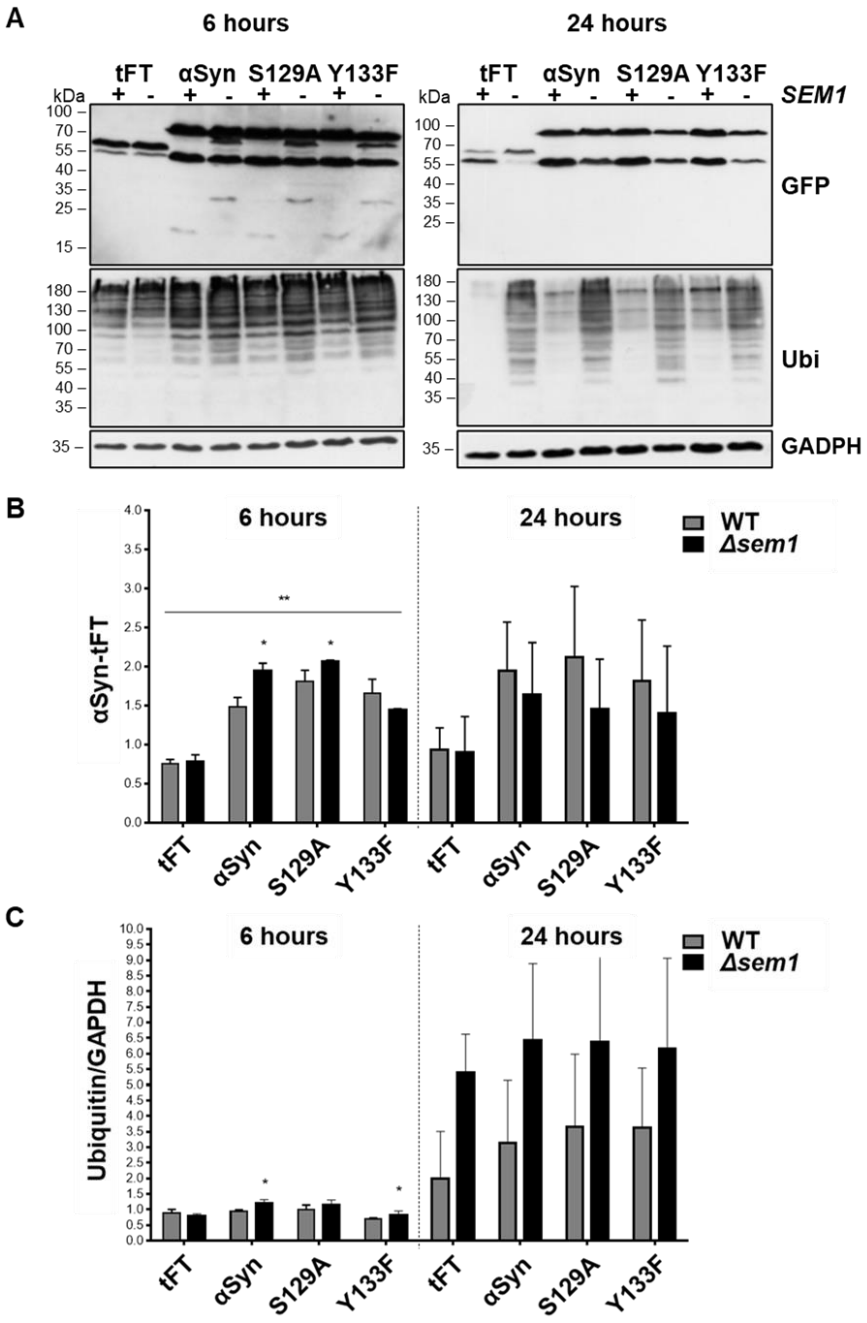

Figure 28. Deletion of *SEM1* affects αSyn turnover and the accumulation of ubiquitinated protein upon expression of αSyn.
(A) Immunoblotting analysis of yeast cells expressing αSyn-tFT, S129A-tFT or Y133F-tFT for 6 or 24 hours in wild type yeast strain (BY4741) (+) and *SEM1* deletion strain (-). Immunoblotting analysis was performed with GFP or ubiquitin (Ubi) antibodies. GAPDH antibody was used as a loading control. (B) Densitometric analysis of the immunodetection of GFP, derived from the tFT-tag to the GAPDH control. The significance of differences was calculated with *t*-test relative to tFT control (*, $p < 0.05$; **, $p < 0.1$). (C) Densitometric analysis of the immunodetection of the ubiquitin conjugates relative to the GAPDH control. The significance of differences was calculated with *t*-test (*$p < 0.05$).

These results demonstrate that Sem1 has a similar impact on the stability of αSyn and S129A, in contrast to Rpn11. This might be attributed to unspecific 20S protein degradation activity, since Sem1 is required for efficient 26S proteasome assembly and absence of Sem1 significantly increases the percentage of 20S proteasomes. This suggests that phosphorylation at S129 promotes the degradation by then26S proteasome, whereas degradation by the 20S activity is independent on pS129.

4. Discussion

α-Synuclein (αSyn) is a protein of presynaptic neurons that is genetically and neuropathologically associated with development of Parkinson's disease (PD). This work shows that αSyn disturbs protein homeostasis in cells by changing stability of proteins. It reveals a complex interplay between αSyn and proteasomal subunits. Expression of αSyn increases the stability of the proteasomal chaperone Rpn14. The study reveals that Rpn14 is a mediator of αSyn-induced 26S proteasome inhibition. Furthermore, it demonstrates that another proteasomal subunit, Rpn11 deubiquitinase, promotes degradation of αSyn.

With the aging population, a number of age-related neurodegenerative disorders are becoming a substantial public health problem. The improved hygiene and health care, healthier lifestyle, better nutrition and more advanced medical care in the developed and developing countries lead to increased life expectancy and fast-growing percentage of people older than 65 (Figure 29). Despite decades of extensive studies and resources invested in research and drug development, no curative treatments are available as most of the causative pathogenic factors are unknown. Therefore, research on human neurodegenerative diseases such as Parkinson's disease (PD) is emerging as an important topic.

αSyn protein is considered to be one of the most important factors in the PD’s pathogenesis. This small intrinsically unfolded neuronal protein of 140 amino acids is found in high concentrations at presynaptic terminals in a soluble form or in fractions bound to the membrane. In pathological conditions αSyn aggregates and accumulates in Lewy bodies, intracellular protein inclusions, which are linked to the selective loss of dopaminergic neurons in the *substantia nigra* in PD. The propensity of αSyn for aggregation can be altered by multiple factors, including its abundant posttranslational modifications.

Accumulation and aggregation of αSyn leads to defects in vesicle trafficking, impaired mitochondrial activity, cell membrane damage, proteasome dysfunction and aggregation of ubiquitinated proteins (Tenreiro *et al*, 2017; Cooper *et al*, 2006; Gitler *et al*, 2009, Gilter *et al*, 2008; Su *et al*, 2010; Soper *et al*, 2008; Zabrocki *et al*, 2008; Outeiro & Lindquist, 2003). Furthermore, it disrupts protein homeostasis, but the exact

mechanism of this process is not well understood. In this study, the effect of αSyn expression on protein stability was investigated in *Saccharomyces cerevisiae* as monitoring of these effects is much easier in this simple eukaryotic reference cell than in complex multicellular systems. Expression of αSyn in yeast leads to αSyn association with the plasma membrane in a highly selective manner and subsequent formation of cytoplasmic inclusions in a concentration-dependent process (Outeiro & Lindquist, 2003; Petroi *et al*, 2012). The cellular disorders in yeast mimic effects associated with αSyn accumulation in neuronal cells in PD (Menezes *et al*, 2015; Outeiro & Lindquist, 2003).

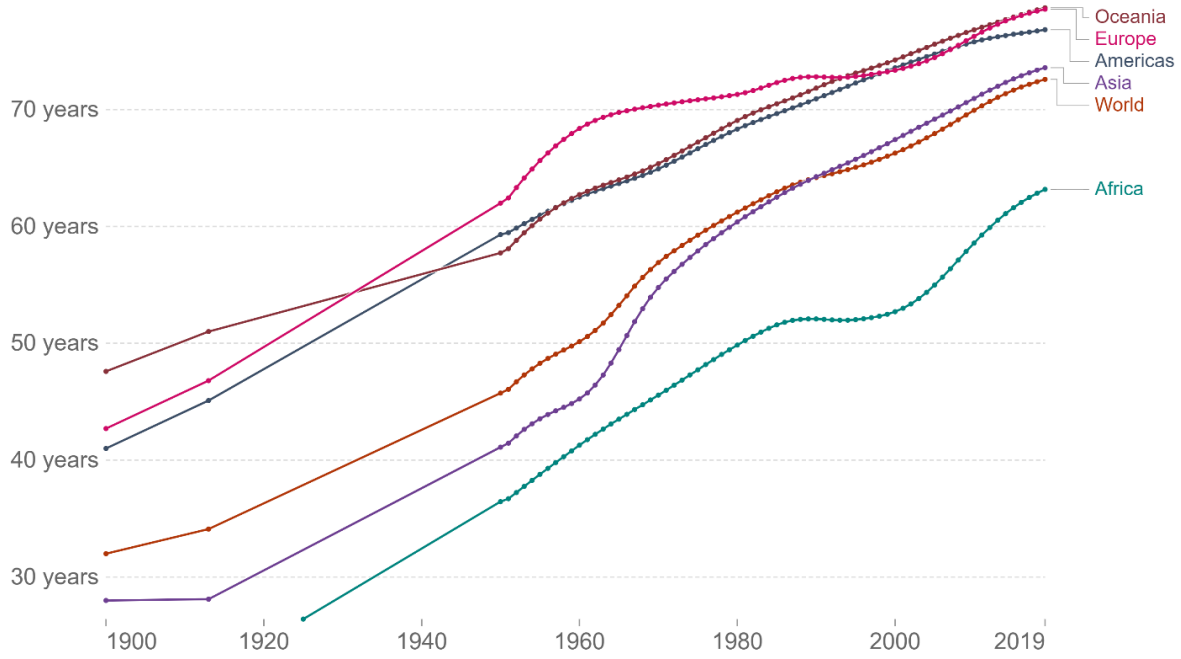

Figure 29. Rising life expectancy around the world (1900-2019).
The chart represents life expectancy at birth, which is defined as the average number of years newborns were expected to live if they were to pass through life subject to age-specific mortality rates over a defined period. It shows that the health transition began at varying times in different regions of the world. In contrast do developed regions, the life expectancy in Africa did not begin to increase until around 1920 and is lower up to the date (Riley, 2005; Zijdeman & Ribeira da Silva, 2015; Nations, 2019; retrieved from: 'https://ourworldindata.org/life-expectancy').

In this study, *Saccharomyces cerevisiae* was employed as a reference cell to examine the molecular mechanisms underlying αSyn induced toxicity and the role of phosphorylation at serine 129 (S129) as a major posttranslational modification of the protein. Proteasome is one of the pathways of αSyn degradation. Therefore, the

interplay between αSyn, the proteasome subunits, and proteasome interacting proteins was the subject of this study. Moreover, the role of S129 as a major posttranslational modification of αSyn, which affects degradation of the protein, was investigated (Figure 30).

4.1. Impact of α-synuclein expression on protein homeostasis

Proteostasis is crucial for the maintenance of cellular functions, which control protein synthesis, folding, translocation, and degradation. Impaired cellular proteostasis is associated with various neurodegenerative diseases, including Parkinson's disease (Lehtonen *et al*, 2019). Perturbation of protein homeostasis in PD can be directly caused by αSyn when imbalance between synthesis and degradation of the protein occurs, and indirectly by affecting other components of the proteostasis network.

αSyn in an aggregated form is a key component of Lewy bodies in the brain of PD patients and plays a crucial role in the disease progression (Poewe *et al*, 2017). Intracellular homeostasis of αSyn is maintained by endogenous regulatory mechanisms, including the ubiquitin-proteasome system (UPS) and the autophagy-lysosome pathway (ALP). ALP appears to be preferred degradation pathway over UPS in the removal of oligomeric forms of αSyn. The accumulation of αSyn is strongly linked to the impairment of these degradation mechanisms (Xilouri *et al*, 2013). Consequently, aberrant proteins are likely to perturb UPS mechanisms, directly or indirectly, and subsequently impair the function of related pathways, resulting in irreversible alterations in the homeostasis of neuronal proteins and degeneration (Cookson, 2009; Sato *et al*, 2018).

Tandem protein fluorescence is a novel technique to measure protein age and stability. It allows to discriminate between estimates of three types of protein populations which are either preferentially short-aged (visualized as green), medium-aged (visualized as yellow) or preferentially higher aged (visualized as red). In his work, tandem protein fluorescence measurement technique revealed that soluble fractions of αSyn phosphorylated at S129 residue is preferentially degraded by the proteasome. Therefore, phosphorylation of αSyn is involved directly in the maintenance of αSyn protein homeostasis. Expression of non-phosphorylated αSyn variant - S129A,

resulted in less significant changes in the yeast proteome, as it was shown in previous studies (Popova *et al*, 2021a).

The global effect of αSyn expression on protein homeostasis has not been thoroughly researched and was subject of this study. The impact of αSyn expression on protein stability was investigated in yeast. The high-throughput screen using the tandem fluorescence timer (tFT) yeast gene library revealed more significant impact of αSyn expression on the changes of protein stability, than S129A variant. Identified proteins with changed stability were enriched in some common biological processes upon expression of αSyn and S129A, such as DNA replication and repair, mitosis and mitochondria. Notably, some biological processes were found to be unique for either αSyn or S129A. Expression of αSyn demonstrated an enrichment of the functional category of mRNA processing, whereas S129A expression was found to change the stability of proteins involved in glycosylation and protein folding. These results indicate that αSyn disturb protein homeostasis in yeast by changing stability of proteins involved in crucial cellular processes. This itself can lead to unpredictable consequences for maintaining a healthy cellular balance. Expression of αSyn overloads proteostasis network and might influence its own stability and degradation. Differences in cellular responses to αSyn and S129A expression indicate the importance of αSyn PTMs on the protein biological properties, with phosphorylation at S129 residue as major PTM conserved from human to the baker's yeast as a eukaryotic reference cell for Morbus Parkinson.

4.2. Impact of α-synuclein expression on 26S proteasome

The proteasome is the key cellular pathway that is responsible for most protein degradation processes. Over the past decades, significant progress has been made in the study of the involvement of the proteasome in almost all aspects of biological processes. In fact, precise control of the proteasome abundance and its proper folding is necessary as aberrant increase or decrease in proteasomal activity is thought to be a causative factor in many diseases. Indeed, intracellular accumulation of proteins such as αSyn is a common feature of various neurodegenerative diseases, including Parkinson's disease. Inhibition of proteasomal degradation leads to the formation of

abnormal protein aggregates, such as αSyn, which subsequently binds to the proteasome in a manner that is correlated with a reduction in protease activity (Dantuma & Bott, 2014; McKinnon *et al*, 2020). Thereby, this suggests the existence of a vicious cycle between proteasome dysfunction and the accumulation of proteins in the pathogenesis of PD. Therefore, it is conceivable for the proteasome to be an appealing target for intervention in PD (Thibaudeau & Smith, 2019; Mishra *et al*, 2018). On the one hand, activation of the proteasome could effectively remove aggregates and have a preventive effect on neurodegeneration in PD. On the other hand, understanding the mechanism by which αSyn aggregation disrupts proteasome function may have potential applications for the disease-modifying treatments. In this study, the impact of αSyn expression on proteasomal activity and interplay with proteasome subunits was investigated.

It has been shown in various studies that αSyn can inhibit proteasomal activity, especially in form of fibrils or oligomers (McKinnon *et al*, 2020). Studies in rats have shown impairment of proteasomal chymotrypsin activity and perturbation of the ubiquitin-dependent degradation pathway, exhibiting an increase in ubiquitin-conjugated aggregates when the A53T αSyn mutant was expressed (Stefanis *et al*, 2001). Notably, also wild-type species of αSyn can lead to inhibition of the proteasome function. Study in human neuroblastoma cells have shown a ~50% reduction in ubiquitin-independent proteasomal degradation while wild-type αSyn was stably expressed (Snyder *et al*, 2003). Studies have shown the existence of proteasomal subunits and LBs in midbrain neurons of PD patients and even revealed direct binding of αSyn filaments, but not monomers, to the 20S proteasomal subunit (Lindersson *et al*, 2004). Furthermore, both monomeric and aggregated αSyn were found to bind *in vitro* to the 19S proteasomal subunit (Snyder *et al*, 2003).

Overexpression of αSyn leads to an impairment of the catalytic activity of the 26S proteasome, which is linked to selective accumulation of αSyn phosphorylated at Ser129 and to the onset of degeneration of dopaminergic neurons and movement disorders (McKinnon *et al*, 2020). Nevertheless, that study suggested toxic effect of the phosphorylation which was also implied in other studies (Chen & Feany, 2005; Karampetsou *et al*, 2017; Ma *et al*, 2016). Although the impact of S129 phosphorylation on αSyn toxicity and aggregation is still controversial, various studies, including this study, support protective role of the phosphorylation (Chau *et al*, 1989; Ghanem *et al*,

2022; Kuwahara *et al*, 2012; Paleologou *et al*, 2008; Popova *et al*, 2021a; Sancenon *et al*, 2012; Tenreiro *et al*, 2014b). Both 20S and 26S proteasomes degrade a fraction of αSyn; however, the preference to which proteasome αSyn is directed vary between αSyn species and experimental conditions. pS129 αSyn is selectively targeted for the proteasomal degradation. Pulse-chase experiments revealed that pS129 α-synuclein is characterized by a much shorter half-life (~55 minutes) than non-phosphorylated α-synuclein (~17 hours). Nevertheless, upon inhibition of the proteasome, the half-life of pS129 is longer (Machiya *et al*, 2010). Studies have shown that proteasome drug inhibition leads to accumulation of soluble αSyn oligomers bound to 26S upon proteasomal inhibition (Emmanouilidou *et al*, 2010). Expression of αSyn resulted in a significant inhibition of proteasomal activity without affecting the levels or assembly of the 26S proteasome. These findings suggest that a subset of αSyn oligomers is targeted to the 26S proteasome for degradation and simultaneously inhibit its function, probably by hampering the access of other proteasomal substrates.

Our study has shown accumulation of αSyn inclusion upon inhibition of the proteasome. Cells expressing αSyn failed to remove the inclusions, suggesting that the proteasome has a major role in clearance of αSyn aggregates. The proteasome inhibition did not affect clearance of S129A variant inclusions, suggesting that the proteasome is involved in the clearance of phosphorylated αSyn. Furthermore, decreased 26S proteasomal activity was demonstrated upon expression of αSyn and the effect was not observed upon expression of non-phosphorylated variant. This study proposes that accumulation of phosphorylated αSyn is a result of dysfunction of proteasome which is the preferential degradation pathway for S129 αSyn, and not a causative cytotoxicity factor.

The existence of distinct α-syn strains characterized by different structural and kinetic properties may explain the different pathological features, disease progression time and α-synucleinopathies severity (Malfertheiner *et al*, 2021). Distinct effects of expression of phosphorylated or non-phosphorylated αSyn might be a result of different conformations of the protein aggregates or fibrils, dependent on PTMs. Suzuki et al. generated different αSyn fibrils from identical αSyn monomer, dependent on salt concentration. When injected into mouse brain, they induced different pathologies (Suzuki *et al*, 2020). The fibrils that were formed with salt induced accumulation of phosphorylated S129 and ubiquitinated proteins, as it is found in LBs.

Furthermore, the 26S activity was drastically reduced in the presence of these fibrils. Only αSyn fibrils grown without salt co-precipitated with purified 26S proteasomes and impaired its activity. The αSyn in these fibrils has more exposed C-terminal region due to electrostatic repulsion and shorter core region. The study suggested that the C-terminal region of αSyn interacts with the 26S proteasome, resulting in impairment of its activity. This study supports our recent findings that αSyn interacts with the Rpt2 proteasome base subunit (Popova *et al*, 2021a). The interaction involves primarily the phosphorylated form of αSyn, which presumably causes proteasome dysfunction and altered pool of ubiquitin conjugates. The mechanism of pS129-dependent αSyn interaction with the proteasome might be due to changed conformation of αSyn C-terminal region, since phosphorylation at S129 gives negative charge to the C-terminal region. The phosphorylated αSyn has exposed C-terminal region with high electric repulsion, similarly to the fibrils formed without salt, which might promote the interaction of pS129 with the 26S proteasome and the inhibition of its activity.

4.3. Interplay between proteasome chaperone Rpn14 and α-synuclein

The inhibition of proteasome by αSyn may result from direct interaction with the proteasome subunits (Lindersson *et al*, 2004; Popova *et al*, 2021a; Snyder *et al*, 2003). For better understanding of the mechanism by which αSyn interferes with the proteasome function, we focused on the proteasome chaperone Rpn14. In this study, Rpn14 was identified as a protein whose stability increases upon expression of αSyn in contrast to non-phosphorylated S129A αSyn, which decreases the stability of Rpn14. We hypothesized that the interference of αSyn with the 26S proteasomal activity might occur on the 26S assembly stage.

Rpn14 binds free 19S RP and assists the dissociation of 19S complexes from the 20S core, changing the balance between proteasome assembly and disassembly toward its disassembly. Increased stability of Rpn14 by αSyn might favor the conformation of the disassembled proteasome or might cause a failure to release Rpn14 from the complex and results in its retention on the proteasome (Figure 30). The expulsion mechanism is very precise. Rpn14 binds Rpt6 and, less robustly, Rpt4 and the function of the chaperon is tightly linked to the C-termini of the Rpt subunits (Park *et al*, 2009; Roelofs *et al*, 2009). Remarkably, insertion of a single residue into Rpt6 four residues

upstream from the C-terminus prevents expulsion of Rpn14 (Park *et al*, 2009). Faulty interactions between the templating ATPases, Rpt4 and Rpt6, and the core particle cause more severe proteasome-assembly defects than mutations in the other ATPases (Rpt1, Rpt2, Rpt3 and Rpt5) (Park *et al*, 2005). Increased stability of Rpn14 due to αSyn expression might change the stability of the Rpn14-Rpt4 and Rpn14-Rpt6 subcomplexes. Defects in the late-docking ATPases are expected to cause a milder defect in proteasome assembly because preceding core-particle interactions with Rpt4 and Rpt6 would steer them towards interacting with specific α-subunits. This corroborates our recent findings, where downregulation of the base subunits Rpt2, Rpt4 or Rpt6 demonstrated a strong synthetic-sick phenotype upon αSyn expression and the effect was stronger than upon downregulation of the lid or or the core subunits (Popova *et al*, 2021a). αSyn might interfere with the 26S proteasome assembly by affecting the stability of Rpn14 or some of the intermediate complexes (Figure 30). In this study, BiFC assay indicated physical interaction between αSyn and Rpn14. Thus, αSyn might compete with the chaperon for its binding to Rpt6 and Rpt4 base subunits. Increased level of Rpn14 was shown to be harmful to yeast cells by causing growth retardation and by enhancing the growth retardation induced by αSyn. It suggests that the increased stability of Rpn14 caused by expression of αSyn can mediate the toxicity, given that upon expression of S129A the growth retardation was not observed as it decreases Rpn14 stability. Although Rpn14 has redundant function with another proteasome chaperon, Nas6, the observed effect was exclusive for Rpn14. It was previously shown that high-copy *RPN14* enhanced the levels of free base but not the RP. High-copy *RPN14* and *NAS6* suppress *rpt6* (*cim3-1*) growth defects, and overexpression of both genes in the same cells further enhances this suppression (Funakoshi *et al*, 2009)

Increased level of Rpn14 led to decreased αSyn inclusion clearance upon inhibition of the proteasome. It suggests that αSyn undermine its own clearance in a complex mechanism as expression of the protein not only inhibits proteasomal activity, but at the same time it leads to increased stability of Rpn14. The effect was not observed when S129A was expressed, supporting previous findings that the proteasome is more involved in degradation of phosphorylated αSyn. Moreover, upon deletion of *RPN14* phosphorylated and non-phosphorylated αSyn inclusions were cleared from the cells in a similar manner, confirming the role of Rpn14 in pS129 αSyn inclusion clearance.

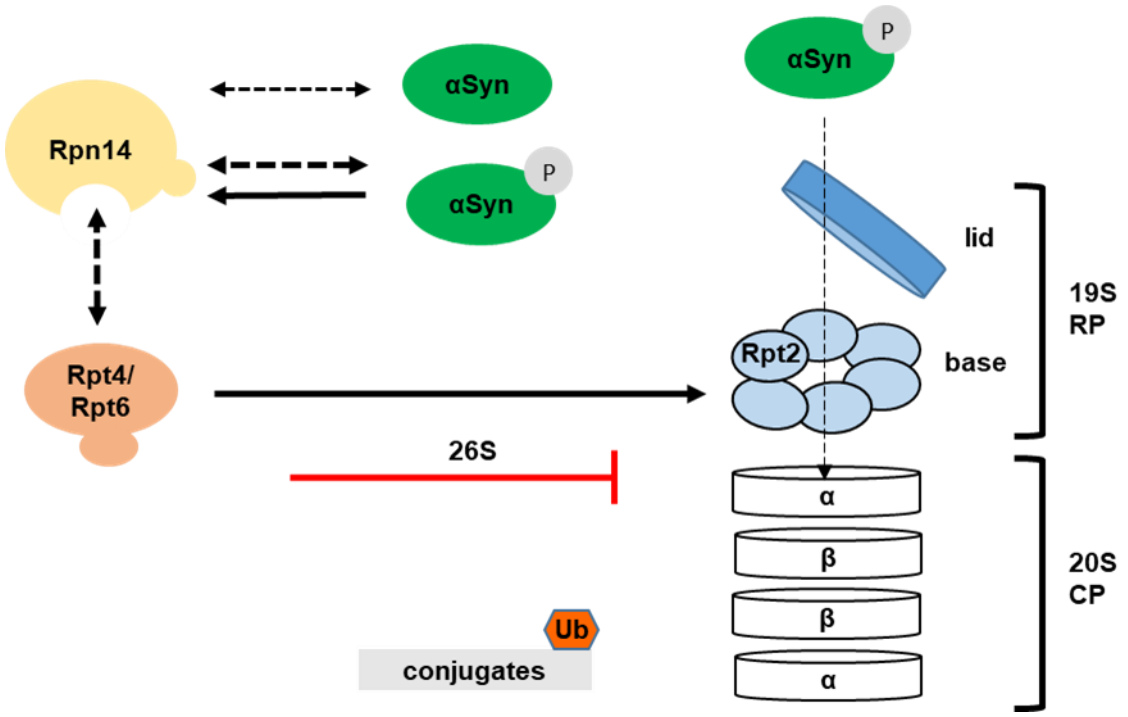

Figure 30. αSyn inhibition of 26S proteasomal activity in yeast is mediated by the proteasome assembly chaperone Rpn14.
Phosphorylated αSyn is a substrate of the 26S proteasome. Rpn14 binds Rpt4 and Rpt6 base subunits, and escorts them to the core particle. The assembly of the base is highly orchestrated process assisted by the proteasomal chaperones with a precise expulsion mechanism. αSyn physically interacts with and stabilizes Rpn14, which on its turn results in proteasome dysfunction and accumulation of pS129 that is normally targeted to the proteasome for degradation. Phosphorylated αSyn and increased levels of Rpn14 lead to accumulation of ubiquitin conjugates when the function of the proteasome is compromised. Increased stability of Rpn14 might stabilize Rpn14 subcomplexes with Rpt4 and Rpt6 and interfere with the expulsion of Rpn14 from the RP sub-complexes, leading to decreased levels of fully assembled proteasomes, accumulation of ubiquitinated proteins and decreased 26S proteasomal activity. Phosphorylated αSyn is in proximity to the Rpt2 base subunit, which probably leads to proteasome dysfunction and altered pool of ubiquitin conjugates. This effect is presumably mediated by elevated levels of Rpn14.

The results have shown decreased 26S proteasomal activity upon overexpression of *RPN14*. The inhibitory effect of excess Rpn14 was contributed, among others, to its role in preventing the association between a premature 19S RP and the 20S CP (Shirozu *et al*, 2015). Notably, it was demonstrated that overexpression of the mammalian homologue of *RPN14*, *PAAF1*, decreases the association between the 20S CP and the 19S RP in a dose-dependent manner. It was suggested that *PAAF1*, by binding to Rpt subunits, might interfere with their association with the 20S CP,

leading to inhibition of the 26S proteasome assembly (Park *et al*, 2005b). These results were reflected in yeast. It was revealed that overexpression of *RPN14* resulted in decreased 26S proteasomal activity and increased free 20S CP and free 19S RP, suggesting that overexpression of *RPN14* inhibits the association between the 20S CP and the 19S RP in yeast as well (Shirozu *et al*, 2015). This study revealed that elevated level of Rpn14 disturbs the function of the 26S proteasome and the degradation of ubiquitin conjugates under proteolytic stress and demonstrated different cellular responses to the expression of *RPN14* and αSyn upon depletion of one the three base subunits Rpt2, Rpt4 or Rpt6. The strongest effect was observed upon downregulation of *RPT2*, which led to accumulation of ubiquitin conjugates upon elevated level of Rpn14 and expression of αSyn. The observed effect was not synergistic, as co-expression of αSyn and *RPN14* led to similar level of accumulation of ubiquitinated proteins, compared to individual expression of αSyn or *RPN14*. This suggests that both, Rpn14 and αSyn, contribute to the impairment of the proteasome as part of the same mechanism. αSyn might render Rpn14 assembly chaperon a mediator of proteasome impairment. It is supported by the fact that non-phosphorylated αSyn has less impact on accumulation of ubiquitin conjugates. Notably, significant accumulation of phosphorylated αSyn was observed at elevated Rpn14 protein level, independently of *RPT2* expression levels. This finding suggests that Rpn14 leads to the increased accumulation of the pS129 fraction by inhibition of phosphorylated αSyn turnover. Similar pattern in accumulation of ubiquitin conjugates was observed upon depletion of Rpt4. Nevertheless, the effect was milder that upon depletion of Rpt2, and no effect of S129A was observed. Downregulation of *RPT6* itself resulted in accumulation of ubiquitinated proteins; however, expression of αSyn or *RPN14* did not increase the level of ubiquitin conjugates in this background and the tendency was similar upon deletion of *RPN14*. Accumulation of pS129 fraction was again observed upon downregulation of *RPT6* regardless the levels of Rpn14 protein.

When excessive amounts of Rpn14 are present in the cell and either *RPT2* or *RPT4* proteasomal base subunits are downregulated, Rpn14 acts as an inhibitor of the proteasome. Interestingly, studies have shown that deletion of only one of the proteasome assembly chaperons, such as *RPN14,* does not lead to cellular growth retardation (Funakoshi *et al*, 2009; Saeki *et al*, 2009). No impact of Rpn14 on cells growth was observed upon depletion of Rpt6, although Rpn14 strongly associates with

this proteasome base subunit (Roelofs *et al*, 2009). Different cellular responses to the expression of Rpn14 and αSyn upon depletion of different base subunits indicate that the mechanism of proteasome impairment by elevated levels of Rpn14 chaperone is not arbitrary. Although Rpt2 is not a direct interaction partner for Rpn14, we have shown that αSyn is in the close proximity to the Rpt2 base subunit and the interaction involves primarily the phosphorylated form of αSyn (Popova *et al*, 2021a). Rpt2 plays a distinct role in the formation and activation of the 26S proteasome by opening the CP 20S entry pore and allowing the translocation of protein substrates into the proteolytic channel for degradation (Grice & Nathan, 2016). Downregulation of this subunit resulted in strong toxicity enhancement even at low αSyn expression levels (Popova *et al*, 2021a). Rpt2 depletion caused αSyn accumulation and development of Lewy body-like inclusions in mice, and neurodegeneration and PD-like symptoms in *Drosophila* (Tanaka *et al*, 2001; Snyder *et al*, 2003). The stronger effect of Rpn14 observed upon depletion of Rpt2 in comparison to the other base subunits may be a consequence of complex interplay between αSyn, Rpn14 and the base subunits. Rpn14 binds Rpt6 and Rpt4, and increased stability of the chaperone caused by αSyn expression may lead to higher stability of Rpn14-Rpt6 and Rpn14-Rpt4 subcomplexes, which in turn alters proteasome assembly. Previously it was reported that loss of the base chaperones results in significant reductions in 26S proteasome levels; however, the quadruple-mutant cells grow normally under physiological conditions (Saeki *et al*, 2009). This result suggests that alternative mechanisms for the base assembly still exist in the cells and might explain why downregulation of *RPT6* and *RPT4* is not as harmful for the cells upon elevated levels of Rpn14 as downregulation of *RPT2.* Therefore, when *RPT2* is downregulated, the effect might have been raised not only from the lack of this subunits, but also from simultaneous depravation of Rpt6 and Rpt4 which are bound to Rpn14 in stable subcomplexes caused by αSyn expression. Subsequently, the effect was exclusively observed upon expression of pS129 αSyn, which is a substrate for the 26S proteasome. pS129 αSyn increases the stability of Rpn14 which in turn results in proteasome dysfunction and accumulation of pS129 that is normally targeted to the UPS for degradation. When *RPN14* is deleted, αSyn has less impact on the proteasomal activity and the accumulation of ubiquitinated protein. Increased stability probably interferes with the expulsion of Rpn14 from the RP sub-complex (Figure 30).

The main finding of this study is that αSyn may indirectly impair the proteasome by increasing the stability of the proteasome chaperone Rpn14. Proteasome impairment associated with neurodegeneration potentially can be caused by physical exposure of αSyn to the regulatory particle, leading to blocking of the proteasome complex at essential sites and changing the composition or stability of the proteasome. Depletion of RP subunits can alter the stoichiometry of the subunits in the cell and disrupt the assembly of the 26S proteasome, resulting in an increased number of compromised proteasomes (Tonoki *et al*, 2009).

4.4. Interplay between Rpn14 and proteasomal activity

Rpn14 is associated specifically with RP but not with the RP-CP holoenzyme (Roelofs *et al*, 2009). Mutation in Rpn14 resulted in proteasome loss-of-function in spite of its absence from the holoenzyme, which results from deficient RP assembly. Deletion of *RPN14* showed reduced level of singly-capped and doubly capped proteasomes. Thus, Rpn14 chaperone is important for RP-CP assembly and for maintaining normal proteasome levels. The assembly of the base is a highly orchestrated process. All four chaperones (Rpn14, Nas6, Nas2, and Hsm3) bind to base subunits of the lid and associate with the C-domains of the Rpt-proteins and negatively regulate the interactions of the base with the CP. On one hand, the interaction is specifically required for assembly itself. Therefore, the chaperones control the timing and ordering of the maturation events by competing with CP for occupancy of the Rpt C-domain.

This study revealed that αSyn affects the proteasomal activity of the cells by increasing the stability of Rpn14 chaperone and hence, the levels of fully assembled chaperones. Both expression of αSyn and elevated level of Rpn14 inhibit the 26S activity, and the effect is not synergistic. Notably, the effect was exclusive for pS129 αSyn and is not observed upon deletion of *RPN14.* No significant effect of S129A was observed. Considering that non-phosphorylated mutant of αSyn decreases the Rpn14 level and in *RPN14* deletion strain αSyn does not increase 26S proteasomal activity, it corroborates the finding that the αSyn-induced decrease of the 26S proteasomal activity is mediated by Rpn14 (Figure 30).

Rpn14 has a redundant function with Nas6 and the excess of the two chaperones might be disadvantages to the cells. It was shown that increased Rpn14 level results in decreased 26S activity. Thus, excess of the chaperone (the same is true for Nas6) is a disadvantage for cells. Expression of *RPN14* or *NAS6* does not affect the amount of the CP or RP; however. an increased 20S activity and decreased 26S activity were observed (Shirozu *et al*, 2015). This indicates that the association of the CP with RP is inhibited upon elevated protein levels of Rpn14 or Nas6 in the cell.

PAAF1 is the mammalian homolog of *RPN14*. *PAAF1* co-purifies with the 19S RP, but not with 20S (Lassot *et al*, 2007; Park *et al*, 2005b). Under the same experimental conditions, 19S and 20S copurify together. This suggests that binding of *PAAF1* with 19S interferes with the stable interaction between the 19S complex and 20S and inhibits the association between them. *PAAF1* was shown to inhibit the proteasomal activity and to lead to accumulation of ubiquitinated proteins.

4.5. Role of Rpn11 on α-synuclein turnover

Rpn11 is a 19S RP lid metalloisopeptidase that removes ubiquitin from substrates targeted for degradation by the 26S proteasome. The deubiquitinase activity of this proteasome subunit promotes degradation. Rpn11 is located in proximity to the ubiquitin receptor Rpn10 and to the ATPase ring within the RP, which form the proteasome substrate entry pore (Kolog Gulko *et al*, 2018). Active substrate translocation by ATPases supposedly delivers the ubiquitin chain to Rpn11, which cuts polyubiquitin at the base of the chain. Consequently, downregulation of Rpn11 leads to an accumulation of ubiquitinated proteins. This study revealed that Rpn11 decreases the stability of αSyn and contributes to the degradation of pS129 αSyn. These results confirm previous findings and show that αSyn phosphorylated at S129 residue is preferentially degraded by the ubiquitin proteasome system. High levels of αSyn lead to depletion of the pool of ubiquitinated proteins. It was suggested that αSyn may alter substrate translocation to the catalytic core and promote ubiquitin and the conjugated substrates degradation. Subsequently, αSyn may evade the DUB activity of Rpn11 and cause depletion of the cellular ubiquitin pool and ubiquitin wasting (Popova *et al*, 2021a). Ubiquitin depletion induces toxicity in yeast (Verma *et al*, 2002).

Impaired Rpn11 function in aged *Drosophila melanogaster* resulted in age-dependent premature accumulation of ubiquitinated proteins, reduced 26S proteasomal activity and intensified neurodegenerative phenotype. Notably, overexpression of Rpn11 recovered 26S proteasomal activity, resulting in extended lifespan (Stefanis *et al*, 2001). Rpn11 is required for appropriate yeast cell morphology, as downregulation of the deubiquitinase leads to aberrant growth upon expression of αSyn.

Another proteasome subunit, Sem1, might indirectly affect αSyn degradation. The role of Sem1 is to maintain association of the lid and base subcomplexes of the regulatory particle (Funakoshi *et al*, 2004). Sem1 is required for stabilization of deubiquitinating enzyme Rpn11 and proper assembly of the 26S proteasome (Kolog Gulko *et al*, 2018). It was previously found that deletion of *SEM1* leads to accumulation of ubiquitin conjugates and disturbs proteasome mediated degradation (Funakoshi *et al*, 2004). This study demonstrated that accumulation of ubiquitinated proteins has similar pattern in *SEM1* deletion mutant and upon *RPN11* downregulation, where accumulation occurred in the cells expressing phosphorylated αSyn. This suggests that the contribution of Rpn11 to αSyn degradation may be mediated by Sem1, by increasing the stability of Rpn11. Nevertheless, in contrast to Rpn11, Sem1 was found to be involved in stabilization of phosphorylated and non-phosphorylated αSyn. Since Sem1 is involved in efficient assembly of the 26S proteasome, this effect could be associated with 20S degradation activity as lack of Sem1 in cells significantly increases the percentage of 20S proteasomes. This suggests that αSyn phosphorylation at S129 residue promotes degradation by the 26S proteasome, whereas degradation by 20S proteasome is independent of pS129.

4.6. Conclusions

Imbalance in protein homeostasis is associated with the onset and progression of Parkinson's disease. This work gives insights into the αSyn-dependent disturbances in cellular protein homeostasis. It reveals a complex interaction between the proteasome and αSyn causing vastly altered proteostasis in yeast as a eukaryotic reference cell for PD. The impact of αSyn on stability of proteins is dependent on the phosphorylation state of αSyn at serine 129 residue, where phosphorylated αSyn has higher influence on proteins stability. The interrelationship between αSyn accumulation

and imbalanced proteostasis are connected to changed protein turnover and proteasome modulation. The main finding of this study is that αSyn increases the stability of 26S proteasome chaperone Rpn14, which mediates the inhibition of the proteasomal activity. It revealed that the proteasomal deubiqutinase Rpn11 decreases αSyn stability and plays a role in the degradation of pS129 αSyn. Dysregulation of proteasomal activity can result in many human diseases, including PD (Bi *et al*, 2021). This work contributes to the understanding of the mechanism of proteasome inhibition by αSyn and provides basis for further studies in higher organisms. Future investigation on the interaction between αSyn and the human homologue of *RPN14* (*PAAF1*) and *RPN11* (*PSMD14*) can give an insight into the mechanism of PD onset and might have a possible medical relevance in human.

5. References

Abeliovich A, Schmitz Y, Fariñ I, Choi-Lundberg D, Ho W-H, Castillo PE, Shinsky N, Manuel J, Verdugo G, Armanini M, *et al* (2000) Mice lacking α-synuclein display functional deficits in the nigrostriatal dopamine system. *Neuron* 25: 239-252

Anderson JP, Walker DE, Goldstein JM, de Laat R, Banducci K, Caccavello RJ, Barbour R, Huang J, Kling K, Lee M, *et al* (2006) Phosphorylation of Ser-129 is the dominant pathological modification of α-synuclein in familial and sporadic Lewy body disease. *J Biol Chem* 281: 29739-29752

Appel-Cresswell S, Vilarino-Guell C, Encarnacion M, Sherman H, Yu I, Shah B, Weir D, Thompson C, Szu-Tu C, Trinh J, *et al* (2013) Alpha-synuclein p.H50Q, a novel pathogenic mutation for Parkinson's disease. *Mov Disord* 28: 811-813

Arawaka S, Wada M, Goto S, Karube H, Sakamoto M, Ren CH, Koyama S, Nagasawa H, Kimura H, Kawanami T, *et al* (2006) The role of G-protein-coupled receptor kinase 5 in pathogenesis of sporadic Parkinson's disease. *J Neurosci* 26: 9227-9238

Baldereschi M, Carlo A di, Vanni P & Grigoletto F (2000) Parkinson's disease and parkinsonism in a longitudinal study: Two-fold higher incidence in men. *Neurology* 55: 1358-1363

Bartels T, Kim NC, Luth ES & Selkoe DJ (2014) N-Alpha-Acetylation of a-Synuclein Increases Its Helical Folding Propensity, GM1 Binding Specificity and Resistance to Aggregation. *PLoS ONE* 9: 103727

Baryshnikova A, Costanzo M, Dixon S, Vizeacoumar FJ, Myers CL, Andrews B & Boone C (2010) Synthetic genetic array (SGA) analysis in *Saccharomyces cerevisiae* and *Schizosaccharomyces pombe*. *Methods in Enzymology* 410: 145-179

Beck-Sickinger AG & Mörl K (2006) Posttranslational Modification of Proteins. Expanding Nature's Inventory. By Christopher T. Walsh. *Angewandte Chemie International Edition* 45: 1020

Ben-Nissan G & Sharon M (2014) Regulating the 20S proteasome ubiquitin-independent degradation pathway. *Biomolecules* 4: 862-884

Bentea E, Verbruggen L & Massie A (2017) The proteasome inhibition model of Parkinson's disease. *J Parkinsons Dis* 7: 31-63

Bertani G (1951) Studies on lysogenesis. I. The mode of phage liberation by lysogenic *Escherichia coli*. *J Bacteriol* 62: 293-300

Beyer K (2006) Synuclein structure, posttranslational modiWcation and alternative splicing as aggregation enhancers. *Acta Neuropathol* 112: 237-251

Bi M, Du X, Jiao Q, Chen X & Jiang H (2021) Expanding the role of proteasome homeostasis in Parkinson's disease: beyond protein breakdown. *Cell Death and Disease* 12: 154

Bonifacino JS & Glick BS (2004) The Mechanisms of Vesicle Budding and Fusion. *Cell* 116: 153-166

Bonifati V, Rizzu P, Squitieri F, Krieger E, Vanacore N, van Swieten JC, Brice A, van Duijn CM, Oostra B, Meco G, *et al* (2003) DJ-1 (PARK7), a novel gene for autosomal recessive, early onset parkinsonism. *Neurological Sciences* 24: 159-160

Botstein D, Chervitz SA & Cherry JM (1997) Yeast as a model organism. *Science* 277: 1259-1260

Braak H, del Tredici K, Rüb U, de Vos RAI, Jansen Steur ENH & Braak E (2003) Staging of brain pathology related to sporadic Parkinson's disease. *Neurobiology of Aging* 24: 197-211

Bradford MM (1976) A rapid and sensitive method for the quantitation of microgram quantities of protein utilizing the principle of protein-dye binding. *Analytical Biochemistry* 72: 248-254

Brodsky JL & Skach WR (2011) Protein folding and quality control in the endoplasmic reticulum: Recent lessons from yeast and mammalian cell systems. *Current Opinion in Cell Biology* 23: 464-475

Buchanan BW, Lloyd ME, Engle SM & Rubenstein EM (2016) Cycloheximide chase analysis of protein degradation in *Saccharomyces cerevisiae*. *J Vis Exp* 110: e53975

Burai R, Ait-Bouziad N, Chiki A & Lashuel HA (2015) Elucidating the role of site-specific nitration of α-synuclein in the pathogenesis of Parkinson's disease via protein semisynthesis and mutagenesis. *J Am Chem Soc* 137: 5041-5052

Burré J, Sharma M & Südhof TC (2018) Cell biology and pathophysiology of α-synuclein. *Cold Spring Harbor Perspectives in Medicine* 8: a024091

Chartier-Harlin MC, Kachergus J, Roumier C, Mouroux V, Douay X, Lincoln S, Levecque C, Larvor L, Andrieux J, Hulihan M, *et al* (2004) Alpha-synuclein locus duplication as a cause of familial Parkinson's disease. *Lancet* 364: 1167-1169

Chau V, Tobias JW, Bachmair A, Marriott D, Ecker DJ, Gonda DK & Varshavsky A (1989) A multiubiquitin chain is confined to specific lysine in a targeted short-lived protein. *Science* 243: 1576-1583

Chen L & Feany MB (2005) α-synuclein phosphorylation controls neurotoxicity and inclusion formation in a *Drosophila* model of Parkinson disease. *Nature Neuroscience* 8: 657-663

Cherry JM, Hong EL, Amundsen C, Balakrishnan R, Binkley G, Chan ET, Christie KR, Costanzo MC, Dwight SS, Engel SR, *et al* (2012) *Saccharomyces* Genome Database: The genomics resource of budding yeast. *Nucleic Acids Research* 40: D700-D705

Chu Y, Dodiya H, Aebischer P, Olanow CW & Kordower JH (2009) Alterations in lysosomal and proteasomal markers in Parkinson's disease: Relationship to alpha-synuclein inclusions. *Neurobiology of Disease* 35: 385-398

Clark RSB, Bayir H & Jenkins LW (2005) Posttranslational protein modifications. *Critical Care Medicine* 33: 12

Cohen-Kaplan V, Livneh I, Avni N, Fabre B, Ziv T, Kwon YT & Ciechanover A (2016) p62- and ubiquitin-dependent stress-induced autophagy of the mammalian 26S proteasome. *Proc Natl Acad Sci U S A* 113: E7490-E7499

Cookson MR (2009) α-Synuclein and neuronal cell death. *Molecular Neurodegeneration* 4: 9

Cooper AA, Gitler AD, Cashikar A, Haynes CM, Hill KJ, Bhullar B, Liu K, Xu K, Strathearn KE, Liu F, *et al* (2006) α-Synuclein blocks ER-Golgi traffic and Rab1 rescues neuron loss in Parkinson's models. *Science* 313: 324-328

Corpet F (1988) Multiple sequence alignment with hierarchical clustering. *Nucleic Acids Res* 16: 10881-10890

Dahodwala N, Shah K, He Y, Wu SS, Schmidt P, Cubillos F & Willis AW (2018) Sex disparities in access to caregiving in Parkinson disease. *Neurology* 90: e48-e54

Dantuma NP & Bott LC (2014) The ubiquitin-proteasome system in neurodegenerative diseases: precipitating factor, yet part of the solution. *Frontiers in Molecular Neuroscience* 7: 70

Dextera DT & Jenner P (2013) Parkinson disease: From pathology to molecular disease mechanisms. *Free Radical Biology and Medicine* 62: 132-144

Dickson DW (2012) Parkinson's disease and parkinsonism: Neuropathology. *Cold Spring Harbor Perspectives in Medicine* 2: a009258

Dorval V & Fraser PE (2006) Small Ubiquitin-like Modifier (SUMO) modification of natively unfolded proteins Tau and α-synuclein. *J Biol Chem* 281: 9919-9924

Duda JE, M-Y Lee V & Trojanowski JQ (2000) Mini-review neuropathology of synuclein aggregates: New insights into mechanisms of neurodegenerative diseases. *J Neurosci Res* 61: 121-127

Ebrahimi-Fakhari D, Cantuti-Castelvetri I, Fan Z, Rockenstein E, Masliah E, Hyman BT, McLean PJ & Unni VK (2011) Distinct roles in vivo for the ubiquitin-proteasome system and the autophagy-lysosomal pathway in the degradation of α-synuclein. *J Neurosci* 31: 14508-14520

Ehlinger A, Park S, Fahmy A, Lary JW, Cole JL, Finley D & Walters KJ (2013) Conformational dynamics of the Rpt6 ATPase in proteasome assembly and Rpn14 binding. *Structure* 21: 753-765

Emamzadeh FN (2016) Alpha-synuclein structure, functions, and interactions. *J Res Med Sci* 21: 29

Emmanouilidou E, Stefanis L & Vekrellis K (2010) Cell-produced α-synuclein oligomers are targeted to, and impair, the 26S proteasome. *Neurobiology of Aging* 31: 953-968

Fearnley JM & Lees AJ (1991) Ageing and Parkinson's disease: substantia nigra regional selectivity. *Brain* 114: 2283-2301

Feigin VL, Krishnamurthi R v., Theadom AM, Abajobir AA, Mishra SR, Ahmed MB, Abate KH, Mengistie MA, Wakayo T, Abd-Allah F, *et al* (2017) Global, regional, and national burden of neurological disorders during 1990-2015: a systematic analysis for the Global Burden of Disease Study 2015. *The Lancet Neurology* 16: 877-897

Feigin VL, Nichols E, Alam T, Bannick MS, Beghi E, Blake N, Culpepper WJ, Dorsey ER, Elbaz A, Ellenbogen RG, *et al* (2019) Global, regional, and national burden of neurological disorders, 1990-2016: a systematic analysis for the Global Burden of Disease Study 2016. *The Lancet Neurology* 18: 459-480

di Fonzo A, Chien HF, Socal M, Giraudo S, Tassorelli C, Iliceto G, Fabbrini G, Marconi R, Fincati E, Abbruzzese G, *et al* (2007) ATP13A2 missense mutations in juvenile parkinsonism and young onset Parkinson disease. *Neurology* 68: 1557

Förster A, Masters EI, Whitby FG, Robinson H & Hill CP (2005) The 1.9 A structure of a proteasome-11S activator complex and implications for proteasome-PAN/PA700 interactions. *Molecular Cell* 18: 589-599

Fujiwara H, Hasegawa M, Dohmae N, Kawashima A, Masliah E, Goldberg MS, Shen J, Takio K & Iwatsubo T (2002) α-Synuclein is phosphorylated in synucleinopathy lesions. *Nature Cell Biology* 4: 160-164

Funakoshi M, Li X, Velichutina I, Hochstrasser M & Kobayashi H (2004) Sem1, the yeast ortholog of a human BRCA2-binding protein, is a component of the proteasome regulatory particle that enhances proteasome stability. *J Cell Sci* 117: 6447-6454

Funakoshi M, Tomko RJ, Kobayashi H & Hochstrasser M (2009) Multiple assembly chaperones govern biogenesis of the proteasome regulatory particle base. *Cell* 137: 887-899

Gallagher SR, Winston SE, Fuller SA & Hurrell JGR (1998) Immunoblotting and Immunodetection. *Current Protocols in Cell Biology* 52: 6.2.1-6.2.28

Gasparini F, Paolo T di & Gomez-Mancilla B (2013) Metabotropic glutamate receptors for Parkinson's disease therapy. *Parkinson's disease* 2013: 196028

Ghanem SS, Majbour NK, Vaikath NN, Ardah MT, Erskine D, Jensen NM, Fayyad M, Sudhakaran IP, Vasili E, Melachroinou K, *et al* (2022) α-Synuclein phosphorylation at serine 129 occurs after initial protein deposition and inhibits seeded fibril formation and toxicity. *Medical Sciences* 119: e2109617119

Giasson BI, Jakes R, Goedert M, Duda JE, Leight S, Trojanowski JQ & Lee VMY (2000) A panel of epitope-specific antibodies detects protein domains distributed throughout human α-synuclein in lewy bodies of Parkinson's disease. *J Neurosci Res* 59: 528-533

Gitler AD, Bevis BJ, Shorter J, Strathearn KE, Hamamichi S, Su LJ, Caldwell KA, Caldwell GA, Rochet JC, McCaffery JM, *et al* (2008) The Parkinson's disease protein alpha-synuclein disrupts cellular Rab homeostasis. *Proc Natl Acad Sci U S A* 105: 145-150

Gitler AD, Chesi A, Geddie ML, Strathearn KE, Hamamichi S, Hill KJ, Caldwell KA, Caldwell GA, Cooper AA, Rochet J-CC, *et al* (2009) Alpha-synuclein is part of a diverse and highly conserved interaction network that includes PARK9 and manganese toxicity. *Nat Genet* 41: 308-315

Glickman MH & Ciechanover A (2002) The ubiquitin-proteasome proteolytic pathway: Destruction for the sake of construction. *Physiol Rev* 82: 373-428

Glickman MH, Rubin DM, Coux O, Wefes I, Pfeifer G, Cjeka Z, Baumeister W, Fried VA & Finley D (1998) A subcomplex of the proteasome regulatory particle required for ubiquitin-conjugate degradation and related to the COP9-signalosome and eIF3. *Cell* 94: 615-623

Goedert M, Jakes R & Spillantini MG (2017) The Synucleinopathies: Twenty Years on. *J Parkinsons Dis* 7: S53-S71

Goffeau A, Barrell BG, Bussey H, Davis RW, Dujon B, Feldmann H, Galibert F, Hoheisel JD, Jacq C, Johnston M, *et al* (1996) Life with 6000 Genes. *Science* 274: 546-567

Goldberg AL (2003) Protein degradation and protection against misfolded or damaged proteins. *Nature* 426: 895-899

Gorbatyuk OS, Li S, Sullivan LF, Chen W, Kondrikova G, Manfredsson FP, Mandel RJ & Muzyczka N (2008) The phosphorylation state of Ser-129 in human alpha-synuclein determines neurodegeneration in a rat model of Parkinson disease. *Proc Natl Acad Sci U S A* 105: 763-768

Greenbaum EA, Graves CL, Mishizen-Eberz AJ, Lupoli MA, Lynch DR, Englander SW, Axelsen PH & Giasson BI (2005) The E46K Mutation in α-Synuclein Increases Amyloid Fibril Formation. *J Biol Chem* 280: 7800-7807

Grice GL & Nathan JA (2016) The recognition of ubiquitinated proteins by the proteasome. *Cellular and Molecular Life Sciences* 73: 3497-3506

Guerrero E, Vasudevaraju P, Hegde ML, Britton GB & Rao KS (2013) Recent advances in α-synuclein functions, advanced glycation, and toxicity: Implications for Parkinson's disease. *Molecular Neurobiology* 47: 525-536

Guthrie C & Fink GR (1991) Guide to yeast genetics and molecular biology. *Methods Enzymol* 194: 1-863

Hamazaki J, Iemura SI, Natsume T, Yashiroda H, Tanaka K & Murata S (2006) A novel proteasome interacting protein recruits the deubiquitinating enzyme UCH37 to 26S proteasomes. *EMBO Journal* 25: 4524-4536

Hanna J & Finley D (2007) A proteasome for all occasions. *FEBS Letters* 581: 2854-2861

Hartwell LH (2002) Yeast and Cancer. *Bioscience Reports* 22: 373-394

Hasegawa M, Fujiwara H, Nonaka T, Wakabayashi K, Takahashi H, Lee VM-Y, Trojanowski JQ, Mann D & Iwatsubo T (2002) Phosphorylated α-synuclein is ubiquitinated in α-synucleinopathy lesions. *J Biol Chem* 277: 49071-49076

Hoffman CS & Winston F (1987) A ten-minute DNA preparation from yeast efficiently releases autonomous plasmids for transformation of *Escherichia coli*. *Gene* 57: 267-272

Hu M, Li P, Song L, Jeffrey PD, Chenova TA, Wilkinson KD, Cohen RE & Shi Y (2005) Structure and mechanisms of the proteasome-associated deubiquitinating enzyme USP14. *EMBO Journal* 24: 3747-3756

Hughes TR (2002) Yeast and drug discovery. *Funct Integr Genomics* 2: 199-211

Huh W-K, Falvo J v, Gerke LC, Carroll AS, Howson RW, Weissman JS & O'Shea EK (2003) Global analysis of protein localization in budding yeast. *Nature* 425: 686-691

Ii K, Ito H, Tanaka K & Hirano A (1997) Immunocytochemical co-localization of the proteasome in ubiquitinated structures in neurodegenerative diseases and the elderly. *J Neuropathol Exp Neurol* 56: 125-131

Inglis KJ, Chereau D, Brigham EF, Chiou SS, Schobel S, Frigon NL, Yu M, Caccavello RJ, Nelson S, Motter R, *et al* (2009) Polo-like kinase 2 (PLK2) phosphorylates alpha-synuclein at serine 129 in central nervous system. *J Biol Chem* 284: 2598-2602

Inoue H, Nojima H & Okayama H (1990) High efficiency transformation of *Escherichia coli* with plasmids. *Gene* 96: 23-28

Ito H, Fukuda Y, Murata K & Kimura A (1983) Transformation of intact yeast cells treated with alkali cations. *J Bacteriol* 153: 163-168

James SL, Abate D, Abate KH, Abay SM, Abbafati C, Abbasi N, Abbastabar H, Abd-Allah F, Abdela J, Abdelalim A, *et al* (2018) Global, regional, and national incidence, prevalence, and years lived with disability for 354 diseases and injuries for 195 countries and territories, 1990-2017: a systematic analysis for the Global Burden of Disease Study 2017. *The Lancet* 392: 1789-1858

Kalia L v & Lang AE (2015) Parkinson's disease. *The Lancet* 386: 896-912

Karampetsou M, Ardah MT, Semitekolou M, Polissidis A, Samiotaki M, Kalomoiri M, Majbour N, Xanthou G, El-Agnaf OMA & Vekrellis K (2017) Phosphorylated exogenous alpha-synuclein fibrils exacerbate pathology and induce neuronal dysfunction in mice. *Scientific Reports* 7: 16533

Khmelinskii A, Blaszczak E, Pantazopoulou M, Fischer B, Omnus DJ, Le Dez G, Brossard A, Gunnarsson A, Barry JD, Meurer M, *et al* (2014) Protein quality control at the inner nuclear membrane. *Nature* 516: 410-413

Khmelinskii A, Keller PJ, Bartosik A, Meurer M, Barry JD, Mardin BR, Kaufmann A, Trautmann S, Wachsmuth M, Pereira G, *et al* (2012) Tandem fluorescent protein timers for in vivo analysis of protein dynamics. *Nat Biotechnol* 30: 708-714

Khmelinskii A & Knop M (2014) Analysis of protein dynamics with tandem fluorescent protein timers. *Methods in molecular biology* 1174: 195-210

Khmelinskii A, Meurer M, Duishoev N, Delhomme N & Knop M (2011) Seamless gene tagging by endonuclease-driven homologous recombination. *PLoS ONE* 6: 1-8

Khmelinskii A, Meurer M, Ho C-T, Besenbeck B, Fuller J, Lemberg MK, Bukau B, Mogk A & Knop M (2016) Incomplete proteasomal degradation of green fluorescent proteins in the context of tandem fluorescent protein timers. *Molecular Biology of the Cell* 27: 360-370

Kim S, Saeki Y, Fukunaga K, Suzuki A, Takagi K, Yamane T, Tanaka K, Mizushima T & Kato K (2010) Crystal structure of yeast Rpn14, a chaperone of the 19 S regulatory particle of the proteasome. *J Biol Chem* 285: 15159-15166

Kitada T, Asakawa S, Hattori N, Matsumine H, Yamamura Y, Minoshima S, Yokochi M, Mizuno Y & Shimizu N (1998) Mutations in the parkin gene cause autosomal recessive juvenile parkinsonism. *Nature* 392: 605-608

Kleinknecht A, Popova B, Lázaro DF, Pinho R, Valerius O, Outeiro TF & Braus GH (2016) C-terminal tyrosine residue modifications modulate the protective phosphorylation of serine 129 of α-synuclein in a yeast model of Parkinson's disease. *PLoS Genet* 12: e1006098

Klionsky DJ, Abdel-Aziz AK, Abdelfatah S, Abdellatif M, Abdoli A, Abel S, Abeliovich H, Abildgaard MH, Abudu YP, Acevedo-Arozena A, *et al* (2021) Guidelines for the use and interpretation of assays for monitoring autophagy. *Autophagy*: 1-382

Klionsky DJ & Emr SD (2000) Autophagy as a Regulated Pathway of Cellular Degradation. *Science* 290: 1717-1721

Kolog Gulko M, Heinrich G, Gross C, Popova B, Valerius O, Neumann P, Ficner R & Braus GH (2018) Sem1 links proteasome stability and specificity to multicellular development. *PLoS Genet* 14: e1007141

Kouli A, Torsney KM & Kuan W-L (2018) Parkinson's Disease: etiology, neuropathology, and pathogenesis. *Parkinson's Disease: Pathogenesis and Clinical Aspects* pp 3-26. Codon Publications

Kowal SL, Dall TM, Chakrabarti R, Storm M v & Jain A (2013) The current and projected economic burden of Parkinson's disease in the United States. *Movement Disorders* 28: 311-318

Krüger R, Kuhn W, Müller T, Woitalla D, Graeber M, Kösel S, Przuntek H, Epplen JT, Schöls L & Riess O (1998) Ala30Pro mutation in the gene encoding α-synuclein in Parkinson's disease. *Nature Genetics* 18: 106-108

Krumova P, Meulmeester E, Garrido M, Tirard M, Hsiao HH, Bossis G, Urlaub H, Zweckstetter M, Kugler S, Melchior F, *et al* (2011) Sumoylation inhibits alpha-synuclein aggregation and toxicity. *J Cell Biol* 194: 49-60

Kuwahara T, Tonegawa R, Ito G, Mitani S & Iwatsubo T (2012) Phosphorylation of α-synuclein protein at ser-129 reduces neuronal dysfunction by lowering its membrane binding property in *Caenorhabditis elegans*. *J Biol Chem* 287: 7098-7109

Laemmli UK (1970) Cleavage of structural proteins during the assembly of the head of bacteriophage T4. *Nature* 227: 680-685

Lashuel HA, Overk CR, Oueslati A & Masliah E (2013) The many faces of α-synuclein: from structure and toxicity to therapeutic target. *Nat Rev Neurosci* 14: 38-48

Lassot I, Latreille D, Rousset E, Sourisseau M, Linares LK, Chable-Bessia C, Coux O, Benkirane M & Kiernan RE (2007) The proteasome regulates HIV-1 transcription by both proteolytic and nonproteolytic mechanisms. *Molecular Cell* 25: 369-383

de Lau LML & Breteler MMB (2006) Epidemiology of Parkinson's disease. *The Lancet Neurology* 5: 525-535

Lee HJ, Khoshaghideh F, Patel S & Lee SJ (2004) Clearance of alpha-synuclein oligomeric intermediates via the lysosomal degradation pathway. *J Neurosci* 24: 1888-1896

Lee PY, Costumbrado J, Hsu CY & Kim YH (2012) Agarose gel electrophoresis for the separation of DNA fragments. *J Vis Exp* 62: e3923

Lehtonen Š, Sonninen TM, Wojciechowski S, Goldsteins G & Koistinaho J (2019) Dysfunction of cellular proteostasis in Parkinson's disease. *Frontiers in Neuroscience* 13: 457

Lesage S, Anheim M, Letournel F, Bousset L, Honore A, Rozas N, Pieri L, Madiona K, Durr A, Melki R, *et al* (2013) G51D alpha-synuclein mutation causes a novel parkinsonian-pyramidal syndrome. *Ann Neurol* 73: 459-471

Li F, Tian G, Langager D, Sokolova V, Finley D & Park S (2017) Nucleotide-dependent switch in proteasome assembly mediated by the Nas6 chaperone. *Proc Natl Acad Sci U S A* 114: 1548-1553

Li J, Uversky VN & Fink AL (2001) Effect of familial Parkinson's disease point mutations A30P and A53T on the structural properties, aggregation, and fibrillation of human α-synuclein. *Biochemistry* 40: 11604-11613

Lindersson E, Beedholm R, Højrup P, Moos T, Gai WP, Hendil KB & Jensen PH (2004) Proteasomal inhibition by α-aynuclein filaments and oligomers. *J Biol Chem* 279: 12924-12934

Liu C, Apodaca J, Davis LE & Rao H (2007) Proteasome inhibition in wild-type yeast *Saccharomyces cerevisiae* cells. *Biotechniques* 42: 158, 160, 162

Lourenço Venda L, Cragg SJ, Buchman VL & Wade-Martins R (2010) α-Synuclein and dopamine at the crossroads of Parkinson's disease. *Trends Neurosci* 33: 559-568

Lundblad M, Decressac M, Mattsson B & Björklund A (2012) Impaired neurotransmission caused by overexpression of α-synuclein in nigral dopamine neurons. *Proc Natl Acad Sci* 109: 3213-3219

Ma M-R, Hu Z-W, Zhao Y-F, Chen Y-X & Li Y-M (2016) Phosphorylation induces distinct alpha-synuclein strain formation. *Scientific Reports* 6: 37130

Machiya Y, Hara S, Arawaka S, Fukushima S, Sato H, Sakamoto M, Koyama S & Kato T (2010) Phosphorylated α-Synuclein at Ser-129 is targeted to the proteasome pathway in a ubiquitin-independent manner. *J Biol Chem* 285: 40732-40744

Madura K (2009) Cell biology: The proteasome assembly line. *Nature* 459: 787-788

Mager WH & Winderickx J (2005) Yeast as a model for medical and medicinal research. *Trends in Pharmacological Sciences* 26: 265-273

Malfertheiner K, Stefanova N & Heras-Garvin A (2021) The concept of α-synuclein strains and how different conformations may explain distinct neurodegenerative disorders. *Frontiers in Neurology* 12: 737195

Marshall RS & Vierstra RD (2018) Proteasome storage granules protect proteasomes from autophagic degradation upon carbon starvation. *Elife* 7: e34532

Marshall RS & Vierstra RD (2019) Dynamic regulation of the 26S proteasome: From synthesis to degradation. *Frontiers in Molecular Biosciences* 6: 40

Mbefo MK, Paleologou KE, Boucharaba A, Oueslati A, Schell H, Fournier M, Olschewski D, Yin G, Zweckstetter M, Masliah E, *et al* (2010) Phosphorylation of synucleins by members of the Polo-like kinase family. *J Biol Chem* 285: 2807-2822

McKinnon C, de Snoo ML, Gondard E, Neudorfer C, Chau H, Ngana SG, O'Hara DM, Brotchie JM, Koprich JB, Lozano AM, *et al* (2020) Early-onset impairment of the ubiquitin-proteasome system in dopaminergic neurons caused by α-synuclein. *Acta Neuropathologica Communications* 8: 17

McNaught KS & Jenner P (2001) Proteasomal function is impaired in substantia nigra in Parkinson's disease. *Neurosci Lett* 297: 191-4

McNaught KSP, Jackson T, JnoBaptiste R, Kapustin A & Olanow CW (2006) Proteasomal dysfunction in sporadic Parkinson's disease. *Neurology* 66: S37-49

McNaught KSP, Mytilineou C, Jnobaptiste R, Yabut J, Shashidharan P, Jennert P & Olanow CW (2002) Impairment of the ubiquitin-proteasome system causes dopaminergic cell death and inclusion body formation in ventral mesencephalic cultures. *J Neurochem* 81: 301-6

Mehra S, Sahay S & Maji SK (2019) α-Synuclein misfolding and aggregation: Implications in Parkinson's disease pathogenesis. *Biochimica et Biophysica Acta (BBA) - Proteins and Proteomics* 1867: 890-908

Menezes R, Tenreiro S, Macedo D, Santos CN & Outeiro TF (2015) From the baker to the bedside: Yeast models of parkinson's disease. *Microbial Cell* 2: 262-279

Mishra R, Upadhyay A, Prajapati VK & Mishra A (2018) Proteasome-mediated proteostasis: Novel medicinal and pharmacological strategies for diseases. *Medicinal Research Reviews* 38: 1916-1973

Mnaimneh S, Davierwala AP, Haynes J, Moffat J, Peng WT, Zhang W, Yang X, Pootoolal J, Chua G, Lopez A, *et al* (2004) Exploration of essential gene functions via titratable promoter alleles. *Cell* 118: 31-44

Munoz AJ, Wanichthanarak K, Meza E & Petranovic D (2012) Systems biology of yeast cell death. *FEMS Yeast Research* 12: 249-265

Murata S, Yashiroda H & Tanaka K (2009) Molecular mechanisms of proteasome assembly. *Nat Rev Mol Cell Biol* 10: 104-115

Nations U (2019) *World Population Prospects 2019* Volume I: Comprehensive Tables

Niederleithinger M (2018) Analysis of the impact of α-synuclein expression on protein dynamics in yeast. *Master thesis, University of Goettingen*

Nuber S, Rajsombath M, Minakaki G, Winkler J, Müller CP, Ericsson M, Caldarone B, Dettmer U & Selkoe DJ (2018) Abrogating native α-synuclein tetramers in mice causes a L-DOPA-responsive motor syndrome closely resembling Parkinson's Disease. *Neuron* 100: 75-90.e5

Okochi M, Walter J, Koyama A, Nakajo S, Baba M, Iwatsubo T, Meijer L, Kahle PJ & Haass C (2000) Constitutive phosphorylation of the Parkinson's disease associated α- synuclein. *J Biol Chem* 275: 390-397

Orozco JL, Andrés Valderrama-Chaparro J, David Pinilla-Monsalve G, Molina-Echeverry MI, Melissa A, Castaño P, Ariza-Araújo Y, Prada SI & Takeuchi Y (2020) Parkinson's disease prevalence, age distribution and staging in Colombia. *Neurology International* 12: 8401

Oueslati A (2016) Implication of Alpha-Synuclein Phosphorylation at S129 in Synucleinopathies: What Have We Learned in the Last Decade? *J Parkinsons Dis* 6: 39-51

Oueslati A, Schneider BL, Aebischer P & Lashuel HA (2013) Polo-like kinase 2 regulates selective autophagic alpha-synuclein clearance and suppresses its toxicity in vivo. *Proc Natl Acad Sci U S A* 110: E3945-E3954

Outeiro TF & Lindquist S (2003) Yeast cells provide insight into alpha-synuclein biology and pathobiology. *Science* 302: 1772-1775

Pajarillo E, Rizor A, Lee J, Aschner M & Lee E (2019) The role of astrocytic glutamate transporters GLT-1 and GLAST in neurological disorders: Potential targets for neurotherapeutics. *Neuropharmacology* 161: 107559

Paleologou KE, Oueslati A, Shakked G, Rospigliosi CC, Kim HY, Lamberto GR, Fernandez CO, Schmid A, Chegini F, Gai WP, *et al* (2010) Phosphorylation at S87 is enhanced in synucleinopathies, inhibits α-synuclein oligomerization, and influences synuclein-membrane interactions. *J Neurosci* 30: 3184-3198

Paleologou KE, Schmid AW, Rospigliosi CC, Kim HY, Lamberto GR, Fredenburg RA, Lansbury PT, Fernandez CO, Eliezer D, Zweckstetter M, *et al* (2008) Phosphorylation at Ser-129 but not the phosphomimics S129E/D inhibits the fibrillation of α-synuclein. *J Biol Chem* 283: 16895-16905

Park S, Roelofs J, Kim W, Robert J, Schmidt M, Gygi SP & Finley D (2009) Hexameric assembly of the proteasomal ATPases is templated through their C termini.

Park Y, Hwang Y-P, Lee J-S, Seo S-H, Yoon SK & Yoon J-B (2005) Proteasomal ATPase-Associated Factor 1 Negatively Regulates Proteasome Activity by Interacting with Proteasomal ATPases. *Molecular and Cellular Biology* 25: 3842-3853

Parkinson J (2002) An essay on the shaking palsy. *J Neuropsychiatry Clin Neurosci* 14: 222-236

Peters LZ, Karmon O, David-Kadoch G, Hazan R, Yu T, Glickman MH & Ben-Aroya S (2015) The protein quality control machinery regulates its misassembled proteasome subunits. *PLoS Genet* 11: e1005178

Petroi D, Popova B, Taheri-Talesh N, Irniger S, Shahpasandzadeh H, Zweckstetter M, Outeiro TF & Braus GH (2012) Aggregate clearance of alpha-synuclein in *Saccharomyces cerevisiae* depends more on autophagosome and vacuole function than on the proteasome. *J Biol Chem* 287: 27567-27579

Poewe W, Seppi K, Tanner CM, Halliday GM, Brundin P, Volkmann J, Schrag A-E & Lang AE (2017) Parkinson disease. *Nature Reviews Disease Primers* 3: 17013

Polymeropoulos MH, Lavedan C, Leroy E, Ide SE, Dehejia A, Dutra A, Pike B, Root H, Rubenstein J, Boyer R, *et al* (1997) Mutation in the α-synuclein gene identified in families with Parkinson's disease. *Science* 276: 2045-2047

Popova B, Galka D, Häffner N, Wang D, Schmitt K, Valerius O, Knop M & Braus GH (2021a) α-synuclein decreases the abundance of proteasome subunits and alters ubiquitin conjugates in yeast. *Cells* 10: 2229

Popova B, Kleinknecht A & Braus GH (2015) Posttranslational Modifications and Clearing of alpha-Synuclein Aggregates in Yeast. *Biomolecules* 5: 617-634

Popova B, Wang D, Pätz C, Akkermann D, Lázaro DF, Galka D, Gulko MK, Bohnsack MT, Möbius W, Bohnsack KE, *et al* (2021b) DEAD-box RNA helicase Dbp4/DDX10 is an enhancer of α-synuclein toxicity and oligomerization. *PLoS Genet* 17: e1009407

Prabakaran S, Lippens G, Steen H & Gunawardena J (2012) Post-translational modification: Nature's escape from genetic imprisonment and the basis for dynamic information encoding. *Wiley Interdiscip Rev Syst Biol and Med* 4: 565-583

Pratt MR, Abeywardana T, Marotta NP & Witt SN (2015) Synthetic proteins and peptides for the direct interrogation of α-synuclein posttranslational modifications. *Biomolecules* 5: 1210-1227

Pronin AN, Morris AJ, Surguchov A & Benovic JL (2000) Synucleins are a novel class of substrates for G protein-coupled receptor kinases. *J Biol Chem* 275: 26515-26522

Qing H, Wong W, McGeer EG & McGeer PL (2009) Lrrk2 phosphorylates alpha synuclein at serine 129: Parkinson disease implications. *Biochem Biophys Res Commun* 387: 149-152

Rabl J, Smith DM, Yu Y, Chang SC, Goldberg AL & Cheng Y (2008) Mechanism of gate opening in the 20S proteasome by the proteasomal ATPases. *Molecular Cell* 30: 360-368

Reggiori F & Klionsky DJ (2013) Autophagic processes in yeast: Mechanism, machinery and regulation. *Genetics* 194: 341-361

Riley JC (2005) Estimates of regional and global life expectancy, 1800-2001. *Population and Development Review* 31: 537-543

Rizek P, Kumar N & Jog MS (2016) An update on the diagnosis and treatment of Parkinson disease. *CMAJ* 188: 1157-1165

Roelofs J, Park S, Haas W, Tian G, McAllister FE, Huo Y, Lee BH, Zhang F, Shi Y, Gygi SP, *et al* (2009) Chaperone-mediated pathway of proteasome regulatory particle assembly. *Nature* 459: 861-865

Rott R, Szargel R, Haskin J, Bandopadhyay R, Lees AJ, Shani V & Engelender S (2011) α-Synuclein fate is determined by USP9X-regulated monoubiquitination. *Proc Natl Acad Sci U S A* 108: 18666-18671

Saeki Y & Tanaka K (2007) Unlocking the Proteasome Door. *Molecular Cell* 27: 865-867

Saeki Y, Toh-e A, Kudo T, Kawamura H & Tanaka K (2009) Multiple Proteasome-Interacting Proteins Assist the Assembly of the Yeast 19S Regulatory Particle. *Cell* 137: 900-913

Saiki RK, Gelfand DH, Stoffel S, Scharf SJ, Higuchi R, Horn GT, Mullis KB & Erlich HA (1988) Primer-Directed Enzymatic Amplification of DNA with a Thermostable DNA Polymerase. *Science* 239: 487-491

Sakata E, Eisele MR & Baumeister W (2021) Molecular and cellular dynamics of the 26S proteasome. *Biochimica et Biophysica Acta - Proteins and Proteomics* 1869: 140583

Salvi M, Trashi E, Marin O, Negro A, Sarno S & Pinna LA (2012) Superiority of PLK-2 as alpha-synuclein phosphorylating agent relies on unique specificity determinants. *Biochem Biophys Res Commun* 418: 156-160

Sancenon V, Lee SA, Patrick C, Griffith J, Paulino A, Outeiro TF, Reggiori F, Masliah E & Muchowski PJ (2012) Suppression of α-synuclein toxicity and vesicle trafficking defects by phosphorylation at S129 in yeast depends on genetic context. *Human Molecular Genetics* 21: 2432-2449

Sanger F, Nicklen S & Coulson AR (1977) DNA sequencing with chain-terminating inhibitors. *Proc Natl Acad Sci U S A* 74: 5463-5467

Sato S, Uchihara T, Fukuda T, Noda S, Kondo H, Saiki S, Komatsu M, Uchiyama Y, Tanaka K & Hattori N (2018) Loss of autophagy in dopaminergic neurons causes Lewy pathology and motor dysfunction in aged mice. *Scientific Reports* 8: 2813

Schmid AB, Nee RJ & Coppieters MW (2013) Reappraising entrapment neuropathies - Mechanisms, diagnosis and management. *Manual Therapy* 18: 449-457

Schmidt M, Hanna J, Elsasser S & Finley D (2005) Proteasome-associated proteins: regulation of a proteolytic machine. *Biological Chemistry* 386: 725-737

Schwartz MD Alan L. P & Ciechanover PhD Aaron MD (1999) The ubiquitin-proteasome pathway and pathogenesis of human diseases. *Annual Review of Medicine* 50: 57-74

Shahpasandzadeh H, Popova B, Kleinknecht A, Fraser PE, Outeiro TF & Braus GH (2014) Interplay between sumoylation and phosphorylation for protection against α-synuclein inclusions. *J Biol Chem* 289: 31224-31240

Sherman F (2002) Getting started with yeast. *Methods in Enzymology* 350: 3-41

Shimura H, Schlossmacher MG, Hattori N, Frosch MP, Trockenbacher A, Schneider R, Mizuno Y, Kosik KS & Selkoe DJ (2001) Ubiquitination of a new form of α-synuclein by parkin from human brain: Implications for Parkinson's disease. *Science* 293: 263-269

Shirozu R, Yashiroda H & Murata S (2015) Identification of minimum Rpn4-responsive elements in genes related to proteasome functions. *FEBS Letters* 589: 933-940

Sikorski RS & Hieter P (1989) A system of shuttle vectors and yeast host strains designed for efficient manipulation of DNA in *Saccharomyces cerevisiae*. *Genetics* 122: 19-27

Singleton AB, Farrer M, Johnson J, Singleton A, Hague S, Kachergus J, Hulihan M, Peuralinna T, Dutra A, Nussbaum R, *et al* (2003) alpha-Synuclein locus triplication causes Parkinson's disease. *Science* 302: 841

Sivaraman T, Kumar TKS, Jayaraman G & Yu C (1997) The mechanism of 2,2,2-trichloroacetic acid-induced protein precipitation. *J Protein Chem* 16: 291-297

Smith DM, Chang S-C, Park S, Finley D, Cheng Y & Goldberg AL (2007) Docking of the proteasomal ATPases' carboxyl termini in the 20S proteasome's alpha ring opens the gate for substrate entry. *Molecular Cell* 27: 731-744

Snyder H, Mensah K, Theisler C, Lee J, Matouschek A & Wolozin B (2003) Aggregated and monomeric α-synuclein bind to the S6′ proteasomal protein and inhibit proteasomal function. *J Biol Chem* 278: 11753-11759

Solla P, Cannas A, Ibba FC, Loi F, Corona M, Orofino G, Marrosu MG & Marrosu F (2012) Gender differences in motor and non-motor symptoms among Sardinian patients with Parkinson's disease. *J Neurol Sci* 323: 33-39

Soper JH, Roy S, Stieber A, Lee E, Wilson RB, Trojanowski JQ, Burd CG & Lee VM (2008) Alpha-synuclein-induced aggregation of cytoplasmic vesicles in *Saccharomyces cerevisiae*. *Mol Biol Cell* 19: 1093-1103

Spillantini MG, Schmidt ML, Lee VM-Y, Trojanowski JQ, Jakes R & Goedert M (1997) α-Synuclein in Lewy bodies. *Nature* 388: 839-840

Stefanis L, Emmanouilidou E, Pantazopoulou M, Kirik D, Vekrellis K & Tofaris GK (2019) How is alpha-synuclein cleared from the cell? *J Neurochem* 150: 577-590

Stefanis L, Larsen KE, Rideout HJ, Sulzer D & Greene LA (2001) Expression of A53T mutant but not wild-type alpha-synuclein in PC12 cells induces alterations of the ubiquitin-dependent degradation system, loss of dopamine release, and autophagic cell death. *J Neurosci* 21: 9549-9560

Su LJ, Auluck PK, Outeiro TF, Yeger-Lotem E, Kritzer JA, Tardiff DF, Strathearn KE, Liu F, Cao S, Hamamichi S, *et al* (2010) Compounds from an unbiased chemical screen reverse both ER-to-Golgi trafficking defects and mitochondrial dysfunction in Parkinson's disease models. *Dis Model Mech* 3: 194-208

Suzuki G, Imura S, Hosokawa M, Katsumata R, Nonaka T, Hisanaga SI, Saeki Y & Hasegawa M (2020) α-synuclein strains that cause distinct pathologies differentially inhibit proteasome. *Elife* 9: 1-21

Tanahashi N, Murakami Y, Minami Y, Shimbara N, Hendil KB & Tanaka K (2000) Hybrid proteasomes. Induction by interferon-γ and contribution to ATP- dependent proteolysis. *J Biol Chem* 275: 14336-14345

Tanaka Y, Engelender S, Igarashi S, Rao RK, Wanner T, Tanzi RE, Sawa A, L. Dawson V, Dawson TM & Ross CA (2001) Inducible expression of mutant α-synuclein decreases proteasome activity and increases sensitivity to mitochondria-dependent apoptosis. *Human Molecular Genetics* 10: 919-926

Tenreiro S, Eckermann K & Outeiro TF (2014a) Protein phosphorylation in neurodegeneration: friend or foe? *Front Mol Neurosci* 7: 42

Tenreiro S, Franssens V, Winderickx J & Outeiro TF (2017) Yeast models of Parkinson's disease-associated molecular pathologies. *Current Opinion in Genetics and Development* 44: 74-83

Tenreiro S, Reimão-Pinto MM, Antas P, Rino J & Wawrzycka D (2014b) Phosphorylation modulates clearance of alpha-synuclein inclusions in a yeast model of Parkinson's disease. *PLoS Genet* 10: e1004302

Tenreiro S, Rosado-Ramos R, Gerhardt E, Favretto F, Magalhães F, Popova B, Becker S, Zweckstetter M, Braus GH & Outeiro TF (2016) Yeast reveals similar molecular mechanisms underlying alpha- and beta-synuclein toxicity. *Human Molecular Genetics* 25: 275-290

Thibaudeau TA & Smith DM (2019) A Practical Review of Proteasome Pharmacology. *Pharmacol Rev* 71: 170-197

Thrower JS, Hoffman L, Rechsteiner M & Pickart CM (2000) Recognition of the polyubiquitin proteolytic signal. *EMBO Journal* 19: 94-102

Tofaris GK, Razzaq A, Ghetti B, Lilley KS & Spillantini MG (2003) Ubiquitination of alpha-synuclein in Lewy bodies is a pathological event not associated with impairment of proteasome function. *J Biol Chem* 278: 44405-44411

Tong AHY & Boone C (2006) Synthetic genetic array analysis in *Saccharomyces cerevisiae*. *Methods Mol Biol* 313: 171-192

Tong AHY & Boone C (2007) 16 High-Throughput Strain Construction and Systematic Synthetic Lethal Screening in *Saccharomyces cerevisiae*. *Methods in Microbiology* 36: 369-386, 706-707

Tonoki A, Kuranaga E, Tomioka T, Hamazaki J, Murata S, Tanaka K & Miura M (2009) Genetic Evidence Linking Age-Dependent Attenuation of the 26S Proteasome with the Aging Process. *Molecular and Cellular Biology* 29: 1095-1106

Tosatto L, Horrocks MH, Dear AJ, Knowles TPJ, Dalla Serra M, Cremades N, Dobson CM & Klenerman D (2015) Single-molecule FRET studies on alpha-synuclein oligomerization of Parkinson's disease genetically related mutants. *Scientific Reports* 5: 16696

Towbin H, Staehelint T & Gordon J (1979) Electrophoretic transfer of proteins from polyacrylamide gels to nitrocellulose sheets: Procedure and some applications. *Proc Natl Acad Sci U S A* 76: 4350-4354

Valente EM, Bentivoglio AR, Dixon PH, Ferraris A, Ialongo T, Frontali M, Albanese A & Wood NW (2001) Localization of a novel locus for autosomal recessive early-onset parkinsonism, PARK6, on human chromosome 1p35-p36. *Am J Hum Genet* 68: 895-900

Verma R, Aravind L, Oania R, McDonald WH, Yates JR, Koonin E v & Deshaies RJ (2002) Role of Rpn11 Metalloprotease in Deubiquitination and Degradation by the 26*S* Proteasome. *Science* 298: 611-615

Vilchez D, Saez I & Dillin A (2014) The role of protein clearance mechanisms in organismal ageing and age-related diseases. *Nature Communications* 5: 5659

Waite KA, Burris A, Vontz G, Lang A & Roelofs J (2022) Proteaphagy is specifically regulated and requires factors dispensable for general autophagy. *J Biol Chem* 298: 101494

Wales P, Pinho R, Lazaro DF & Outeiro TF (2013) Limelight on alpha-synuclein: pathological and mechanistic implications in neurodegeneration. *J Parkinsons Dis* 3: 415-459

Wang S, Xu B, Liou LC, Ren Q, Huang S, Luo Y, Zhang Z & Witt SN (2012) alpha-Synuclein disrupts stress signaling by inhibiting polo-like kinase Cdc5/Plk2. *Proc Natl Acad Sci U S A* 109: 16119-16124

Wang W & Malcolm BA (1999) Two-Stage PCR Protocol Allowing Introduction of Multiple Mutations, Deletions and Insertions Using QuikChangeTM Site-Directed Mutagenesis. *Biotechniques* 26: 680-682

Wanneveich M, Moisan F, Jacqmin-Gadda H, Elbaz A & Joly P (2018) Projections of prevalence, lifetime risk, and life expectancy of Parkinson's disease (2010-2030) in France. *Movement Disorders* 33: 1449-1455

Waxman EA & Giasson BI (2008) Specificity and regulation of casein kinase-mediated phosphorylation of alpha-synuclein. *J Neuropathol Exp Neurol* 67: 402-416

Webb JL, Ravikumar B, Atkins J, Skepper JN & Rubinsztein DC (2003) Alpha-Synuclein is degraded by both autophagy and the proteasome. *J Biol Chem* 278: 25009-25013

Weston LJ, Cook ZT, Stackhouse TL, Sal MK, Schultz BI, Tobias ZJC, Osterberg VR, Brockway NL, Pizano S, Glover G, *et al* (2021) In vivo aggregation of presynaptic alpha-synuclein is not influenced by its phosphorylation at serine-129. *Neurobiology of Disease* 152: 105291

Wijeratne T, Kumagai N, Rahman M, Wang Z, Ou Z, Pan J, Tang S, Duan D, Yu D & Nong H (2021) Global Trends in the Incidence, Prevalence, and Years Lived With Disability of Parkinson's Disease in 204 Countries/Territories From 1990 to 2019. *Frontiers in Public Health* 9: 776847

Xilouri M, Brekk OR & Stefanis L (2013) Alpha-synuclein and Protein Degradation Systems: a Reciprocal Relationship. *Molecular Neurobiology* 47: 537-551

Xu L, Nussinov R & Ma B (2016) Coupling of the Non-Amyloid-Component (NAC) Domain and the KTK(E/Q)GV Repeats Stabilize the α-Synuclein Fibrils HHS Public Access. *Eur J Med Chem* 121: 841-850

Yamada K & Iwatsubo T (2018) Extracellular α-synuclein levels are regulated by neuronal activity. *Molecular Neurodegeneration* 13: 9

Yang A, Ha S, Ahn J, Kim R, Kim S, Lee Y, Kim J, Söll D, Lee HY & Park HS (2016) A chemical biology route to site-specific authentic protein modifications. *Science* 354: 623-626

Yao T, Song L, Xu W, Demartino GN, Florens L, Swanson SK, Washburn MP, Conaway RC, Weliky Conaway J & Cohen RE (2006) Proteasome recruitment and activation of the Uch37 deubiquitinating enzyme by Adrm1. *Nature cell biology* 8: 994-1002

Zabrocki P, Bastiaens I, Delay C, Bammens T, Ghillebert R, Pellens K, de Virgilio C, van Leuven F & Winderickx J (2008) Phosphorylation, lipid raft interaction and traffic of alpha-synuclein in a yeast model for Parkinson. *Biochim Biophys Acta* 1783: 1767-1780

Zarranz JJ, Alegre J, Gómez-Esteban JC, Lezcano E, Ros R, Ampuero I, Vidal L, Hoenicka J, Rodriguez O, Atarés B, *et al* (2004) The new mutation, E46K, of α-synuclein causes parkinson and Lewy body dementia. *Annals of Neurology* 55: 164-173

Zijdeman R & Ribeira da Silva F (2015) Life Expectancy at Birth (Total). *IISH Data Collection* 1

Zimprich A, Biskup S, Leitner P, Lichtner P, Farrer M, Lincoln S, Kachergus J, Hulihan M, Uitti RJ, Calne DB, *et al* (2004) Mutations in LRRK2 cause autosomal-dominant parkinsonism with pleomorphic pathology. *Neuron* 44: 601-607.

Supplementary material

Table S1. Genes encoding proteins with significantly changed stability upon expression of αSyn in comparison to the empty vector (EV) control.
Ratio represents log2 from mCherry/sfGFP fluorescence intensities. $RatioDiff_{(EV-\alpha Syn)}$ represents $log2(R_{EV})$-$log2(R_{\alpha Syn})$ and is a measure for changed stability. Negative RatioDiff indicates stabilization of the fusion protein upon αSyn expression.

ORF	Gene	Name	Ratio (EV)	Ratio (αSyn)	RatioDiff (EV-αSyn)	p-value (EV- αSyn)
YGR142W	*BTN2*	BaTteN disease	-5.27	0.85	-6.12	0.01
YGL004C	*RPN14*	Regulatory Particle Non-ATPase	0.52	6.01	-5.49	0.00
YDR185C	*UPS3*	UnProceSsed	-2.89	2.55	-5.44	0.00
YOR244W	*ESA1*	Catalytic subunit of the histone acetyltransferase complex	-0.73	4.46	-5.20	0.01
YDL048C	*STP4*	protein with similarity to Stp1p	-5.28	-0.11	-5.18	0.00
YPL026C	*SKS1*	Suppressor Kinase of SNF3	-3.72	1.40	-5.12	0.00
YOR344C	*TYE7*	Ty1-mediated Expression	-5.68	-0.74	-4.94	0.00
YGR238C	*KEL2*	KELch repeat	-0.32	4.49	-4.80	0.00
YDR523C	*SPS1*	SPorulation Specific	-2.14	2.62	-4.75	0.00
YDR279W	*RNH202*	RNase H	0.38	5.02	-4.64	0.00
YCL039W	*GID7*	Glucose Induced Degradation deficient	-3.16	1.46	-4.63	0.00
YDL063C	*SYO1*	SYnchronized impOrt or SYmpOrtin	0.29	4.90	-4.61	0.01
YFL007W	*BLM10*	BLeoMycin resistance	-2.63	1.96	-4.58	0.00
YEL006W	*YEA6*	Mitochondrial NAD+ transporter	-3.27	1.26	-4.54	0.01
YKR054C	*DYN1*	DYNein	-1.43	3.09	-4.52	0.00
YNL172W	*APC1*	Anaphase Promoting Complex subunit	-2.51	2.00	-4.51	0.00
YOL043C	*NTG2*	eNdonuclease Three-like Glycosylase	-0.60	3.90	-4.49	0.00
YOL116W	*MSN1*	Multicopy suppressor of SNF1 mutation	-0.71	3.70	-4.42	0.00
YCL061C	*MRC1*	Mediator of the Replication Checkpoint	-1.31	3.07	-4.38	0.00
YMR199W	*CLN1*	CycLiN	-3.97	0.38	-4.35	0.01
YGR044C	*RME1*	Regulator of MEiosis	-3.76	0.59	-4.35	0.00
YIL087C	*AIM19*	Altered Inheritance rate of Mitochondria	-3.60	0.71	-4.31	0.00
YHR061C	*GIC1*	GTPase Interactive Component	-2.67	1.61	-4.28	0.00
YML099C	*ARG81*	ARGinine requiring	-2.76	1.46	-4.22	0.01
YHR034C	*PIH1*	Protein Interacting with Hsp90	-0.38	3.84	-4.21	0.00
YMR135C	*GID8*	Glucose Induced Degradation deficient	-3.61	0.60	-4.21	0.00
YNR031C	*SSK2*	Suppressor of Sensor Kinase	0.99	5.18	-4.20	0.00
YMR056C	*AAC1*	ADP/ATP Carrier	-3.13	1.05	-4.18	0.01
YMR225C	*MRPL44*	Mitochondrial Ribosomal Protein, Large subunit	-0.99	3.15	-4.13	0.01
YMR137C	*PSO2*	PSOralen derivative sensitive	-2.22	1.91	-4.13	0.00
YBL084C	*CDC27*	Cell Division Cycle	-2.07	2.05	-4.12	0.00
YDR026C	*NSI1*	NTS1 SIlencing protein 1	-1.80	2.32	-4.12	0.00

YOR355W	*GDS1*	Involved in histone H4 acetylation	-3.94	0.16	-4.10	0.00
YLR247C	*IRC20*	Increased Recombination Centers	-1.43	2.66	-4.09	0.01
YLR385C	*SWC7*	SWr Complex	1.56	5.63	-4.07	0.00
YPL141C	*FRK1*	Fatty acyl-CoA synthetase and RNA processing-associated Kinase	-1.83	2.24	-4.07	0.00
YKL125W	*RRN3*	Regulation of RNA polymerase I	-2.73	1.31	-4.04	0.00
YIR017C	*MET28*	METhionine	-2.96	1.06	-4.02	0.00
YNL155W	*CUZ1*	Cdc48-associated UBL/Zn-finger protein	-3.71	0.29	-4.00	0.01
YMR198W	*CIK1*	Chromosome Instability and Karyogamy	-2.49	1.51	-4.00	0.00
YPL076W	*GPI2*	GlycosylPhosphatidylInositol anchor biosynthesis	-0.59	3.41	-4.00	0.01
YER013W	*PRP22*	Pre-mRNA Processing	-2.63	1.35	-3.98	0.00
YOR279C	*RFM1*	Repression Factor of Middle sporulation element	-2.73	1.24	-3.97	0.01
YLR023C	*IZH3*	Implicated in Zinc Homeostasis	-4.08	-0.11	-3.96	0.01
YNL082W	*PMS1*	PostMeiotic Segregation	-2.66	1.30	-3.95	0.00
YKL185W	*ASH1*	Asymmetric Synthesis of HO	-3.08	0.87	-3.95	0.00
YDR375C	*BCS1*	ubiquinol-cytochrome c reductase (bc1) Synthesis	-2.25	1.69	-3.94	0.00
YGL139W	*FLC3*	FLavin Carrier	-1.46	2.47	-3.92	0.01
YGL229C	*SAP4*	Sit4 Associated Protein	-2.03	1.86	-3.89	0.00
YDR118W	*APC4*	Anaphase Promoting Complex	-1.73	2.15	-3.88	0.00
YNL257C	*SIP3*	SNF1-Interacting Protein	-1.22	2.66	-3.88	0.00
YDR266C	*HEL2*	Histone E3 Ligase	-1.61	2.24	-3.85	0.00
YKL179C	*COY1*	CASP Of Yeast	-1.74	2.10	-3.84	0.00
YJL025W	*RRN7*	Regulation of RNA polymerase I	-1.18	2.61	-3.79	0.00
YML109W	*ZDS2*	Zillion Different Screens	-1.97	1.81	-3.78	0.00
YER173W	*RAD24*	RADiation sensitive	-0.75	3.01	-3.76	0.00
YOR346W	*REV1*	REVersionless	-0.39	3.37	-3.76	0.01
YLR098C	*CHA4*	Catabolism of Hydroxy Amino acids	-1.65	2.11	-3.76	0.01
YNR045W	*PET494*	PETite colonies	-1.57	2.17	-3.74	0.00
YDR052C	*DBF4*	DumbBell Former	-2.24	1.50	-3.73	0.00
YER124C	*DSE1*	Daughter Specific Expression	-4.10	-0.37	-3.73	0.00
YDR443C	*SSN2*	Suppressor of SNf1	-0.53	3.17	-3.70	0.00
YMR048W	*CSM3*	Chromosome Segregation in Meiosis	-1.27	2.42	-3.69	0.01
YKR022C	*NTR2*	NineTeen complex Related protein	-1.10	2.57	-3.66	0.00
YLR003C	*CMS1*	Complementation of Mcm-10 Suppressor	-2.83	0.82	-3.65	0.00
YIL050W	*PCL7*	Pho85 CycLin	-3.20	0.44	-3.64	0.00
YDR076W	*RAD55*	RADiation sensitive	-1.28	2.33	-3.62	0.01
YJL139C	*YUR1*	Yeast Unknown Reading frame	-1.43	2.18	-3.61	0.00
YLR105C	*SEN2*	Splicing ENdonuclease	-1.56	2.02	-3.59	0.00
YOR337W	*TEA1*	Ty Enhancer Activator	-1.71	1.86	-3.57	0.00
YKL078W	*DHR2*	DEAH-box RNA helicase	-1.26	2.29	-3.55	0.00
YGL162W	*SUT1*	Sterol UpTake	-1.10	2.44	-3.55	0.01

YLR135W	*SLX4*	Synthetic Lethal of unknown (X) function	-1.32	2.22	-3.54	0.00
YDR439W	*LRS4*	Loss of RDNA Silencing	-1.87	1.67	-3.54	0.00
YOR162C	*YRR1*	Yeast Reveromycin-A Resistant	-2.10	1.43	-3.54	0.00
YDR125C	*ECM18*	ExtraCellular Mutant	-1.32	2.21	-3.53	0.00
YBR008C	*FLR1*	FLuconazole Resistance	-1.90	1.63	-3.53	0.00
YAR031W	*PRM9*	Pheromone-Regulated Membrane protein	-0.61	2.91	-3.52	0.00
YFL004W	*VTC2*	Vacuolar Transporter Chaperone	-3.14	0.38	-3.52	0.00
YIR005W	*IST3*	Increased Sodium Tolerance	-1.73	1.77	-3.50	0.00
YBL063W	*KIP1*	KInesin related Protein	-1.13	2.36	-3.49	0.01
YNL321W	*VNX1*	Vacuolar Na+/H+ eXchanger	-1.41	2.06	-3.48	0.00
YBR042C	*CST26*	Chromosome STability	-1.08	2.39	-3.47	0.00
YPL179W	*PPQ1*	Protein Phosphatase Q	-2.27	1.19	-3.46	0.00
YKL074C	*MUD2*	Mutant U1 Die	-1.83	1.63	-3.46	0.00
YOL100W	*PKH2*	Pkb-activating Kinase Homolog	-1.18	2.28	-3.46	0.00
YJL110C	*GZF3*	Gata Zinc Finger protein	-2.43	1.02	-3.45	0.00
YJR097W	*JJJ3*	J-protein (Type III)	-1.27	2.17	-3.44	0.00
YKL043W	*PHD1*	PseudoHyphal Determinant	-1.66	1.77	-3.43	0.00
YOR373W	*NUD1*	Mitotic exit network (MEN) scaffold protein	-0.69	2.74	-3.43	0.00
YOR311C	*DGK1*	DiacylGlycerol Kinase	-0.90	2.53	-3.43	0.00
YMR224C	*MRE11*	Meiotic REcombination	-1.29	2.13	-3.42	0.00
YNL053W	*MSG5*	Multicopy Suppressor of GPA1	-2.24	1.18	-3.42	0.00
YOL105C	*WSC3*	Cell wall integrity and Stress response Component	-0.97	2.44	-3.41	0.00
YHR036W	*BRL1*	BRr6 Like protein	-1.24	2.17	-3.41	0.00
YKL101W	*HSL1*	Histone Synthetic Lethal	-1.28	2.11	-3.39	0.00
YOR025W	*HST3*	Homolog of SIR Two (SIR2)	-2.60	0.77	-3.37	0.00
YJL004C	*SYS1*	Suppressor of Ypt Six	-1.03	2.33	-3.37	0.00
YCR018C	*SRD1*	Involved in the processing of pre-rRNA	-2.48	0.88	-3.37	0.00
YKR077W	*MSA2*	Mbf and Sbf Associated	-3.19	0.17	-3.36	0.00
YPL230W	*USV1*	Up in StarVation	-2.38	0.96	-3.35	0.00
YDR184C	*ATC1*	Aip Three Complex	-1.78	1.57	-3.35	0.00
YAL041W	*CDC24*	Cell Division Cycle	-0.33	2.99	-3.32	0.00
YBR065C	*ECM2*	ExtraCellular Mutant	-0.87	2.45	-3.32	0.00
YDR247W	*VHS1*	Viable in a Hal3 Sit4 background	-2.29	1.02	-3.31	0.00
YLR193C	*UPS1*	UnProceSsed	-2.58	0.68	-3.26	0.00
YER033C	*ZRG8*	Zinc Regulated Gene	-1.73	1.52	-3.24	0.00
YKL033W	*TTI1*	Two Tel2-Interacting protein	-1.18	2.06	-3.24	0.00
YIL017C	*VID28*	Vacuolar Import and Degradation	-1.24	1.99	-3.23	0.00
YER167W	*BCK2*	Bypass of C Kinase	-1.34	1.88	-3.23	0.00
YFL029C	*CAK1*	Cdk-Activating Kinase	-1.21	2.01	-3.22	0.01
YLR183C	*TOS4*	Target Of Sbf	-2.44	0.78	-3.22	0.00
YOL077W-A	*ATP19*	ATP synthase	-3.55	-0.33	-3.21	0.00

YOR127W	*RGA1*	Rho GTPase Activating Protein	-1.16	2.05	-3.21	0.01
YDR323C	*PEP7*	carboxyPEPtidase Y-deficient	-1.17	2.03	-3.20	0.00
YML071C	*COG8*	Conserved Oligomeric Golgi complex	-1.31	1.89	-3.20	0.01
YGR206W	*MVB12*	MultiVesicular Body sorting factor of 12 kilodaltons	-1.52	1.67	-3.19	0.00
YGL222C	*EDC1*	Enhancer of mRNA DeCapping	-2.99	0.19	-3.18	0.00
YPL242C	*IQG1*	IQGAP-related protein	-1.20	1.98	-3.18	0.00
YNL230C	*ELA1*	ELongin A	-0.91	2.23	-3.13	0.00
YLR442C	*SIR3*	Silent Information Regulator	-1.20	1.93	-3.13	0.00
YJR089W	*BIR1*	Baculoviral IAP Repeat-containing protein	-1.05	2.07	-3.12	0.00
YMR119W	*ASI1*	Amino acid Sensor-Independent	-0.56	2.56	-3.12	0.00
YLR127C	*APC2*	Anaphase Promoting Complex	-1.52	1.60	-3.12	0.00
YLR401C	*DUS3*	DihydroUridine Synthase	-1.26	1.86	-3.11	0.00
YGR251W	*NOP19*	NucleOlar Protein	-0.49	2.62	-3.11	0.00
YBR083W	*TEC1*	Transposon Enhancement Control	-1.54	1.57	-3.10	0.00
YDR189W	*SLY1*	Suppressor of Loss of Ypt1	0.19	3.29	-3.10	0.00
YMR172W	*HOT1*	High-Osmolarity-induced Transcription	-1.19	1.89	-3.09	0.00
YLR034C	*SMF3*	Involved in iron homeostasis	-2.86	0.21	-3.07	0.00
YMR268C	*PRP24*	Pre-mRNA Processing	-0.63	2.44	-3.07	0.01
YPL133C	*RDS2*	Regulator of Drug Sensitivity	-1.65	1.39	-3.05	0.00
YDL070W	*BDF2*	BromoDomain Factor	-2.25	0.79	-3.04	0.00
YMR036C	*MIH1*	Mitotic Inducer Homolog	-0.34	2.69	-3.03	0.01
YAL031C	*GIP4*	Glc7 Interacting Protein	-0.71	2.30	-3.02	0.00
YFL033C	*RIM15*	Regulator of IME2	-0.50	2.52	-3.02	0.00
YGR169C	*PUS6*	PseudoUridine Synthase	-1.42	1.59	-3.01	0.00
YOR271C	*FSF1*	Fungal SideroFlexin 1	-0.35	2.66	-3.01	0.00
YGR099W	*TEL2*	TELomere maintenance	-1.12	1.89	-3.00	0.00
YJL198W	*PHO90*	PHOsphate metabolism	-1.18	1.82	-3.00	0.00
YAL056W	*GPB2*	Regulator of cAMP-PKA signaling	-0.51	2.47	-2.98	0.00
YDR464W	*SPP41*	Suppressor of PrP4	-0.90	2.08	-2.98	0.00
YNL023C	*FAP1*	FKBP12-Associated Protein	-0.50	2.47	-2.97	0.00
YGL175C	*SAE2*	Sporulation in the Absence of spo Eleven	-0.14	2.83	-2.97	0.01
YBR179C	*FZO1*	FuZzy Onions homolog	-1.77	1.18	-2.95	0.00
YIR015W	*RPR2*	RNase P Ribonucleoprotein	-1.75	1.20	-2.95	0.00
YPR134W	*MSS18*	Mitochondrial Splicing System	-0.40	2.54	-2.94	0.00
YNL063W	*MTQ1*	Methyltransferase	-0.80	2.13	-2.93	0.01
YPR031W	*NTO1*	NuA Three Orf	-1.19	1.73	-2.92	0.00
YMR232W	*FUS2*	cell FUSion	-1.22	1.70	-2.92	0.00
YPL157W	*TGS1*	TrimethylGuanosine Synthase	-1.02	1.89	-2.91	0.00
YNL133C	*FYV6*	Function required for Yeast Viability	-0.46	2.45	-2.91	0.00
YPR140W	*TAZ1*	TAfaZzin	-0.75	2.16	-2.91	0.00
YGL065C	*ALG2*	Asparagine-Linked Glycosylation	0.22	3.13	-2.91	0.00

YIL061C	*SNP1*	Component of U1 snRNP	-1.45	1.45	-2.91	0.00
YBL102W	*SFT2*	Suppressor of sed Five Ts	0.31	3.21	-2.90	0.00
YGL240W	*DOC1*	Destruction Of Cyclin B	-0.62	2.28	-2.89	0.00
YBR168W	*PEX32*	PEroXisome related	-0.73	2.15	-2.89	0.00
YNR011C	*PRP2*	Pre-mRNA Processing	-1.55	1.32	-2.87	0.00
YKL146W	*AVT3*	Amino acid Vacuolar Transport	-1.57	1.30	-2.87	0.00
YLR371W	*ROM2*	RhO1 Multicopy suppressor	-1.11	1.75	-2.86	0.01
YNL129W	*NRK1*	Nicotinamide Riboside Kinase	-1.36	1.50	-2.86	0.00
YKR084C	*HBS1*	Hsp70 subfamily B Suppressor	-0.92	1.94	-2.86	0.00
YPL022W	*RAD1*	RADiation sensitive	-0.49	2.37	-2.86	0.00
YOR315W	*SFG1*	SuperFicial pseudohyphal Growth	-2.10	0.76	-2.86	0.00
YDL111C	*RRP42*	Ribosomal RNA Processing	0.86	3.70	-2.84	0.00
YBR257W	*POP4*	Processing Of Precursor RNAs	-0.93	1.91	-2.84	0.00
YDR448W	*ADA2*	transcriptional ADAptor	-1.44	1.39	-2.83	0.01
YMR288W	*HSH155*	Human Sap Homolog	-0.51	2.33	-2.83	0.00
YGR134W	*CAF130*	CCR4 Associated Factor	-1.04	1.79	-2.83	0.01
YNL027W	*CRZ1*	Calcineurin-Responsive Zinc finger	-0.90	1.92	-2.83	0.00
YLR068W	*FYV7*	Function required for Yeast Viability	-0.66	2.16	-2.82	0.01
YDR252W	*BTT1*	BTf Three	-1.30	1.51	-2.81	0.00
YCR082W	*AHC2*	Ada Histone acetyltransferase complex Component	-2.39	0.42	-2.81	0.00
YAR003W	*SWD1*	Set1c, WD40 repeat protein	0.24	3.05	-2.81	0.01
YLR107W	*REX3*	Rna EXonuclease	-1.03	1.77	-2.80	0.00
YJL056C	*ZAP1*	Zinc-responsive Activator Protein	-1.88	0.92	-2.80	0.00
YER142C	*MAG1*	3-MethylAdenine DNA Glycosylase	-0.48	2.31	-2.79	0.00
YOL028C	*YAP7*	Yeast AP-1	-1.43	1.36	-2.79	0.00
YBR095C	*RXT2*	Component of histone deacetylase Rpd3L complex	-0.46	2.32	-2.78	0.00
YPL267W	*ACM1*	APC/C[Cdh1] Modulator	-1.99	0.78	-2.77	0.00
YNL273W	*TOF1*	TOpoisomerase I-interacting Factor	-0.55	2.22	-2.77	0.00
YLR215C	*CDC123*	Cell Division Cycle	-0.10	2.67	-2.76	0.00
YNL068C	*FKH2*	ForK head Homolog	-1.23	1.53	-2.76	0.00
YOL113W	*SKM1*	STE20/PAK homologous Kinase related to Morphogenesis	-0.85	1.91	-2.76	0.00
YML076C	*WAR1*	Weak Acid Resistance	-0.79	1.97	-2.76	0.00
YPL256C	*CLN2*	CycLiN	-2.34	0.40	-2.75	0.00
YGR096W	*TPC1*	Thiamine Pyrophosphate Carrier	-0.50	2.25	-2.74	0.01
YNL298W	*CLA4*	CLn Activity dependant	-0.28	2.45	-2.73	0.00
YDR410C	*STE14*	STErile	0.00	2.73	-2.73	0.00
YOL072W	*THP1*	Tho2/Hpr1 Phenotype	-0.35	2.38	-2.73	0.01
YNR023W	*SNF12*	Sucrose NonFermenting	-0.79	1.94	-2.73	0.00
YNL213C	*RRG9*	Required for Respiratory Growth	-0.78	1.95	-2.73	0.00
YPL155C	*KIP2*	KInesin related Protein	-0.97	1.75	-2.73	0.00

YEL059C-A	*SOM1*	SOrting Mitochondrial	-0.31	2.42	-2.72	0.00
YNR055C	*HOL1*	HistidinOl	-0.42	2.30	-2.72	0.00
YDR291W	*HRQ1*	Homologous to RecQ protein	-0.64	2.08	-2.72	0.00
YDL087C	*LUC7*	Lethal Unless Cap-binding complex is produced	-1.37	1.34	-2.72	0.00
YHR164C	*DNA2*	DNA synthesis defective	-0.04	2.67	-2.71	0.01
YPL115C	*BEM3*	Bud EMergence	-0.82	1.87	-2.70	0.00
YDR219C	*MFB1*	Mitochondria-associated F-Box protein	-1.62	1.08	-2.70	0.00
YBR195C	*MSI1*	Multicopy Suppressor of IRA1	-0.83	1.86	-2.69	0.00
YDR376W	*ARH1*	Adrenodoxin Reductase Homolog	-0.20	2.48	-2.68	0.00
YBR097W	*VPS15*	Vacuolar Protein Sorting	-0.85	1.83	-2.68	0.00
YHR090C	*YNG2*	Yeast iNG1 homolog	-0.86	1.82	-2.68	0.00
YLR265C	*NEJ1*	Nonhomologous End-Joining defective	-0.82	1.84	-2.67	0.00
YMR127C	*SAS2*	Something About Silencing	0.67	3.34	-2.66	0.00
YCR092C	*MSH3*	MutS Homolog	-0.53	2.13	-2.66	0.00
YMR138W	*CIN4*	Chromosome INstability	-1.01	1.65	-2.66	0.00
YJL191W	*RPS14B*	Ribosomal Protein of the Small subunit	-1.97	0.69	-2.66	0.00
YGL113W	*SLD3*	Synthetically Lethal with Dpb11-1	-0.17	2.49	-2.66	0.00
YLR451W	*LEU3*	LEUcine biosynthesis	-1.58	1.07	-2.65	0.00
YER107C	*GLE2*	GLFG LEthal	-1.29	1.35	-2.64	0.01
YIL009W	*FAA3*	Fatty Acid Activation	-0.62	2.00	-2.62	0.00
YER075C	*PTP3*	Protein Tyrosine Phosphatase	-0.85	1.78	-2.62	0.00
YCR024C	*SLM5*	Synthetic Lethal with Mss4	-0.10	2.52	-2.62	0.00
YCL055W	*KAR4*	KARyogamy	-0.68	1.94	-2.62	0.00
YLR115W	*CFT2*	Cleavage Factor Two	-0.51	2.10	-2.61	0.00
YDR437W	*GPI19*	Glycosyl PhosphatidylInositol anchor biosynthesis	-1.03	1.58	-2.61	0.00
YPL140C	*MKK2*	Mitogen-activated Kinase Kinase	-1.55	1.06	-2.61	0.00
YHR171W	*ATG7*	AuTophaGy related	-0.40	2.21	-2.60	0.01
YGR171C	*MSM1*	Mitochondrial aminoacyl-tRNA Synthetase, Methionine	-0.26	2.34	-2.60	0.00
YDL080C	*THI3*	THIamine metabolism	-0.58	2.02	-2.59	0.01
YKL114C	*APN1*	APurinic/apyrimidinic eNdonuclease	-0.94	1.65	-2.59	0.00
YMR292W	*GOT1*	GOlgi Transport	0.03	2.62	-2.59	0.00
YKL004W	*AUR1*	AUreobasidin A Resistance	-0.70	1.89	-2.59	0.00
YER132C	*PMD1*	Paralog of MDS3	-0.58	2.00	-2.59	0.00
YHR102W	*KIC1*	Kinase that Interacts with Cdc31p	-0.90	1.69	-2.59	0.01
YJL091C	*GWT1*	GPI-anchored Wall protein Transfer	0.02	2.61	-2.59	0.00
YKR031C	*SPO14*	SPOrulation	0.13	2.71	-2.58	0.01
YDR440W	*DOT1*	Disruptor Of Telomeric silencing	0.07	2.64	-2.58	0.00
YBL060W	*YEL1*	Yeast EFA6-Like	-0.85	1.72	-2.57	0.00
YDL036C	*PUS9*	PseudoUridine Synthase	-0.51	2.06	-2.57	0.00
YMR285C	*NGL2*	Involved in 5.8S rRNA processing	-1.49	1.07	-2.57	0.00

YBR239C	*ERT1*	Ethanol Regulated Transcription factor	-0.93	1.63	-2.56	0.00
YLR452C	*SST2*	SuperSensiTive	-0.41	2.15	-2.56	0.00
YHR031C	*RRM3*	rDNA Recombination Mutation	-0.93	1.63	-2.56	0.00
YDR473C	*PRP3*	Pre-mRNA Processing	-1.03	1.52	-2.55	0.00
YER054C	*GIP2*	Glc7-Interacting Protein	-1.27	1.27	-2.54	0.00
YLR136C	*TIS11*	similar to the mammalian TPA Induced Sequence gene family	-2.36	0.18	-2.54	0.00
YNL073W	*MSK1*	Mitochondrial aminoacyl-tRNA Synthetase, lysine (K)	0.63	3.16	-2.53	0.00
YMR201C	*RAD14*	RADiation sensitive	-1.00	1.53	-2.53	0.00
YDR206W	*EBS1*	Est1-like Bcy1 Suppressor	-0.91	1.61	-2.52	0.00
YJL098W	*SAP185*	Sit4 Associated Protein	-1.13	1.40	-2.52	0.00
YGR102C	*GTF1*	Glutaminyl Transamidase subunit F	-0.69	1.83	-2.52	0.00
YMR280C	*CAT8*	CATabolite repression	-0.95	1.56	-2.52	0.00
YMR060C	*SAM37*	Sorting and Assembly Machinery	-0.15	2.36	-2.51	0.00
YER088C	*DOT6*	Disruptor Of Telomeric silencing	-1.57	0.94	-2.51	0.00
YLR382C	*NAM2*	Nuclear Accommodation of Mitochondria	-0.38	2.13	-2.50	0.00
YKL062W	*MSN4*	Multicopy suppressor of SNF1 mutation	-1.99	0.51	-2.50	0.00
YGR002C	*SWC4*	SWr Complex	-1.42	1.08	-2.50	0.00
YDR004W	*RAD57*	RADiation sensitive	-0.23	2.27	-2.50	0.00
YGR062C	*COX18*	Cytochrome c OXidase	-1.08	1.40	-2.48	0.00
YLR228C	*ECM22*	ExtraCellular Mutant	-1.14	1.34	-2.48	0.01
YNL242W	*ATG2*	AuTophaGy related	-0.37	2.11	-2.48	0.00
YDR423C	*CAD1*	CADmium resistance	-1.13	1.35	-2.47	0.00
YLR085C	*ARP6*	Actin-Related Protein	-0.56	1.91	-2.47	0.01
YMR211W	*DML1*	Drosophila melanogaster Misato-Like protein	-0.27	2.20	-2.47	0.01
YER147C	*SCC4*	Sister Chromatid Cohesion	-0.59	1.88	-2.46	0.00
YDR495C	*VPS3*	Vacuolar Protein Sorting	-0.21	2.25	-2.46	0.00
YOL080C	*REX4*	Rna EXonuclease	0.22	2.67	-2.46	0.00
YNL233W	*BNI4*	Bud Neck Involved	-0.83	1.62	-2.45	0.00
YNR004W	*SWM2*	Synthetic With mud2-delta	-0.53	1.92	-2.45	0.00
YJR047C	*ANB1*	ANaeroBically induced	-0.43	2.02	-2.44	0.01
YML111W	*BUL2*	Binds Ubiquitin Ligase	-0.18	2.26	-2.44	0.00
YJR055W	*HIT1*	HIgh Temperature growth	-0.44	1.99	-2.43	0.00
YDL030W	*PRP9*	Pre-mRNA Processing	-0.62	1.81	-2.42	0.00
YLR272C	*YCS4*	Yeast Condensin Subunit	-1.08	1.35	-2.42	0.00
YGL059W	*PKP2*	Protein Kinase of PDH	-1.07	1.35	-2.42	0.00
YLR077W	*FMP25*	Found in Mitochondrial Proteome	-0.02	2.40	-2.41	0.00
YKR049C	*FMP46*	Found in Mitochondrial Proteome	-0.55	1.86	-2.41	0.01
YCR033W	*SNT1*	SaNT domains	-0.64	1.77	-2.41	0.00
YBR193C	*MED8*	MEDiator complex	-0.59	1.81	-2.41	0.01
YML059C	*NTE1*	Neuropathy Target Esterase	0.04	2.44	-2.40	0.00
YKL020C	*SPT23*	SuPpressor of Ty	-0.84	1.57	-2.40	0.00

YER162C	*RAD4*	RADiation sensitive	-0.16	2.23	-2.39	0.00
YGL226C-A	*OST5*	OligoSaccharylTransferase	0.39	2.77	-2.38	0.00
YDL001W	*RMD1*	Required for Meiotic nuclear Division	-0.90	1.48	-2.38	0.00
YGL166W	*CUP2*	Copper-binding transcription factor	-0.87	1.50	-2.37	0.00
YDR288W	*NSE3*	Non SMC Element	-0.45	1.92	-2.37	0.00
YOL056W	*GPM3*	Glycerate PhosphoMutase	-1.52	0.84	-2.36	0.00
YPL138C	*SPP1*	Set1c, Phd finger Protein	-0.67	1.69	-2.36	0.00
YLR188W	*MDL1*	MultiDrug resistance-Like	-0.99	1.37	-2.36	0.01
YGL085W	*LCL3*	Long Chronological Lifespan 3	-0.65	1.70	-2.36	0.01
YOR228C	*MCP1*	Mdm10 Complementing Protein	-0.79	1.56	-2.35	0.00
YPL072W	*UBP16*	UBiquitin-specific Protease	0.11	2.46	-2.35	0.01
YHR041C	*SRB2*	Suppressor of RNA polymerase B	-0.41	1.93	-2.34	0.00
YHR116W	*COX23*	Cytochrome OXidase	1.17	3.51	-2.34	0.00
YOR249C	*APC5*	Anaphase Promoting Complex	-1.23	1.11	-2.34	0.00
YLR051C	*FCF2*	Faf1p Copurifying Factor	-0.64	1.69	-2.33	0.01
YLR086W	*SMC4*	Structural Maintenance of Chromosomes	-0.85	1.48	-2.33	0.00
YIL079C	*AIR1*	Arginine methyltransferase-Interacting RING finger protein	-0.54	1.79	-2.33	0.00
YNL078W	*NIS1*	Neck protein Interacting with Septins	-0.65	1.68	-2.33	0.00
YBR055C	*PRP6*	Pre-mRNA Processing	-0.83	1.50	-2.32	0.00
YIL056W	*VHR1*	VHt1 Regulator	-1.10	1.23	-2.32	0.00
YFR048W	*RMD8*	Required for Meiotic nuclear Division	0.56	2.89	-2.32	0.00
YPL177C	*CUP9*	Transcriptional repressor	-2.17	0.14	-2.31	0.00
YLR130C	*ZRT2*	Zinc-Regulated Transporter	-0.85	1.46	-2.31	0.00
YER111C	*SWI4*	SWItching deficient	-0.82	1.50	-2.31	0.00
YJL203W	*PRP21*	Pre-mRNA Processing	-0.72	1.59	-2.31	0.00
YHL025W	*SNF6*	Sucrose NonFermenting	-0.08	2.23	-2.31	0.00
YPR147C	*YPR147C*	Bifunctional triacylglycerol lipase	-1.72	0.34	-2.06	0.01
YBR291C	*CTP1*	Citrate Transport Protein	-1.81	0.07	-1.88	0.00
YOL013C	*HRD1*	HMG-coA Reductase Degradation	-0.30	1.56	-1.86	0.00
YPR049C	*ATG11*	AuTophaGy related	0.00	1.62	-1.62	0.00
YNL185C	*MRPL19*	Mitochondrial Ribosomal Protein, Large subunit	-0.52	1.01	-1.53	0.00
YPR174C	*CSA1*	Cdc5 SPB Anchor	0.04	1.52	-1.48	0.00
YGR084C	*MRP13*	Mitochondrial Ribosomal Protein	-0.02	1.37	-1.39	0.00
YIL107C	*PFK26*	6-PhosphoFructo-2-Kinase	0.04	1.35	-1.31	0.00
YHR001W-A	*QCR10*	ubiQuinol-cytochrome C oxidoReductase	-2.93	-1.64	-1.29	0.00
YMR098C	*ATP25*	ATPase	0.28	1.57	-1.29	0.00
YPR114W	*YPR114W*	Similar to ceramide synthases	1.93	3.22	-1.28	0.00
YLL008W	*DRS1*	Deficiency of Ribosomal Subunits	0.41	1.60	-1.18	0.00
YMR208W	*ERG12*	ERGosterol biosynthesis	-0.82	0.34	-1.17	0.00
YOL082W	*ATG19*	AuTophaGy related	0.09	1.07	-0.98	0.00
YER035W	*EDC2*	Enhancer of mRNA DeCapping	-1.51	-0.54	-0.97	0.00

YDL222C	*FMP45*	Found in Mitochondrial Proteome	0.46	1.41	-0.95	0.00
YDL064W	*UBC9*	UBiquitin-Conjugating	0.11	0.95	-0.84	0.00
YCR021C	*HSP30*	Heat Shock Protein	0.60	1.43	-0.83	0.00
YNL137C	*NAM9*	Nuclear Accommodation of Mitochondria	-0.12	0.67	-0.79	0.01
YIL111W	*COX5B*	Cytochrome c OXidase	-0.28	0.45	-0.73	0.00
YDR342C	*HXT7*	HeXose Transporter	1.05	1.76	-0.70	0.00
YDR343C	*HXT6*	HeXose Transporter	0.42	1.07	-0.65	0.00
YLR290C	*COQ11*	COenzyme Q	0.19	0.81	-0.62	0.00
YER103W	*SSA4*	Stress-Seventy subfamily A	-0.17	0.45	-0.61	0.00
YML081C-A	*ATP18*	ATP synthase	-0.63	-0.07	-0.57	0.00
YBR169C	*SSE2*	Stress Seventy subfamily E	0.11	0.58	-0.46	0.00
YNL052W	*COX5A*	Cytochrome c OXidase	0.20	0.66	-0.46	0.00
YPL061W	*ALD6*	ALdehyde Dehydrogenase	-0.11	0.34	-0.46	0.00
YPL004C	*LSP1*	Long chain bases Stimulate Phosphorylation	0.31	0.76	-0.45	0.00
YFL014W	*HSP12*	Heat Shock Protein	0.29	0.72	-0.43	0.00
YML128C	*MSC1*	Meiotic Sister-Chromatid recombination	0.56	0.99	-0.43	0.00
YDR432W	*NPL3*	Nuclear Protein Localization	0.95	1.37	-0.42	0.00
YBR072W	*HSP26*	Heat Shock Protein	1.07	1.49	-0.42	0.00
YNL055C	*POR1*	PORin	-3.14	-2.73	-0.41	0.00
YMR175W	*SIP18*	Salt Induced Protein	0.32	0.71	-0.40	0.00
YDL223C	*HBT1*	HuB1 Target	0.41	0.80	-0.39	0.00
YDR225W	*HTA1*	Histone h Two A	0.12	0.51	-0.39	0.00
YGL245W	*GUS1*	GlUtamyl-tRNA Synthetase	-0.09	0.30	-0.38	0.00
YPR069C	*SPE3*	SPErmidine auxotroph	0.41	0.78	-0.38	0.01
YDR033W	*MRH1*	Membrane protein Related to Hsp30p	0.08	0.46	-0.37	0.00
YNL016W	*PUB1*	PolyUridylate Binding	-0.10	0.27	-0.37	0.00
YNR018W	*RCF2*	Respiratory superComplex Factor	0.31	0.69	-0.37	0.00
YMR092C	*AIP1*	Actin Interacting Protein	0.01	0.38	-0.37	0.00
YHR193C	*EGD2*	Enhancer of Gal4 DNA binding	-0.01	0.35	-0.37	0.00
YKL035W	*UGP1*	UDP-glucose pyrophosphorylase	0.14	0.51	-0.37	0.00
YBL003C	*HTA2*	Histone h Two A	0.01	0.37	-0.36	0.00
YIL053W	*GPP1*	Glycerol-3-Phosphate Phosphatase	0.05	0.40	-0.36	0.00
YNR016C	*ACC1*	Acetyl-CoA Carboxylase	0.14	0.50	-0.35	0.01
YOR187W	*TUF1*	Mitochondrial translation elongation factor Tu (EF-Tu)	0.26	0.60	-0.34	0.00
YJL088W	*ARG3*	ARGinine requiring	0.41	0.75	-0.34	0.00
YLR180W	*SAM1*	S-AdenosylMethionine requiring	0.16	0.49	-0.33	0.00
YFR053C	*HXK1*	HeXoKinase	0.05	0.39	-0.33	0.00
YOR232W	*MGE1*	Mitochondrial GrpE	0.09	0.42	-0.33	0.00
YBR011C	*IPP1*	Inorganic PyroPhosphatase	-0.11	0.22	-0.33	0.00
YGL008C	*PMA1*	Plasma Membrane ATPase	0.31	0.64	-0.33	0.00
YDR012W	*RPL4B*	Ribosomal Protein of the Large subunit	0.05	0.38	-0.33	0.00

YGL105W	*ARC1*	Aminoacyl-tRNA synthetase Cofactor	-0.04	0.27	-0.31	0.00
YHR087W	*RTC3*	Restriction of Telomere Capping	0.43	0.73	-0.31	0.01
YNL096C	*RPS7B*	Ribosomal Protein of the Small subunit	0.00	0.30	-0.31	0.00
YBL002W	*HTB2*	Histone h Two B	0.12	0.42	-0.31	0.00
YGL256W	*ADH4*	Alcohol DeHydrogenase	0.72	1.03	-0.30	0.00
YBR088C	*POL30*	POLymerase	0.72	0.49	0.22	0.01
YJR121W	*ATP2*	ATP synthase	1.11	0.75	0.36	0.01
YLR304C	*ACO1*	ACOnitase	1.31	0.53	0.78	0.01
YOR062C	*YOR062C*	Similar to Reg1	0.37	-0.65	1.02	0.04
YLR355C	*ILV5*	IsoLeucine-plus-Valine requiring	4.63	3.58	1.04	0.01

Table S2. Genes encoding proteins with significantly changed stability upon expression of S129A in comparison to the empty vector (EV) control.
Ratio represents log2 from mCherry/sfGFP fluorescence intensities. $RatioDiff_{(EV\text{-}S129A)}$ represents $log2(R_{EV})$-$log2(R_{S129A})$ and is a measure for changed stability. Negative RatioDiff indicates stabilization of the fusion protein upon S129A expression.

ORF	**Gene**	**Name**	**Ratio (EV)**	**Ratio (S129A)**	**RatioDiff (EV-S129A)**	**p-value (EV- S129A)**
YDR185C	*UPS3*	UnProceSsed	-2.89	2.27	-5.16	0.01
YGL139W	*FLC3*	FLavin Carrier	-1.46	3.58	-5.03	0.01
YMR066W	*SOV1*	Synthesis Of Var	-0.73	4.00	-4.73	0.01
YDR026C	*NSI1*	NTS1 SIlencing protein 1	-1.80	2.62	-4.42	0.01
YMR198W	*CIK1*	Chromosome Instability and Karyogamy	-2.49	1.63	-4.12	0.01
YMR048W	*CSM3*	Chromosome Segregation in Meiosis	-1.27	2.81	-4.08	0.01
YLR247C	*IRC20*	Increased Recombination Centers	-1.43	2.47	-3.90	0.01
YGL162W	*SUT1*	Sterol UpTake	-1.10	2.55	-3.65	0.01
YNL230C	*ELA1*	ELongin A	-0.91	2.74	-3.64	0.01
YGR134W	*CAF130*	CCR4 Associated Factor	-1.04	2.54	-3.57	0.01
YPL005W	*AEP3*	ATPase ExPression	0.15	3.72	-3.57	0.01
YPL139C	*UME1*	Unscheduled Meiotic gene Expression	-0.58	2.96	-3.54	0.01
YER173W	*RAD24*	RADiation sensitive	-0.75	2.76	-3.51	0.01
YGR200C	*ELP2*	ELongator Protein	0.83	4.27	-3.45	0.01
YIL098C	*FMC1*	Formation of Mitochondrial Complexes	-0.14	3.25	-3.39	0.01
YDR076W	*RAD55*	RADiation sensitive	-1.28	2.07	-3.35	0.01
YDR118W	*APC4*	Anaphase Promoting Complex	-1.73	1.58	-3.31	0.01
YER013W	*PRP22*	Pre-mRNA Processing	-2.63	0.66	-3.29	0.01
YBR257W	*POP4*	Processing Of Precursor RNAs	-0.93	2.27	-3.20	0.01
YNL023C	*FAP1*	FKBP12-Associated Protein	-0.50	2.69	-3.19	0.01
YDR125C	*ECM18*	ExtraCellular Mutant	-1.32	1.83	-3.15	0.01

YBR008C	*FLR1*	FLuconazole Resistance	-1.90	1.21	-3.11	0.01
YKL033W	*TTI1*	Two Tel2-Interacting protein	-1.18	1.92	-3.10	0.01
YMR223W	*UBP8*	UBiquitin-specific processing Protease	0.66	3.64	-2.98	0.01
YIR005W	*IST3*	Increased Sodium Tolerance	-1.73	1.20	-2.93	0.01
YLR371W	*ROM2*	RhO1 Multicopy suppressor	-1.11	1.79	-2.89	0.01
YHR164C	*DNA2*	DNA synthesis defective	-0.04	2.85	-2.89	0.01
YGR206W	*MVB12*	MultiVesicular Body sorting factor of 12 kilodaltons	-1.52	1.35	-2.87	0.01
YKL125W	*RRN3*	Regulation of RNA polymerase I	-2.73	0.09	-2.82	0.01
YNL321W	*VNX1*	Vacuolar Na+/H+ eXchanger	-1.41	1.40	-2.81	0.01
YMR127C	*SAS2*	Something About Silencing	0.67	3.47	-2.79	0.01
YFL007W	*BLM10*	BLeoMycin resistance	-2.63	0.15	-2.77	0.01
YGR251W	*NOP19*	NucleOlar Protein	-0.49	2.25	-2.74	0.01
YBR065C	*ECM2*	ExtraCellular Mutant	-0.87	1.84	-2.72	0.01
YNL082W	*PMS1*	PostMeiotic Segregation	-2.66	0.04	-2.70	0.01
YGL240W	*DOC1*	Destruction Of Cyclin B	-0.62	2.07	-2.69	0.01
YCL039W	*GID7*	Glucose Induced Degradation deficient	-3.16	-0.50	-2.67	0.01
YKR093W	*PTR2*	Peptide TRansport	0.49	3.13	-2.65	0.01
YGR044C	*RME1*	Regulator of MEiosis	-3.76	-1.11	-2.64	0.01
YBL084C	*CDC27*	Cell Division Cycle	-2.07	0.54	-2.61	0.01
YKR084C	*HBS1*	Hsp70 subfamily B Suppressor	-0.92	1.67	-2.59	0.01
YML076C	*WAR1*	Weak Acid Resistance	-0.79	1.76	-2.55	0.01
YPR134W	*MSS18*	Mitochondrial Splicing System	-0.40	2.14	-2.54	0.01
YKL078W	*DHR2*	DEAH-box RNA helicase	-1.26	1.25	-2.51	0.01
YHR102W	*KIC1*	Kinase that Interacts with Cdc31p	-0.90	1.58	-2.48	0.01
YKL185W	*ASH1*	Asymmetric Synthesis of HO	-3.08	-0.61	-2.47	0.01
YER147C	*SCC4*	Sister Chromatid Cohesion	-0.59	1.86	-2.44	0.01
YMR232W	*FUS2*	cell FUSion	-1.22	1.21	-2.43	0.01
YLR115W	*CFT2*	Cleavage Factor Two	-0.51	1.90	-2.42	0.01
YBL018C	*POP8*	Processing Of Precursor RNAs	-0.09	2.30	-2.39	0.01
YAR014C	*BUD14*	BUD site selection	-0.49	1.89	-2.38	0.01
YEL059C-A	*SOM1*	SOrting Mitochondrial	-0.31	2.02	-2.33	0.01
YLR127C	*APC2*	Anaphase Promoting Complex	-1.52	0.78	-2.30	0.01
YLR215C	*CDC123*	Cell Division Cycle	-0.10	2.08	-2.18	0.01
YMR098C	*ATP25*	ATPase	0.28	1.16	-0.88	0.01
YLL008W	*DRS1*	Deficiency of Ribosomal Subunits	0.41	1.18	-0.76	0.01
YMR208W	*ERG12*	ERGosterol biosynthesis	-0.82	-0.35	-0.47	0.01
YJR121W	*ATP2*	ATP synthase	1.11	0.54	0.57	0.01
YBR146W	*MRPS9*	Mitochondrial Ribosomal Protein, Small subunit	-0.65	-3.18	2.53	0.01

Table S3. Genes encoding proteins with significantly changed stability upon expression of S129A in comparison to αSyn.

Ratio represents log2 from mCherry/sfGFP fluorescence intensities. $RatioDiff_{(\alpha Syn\text{-}S129A)}$ represents $log2(_{\alpha Syn})$-$log2(R_{S129A})$ and is a measure for changed stability. Negative RatioDiff indicates stabilization of the fusion protein upon αSyn expression in comparison to S129A expression.

ORF	Gene	Name	Ratio (αSyn)	Ratio (S129A)	RatioDiff (S129A-αSyn)	p-value (S129A-αSyn
YER032W	*FIR1*	Factor Interacting with REF2	2.00	-2.12	-4.12	0.01
YOR244W	*ESA1*	Catalytic subunit of the histone acetyltransferase complex	4.46	0.57	-3.89	0.02
YNR031C	*SSK2*	Suppressor of Sensor Kinase	5.18	1.29	-3.89	0.00
YGL004C	*RPN14*	Regulatory Particle Non-ATPase	6.01	2.22	-3.79	0.00
YDR279W	*RNH202*	RNase H	5.02	1.73	-3.29	0.01
YOR064C	*YNG1*	Yeast iNG1 homolog	2.02	-1.13	-3.15	0.01
YGR238C	*KEL2*	KELch repeat	4.49	1.43	-3.06	0.00
YLR003C	*CMS1*	Complementation of Mcm-10 Suppressor	0.82	-2.14	-2.96	0.00
YKR054C	*DYN1*	DYNein	3.09	0.35	-2.74	0.02
YLR023C	*IZH3*	Implicated in Zinc Homeostasis	-0.11	-2.85	-2.73	0.01
YBR146W	*MRPS9*	Mitochondrial Ribosomal Protein, Small subunit	-0.51	-3.18	-2.66	0.00
YHR034C	*PIH1*	Protein Interacting with Hsp90	3.84	1.18	-2.66	0.00
YDR189W	*SLY1*	Suppressor of Loss of Ypt1	3.29	0.67	-2.62	0.00
YMR137C	*PSO2*	PSOralen derivative sensitive	1.91	-0.71	-2.61	0.03
YOL116W	*MSN1*	Multicopy suppressor of SNF1 mutation	3.70	1.10	-2.60	0.01
YPR147C	YPR147C	Bifunctional triacylglycerol lipase	0.34	-2.18	-2.52	0.00
YDR052C	*DBF4*	DumbBell Former	1.50	-0.90	-2.39	0.01
YBL102W	*SFT2*	Suppressor of sed Five Ts	3.21	0.84	-2.37	0.00
YOR265W	*RBL2*	Rescues Beta-tubulin Lethality	4.53	2.23	-2.31	0.00
YKL179C	*COY1*	CASP Of Yeast	2.10	-0.21	-2.31	0.00
YKR077W	*MSA2*	Mbf and Sbf Associated	0.17	-2.09	-2.26	0.00
YIL119C	*RPI1*	Ras-cAMP Pathway Inhibitor	0.31	-1.91	-2.22	0.02
YDR362C	*TFC6*	Transcription Factor C	1.42	-0.73	-2.15	0.01
YMR201C	*RAD14*	RADiation sensitive	1.53	-0.62	-2.15	0.00
YNL257C	*SIP3*	SNF1-Interacting Protein	2.66	0.53	-2.13	0.01
YDR043C	*NRG1*	Negative Regulator of Glucose-repressed genes	-0.29	-2.42	-2.12	0.00
YGL065C	*ALG2*	Asparagine-Linked Glycosylation	3.13	1.02	-2.11	0.00
YKL184W	*SPE1*	SPErmidine auxotroph	-0.83	-2.94	-2.11	0.00
YOR311C	*DGK1*	DiacylGlycerol Kinase	2.53	0.44	-2.09	0.02
YPL179W	*PPQ1*	Protein Phosphatase Q	1.19	-0.90	-2.09	0.02
YDL048C	*STP4*	protein with similarity to Stp1p	-0.11	-2.19	-2.08	0.00
YAR031W	*PRM9*	Pheromone-Regulated Membrane protein	2.91	0.84	-2.08	0.01

YDR375C	*BCS1*	ubiquinol-cytochrome c reductase (bc1) Synthesis	1.69	-0.37	-2.06	0.02
YLR183C	*TOS4*	Target Of Sbf	0.78	-1.25	-2.03	0.01
YBR058C-A	*TSC3*	Temperature-sensitive Suppressors of Csg2 mutants	0.55	-1.46	-2.02	0.00
YML027W	*YOX1*	Yeast homeobOX	-0.56	-2.57	-2.01	0.02
YOL013C	*HRD1*	HMG-coA Reductase Degradation	1.56	0.08	-1.48	0.00
YBR291C	*CTP1*	Citrate Transport Protein	0.07	-1.26	-1.33	0.00
YPR049C	*ATG11*	AuTophaGy related	1.62	0.78	-0.84	0.01
YIL107C	*PFK26*	6-PhosphoFructo-2-Kinase	1.35	0.52	-0.83	0.00
YNL185C	*MRPL19*	Mitochondrial Ribosomal Protein, Large subunit	1.01	0.18	-0.83	0.02
YGR084C	*MRP13*	Mitochondrial Ribosomal Protein	1.37	0.71	-0.66	0.00
YDL064W	*UBC9*	UBiquitin-Conjugating	0.95	0.40	-0.55	0.00
YLR290C	*COQ11*	COenzyme Q	0.81	0.40	-0.41	0.00
YBR072W	*HSP26*	Heat Shock Protein	1.49	1.17	-0.32	0.00
YPL004C	*LSP1*	Long chain bases Stimulate Phosphorylation	0.76	0.46	-0.30	0.00
YNL055C	*POR1*	PORin	-2.73	-2.98	-0.26	0.00
YKL173W	*SNU114*	Small NUclear ribonucleoprotein associated	-0.31	0.53	0.84	0.00
YGL113W	*SLD3*	Synthetically Lethal with Dpb11-1	2.49	3.40	0.92	0.02
YLR355C	*ILV5*	IsoLeucine-plus-Valine requiring	3.58	4.59	1.00	0.01
YML116W	*ATR1*	AminoTriazole Resistance	2.44	3.79	1.35	0.01
YDL043C	*PRP11*	Pre-mRNA Processing	1.36	2.98	1.62	0.01
YMR223W	*UBP8*	UBiquitin-specific processing Protease	1.87	3.64	1.77	0.02
YGR016W	YGR016W	Uncharacterized ORF	2.78	4.60	1.83	0.00
YDR016C	*DAD1*	Duo1 And Dam1 interacting	1.44	3.32	1.88	0.00

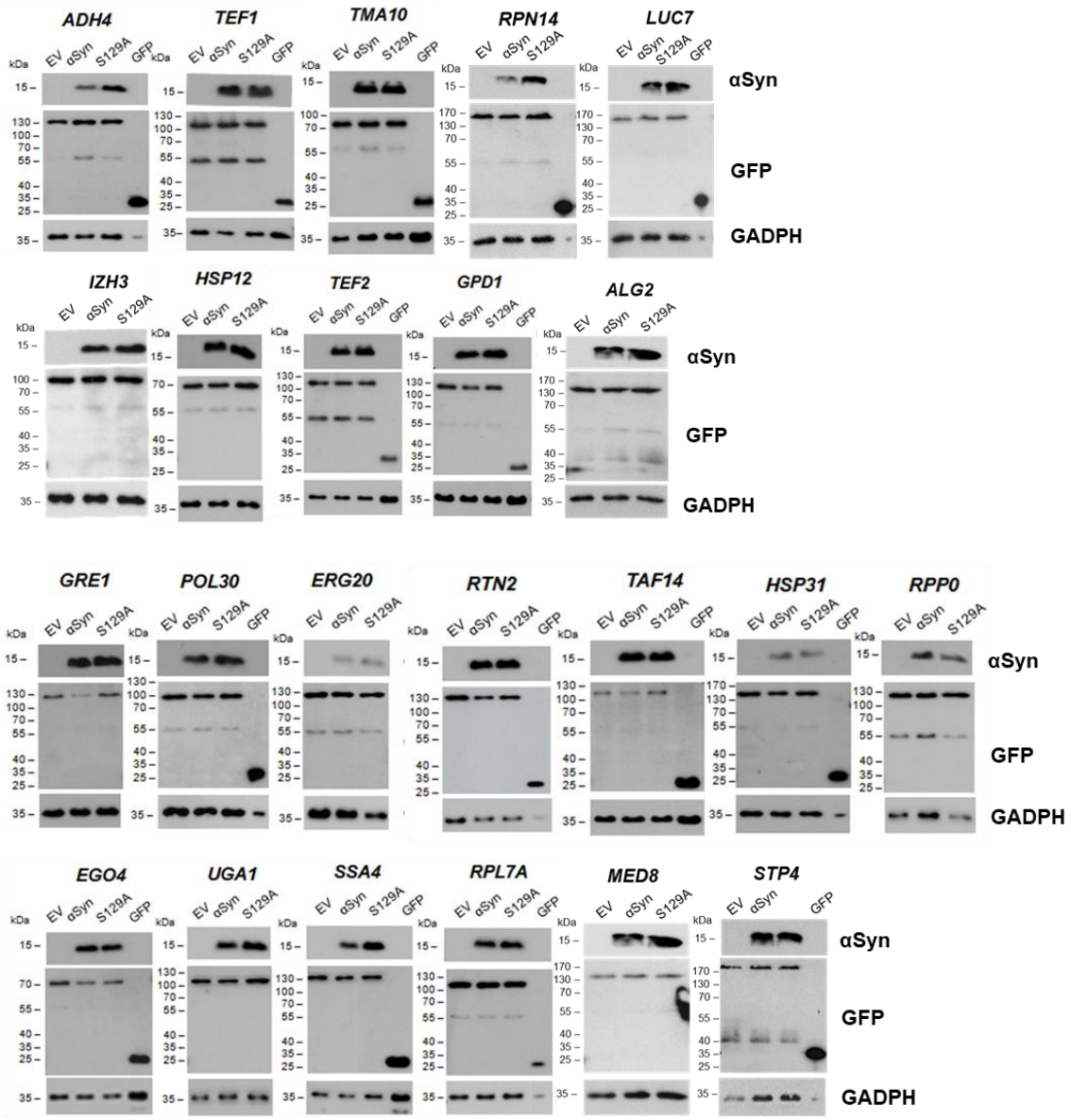

Figure S1. Immunoblotting analysis of the tFT-screen candidates from different functional categories and different groups expression levels.
Crude protein extracts were prepared from yeast cells after 6 h induction of protein expression in galactose-containing medium. GFP antibody was used for detection of protein levels tagged with tFT. αSyn identifies the presence of the protein and anti-GAPDH was used as a loading control. Crude protein extract from cells, expressing GFP were used as a control (EV).

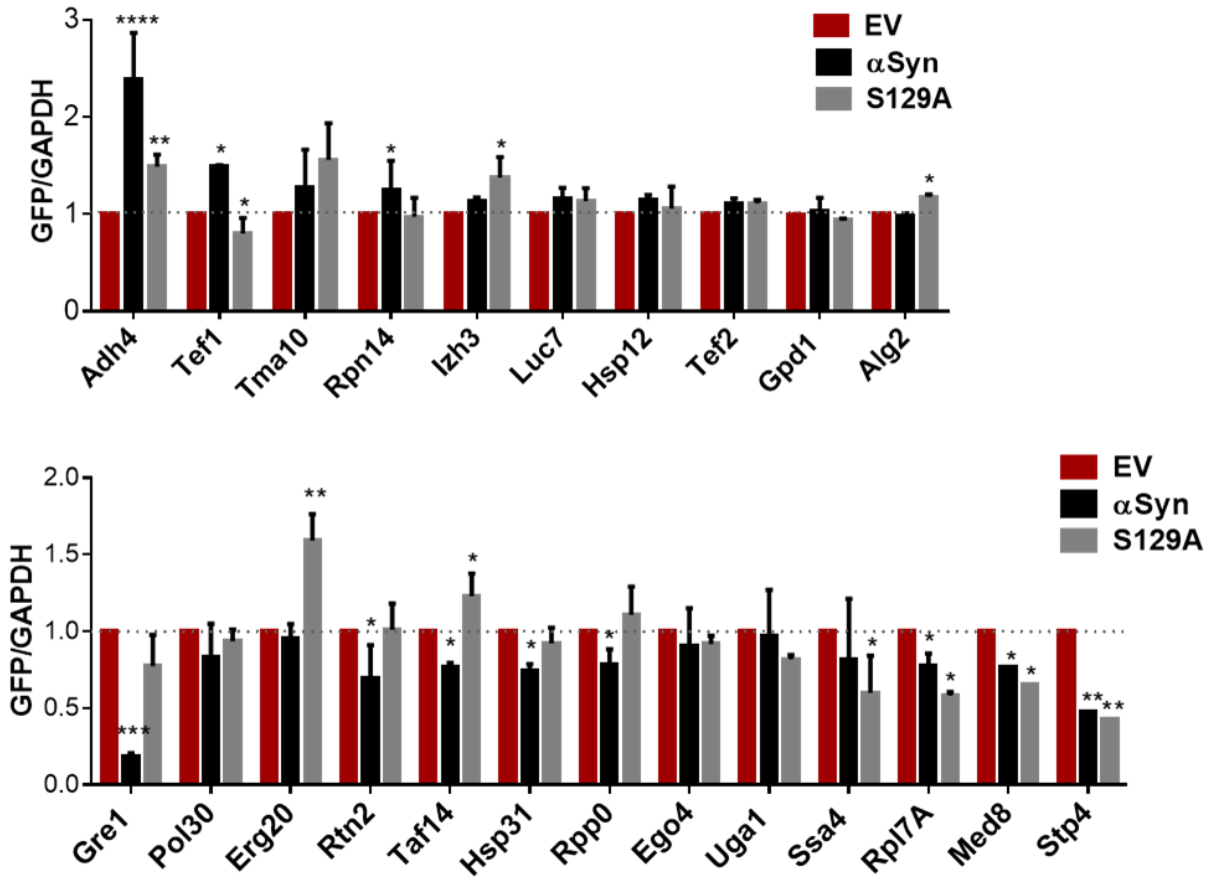

Figure S2. Quantification of the steady-state proteins levels (from Figure II) upon αSyn or S129A expression in yeast.
Protein levels were quantified from densitometric images of the immunodetection of GFP signal using ImageJ software. For each strain, the results were normalised to the corresponding empty vector control. Significance of differences was calculated with 2-way ANOVA test versus control cells (*p < 0.05; **p < 0.01; ****p < 0.0001; n=2).

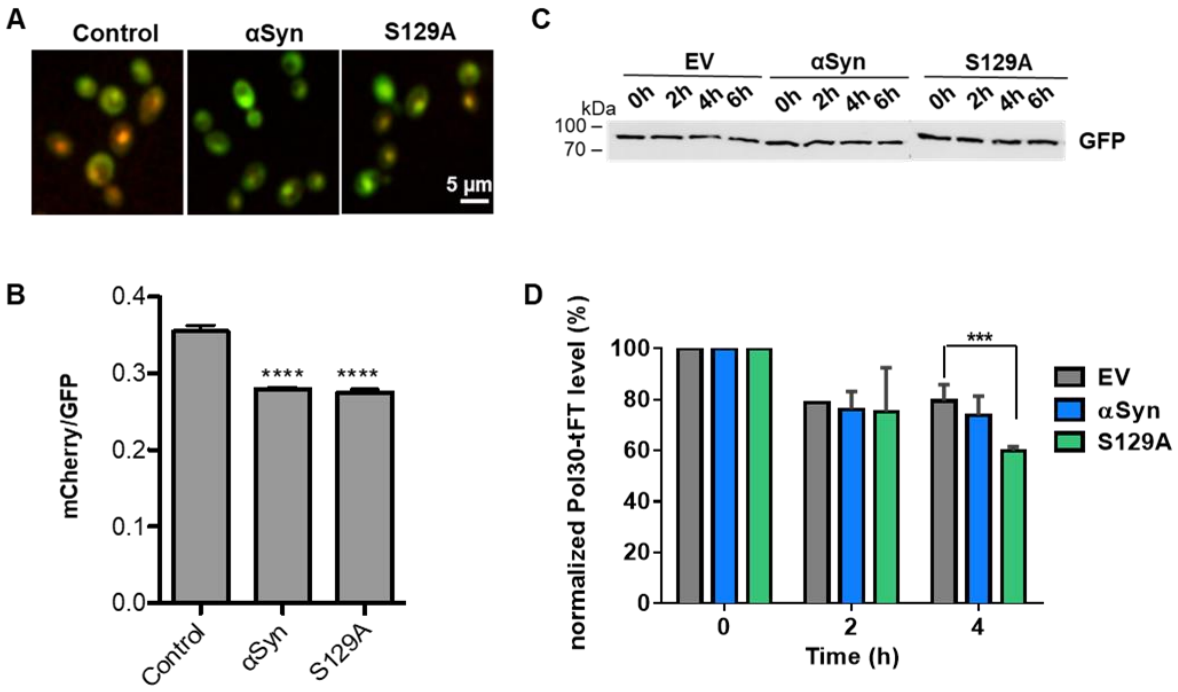

Figure S3. Expression of αSyn decreases stability of Pol30.
(A) Life cell fluorescence microscopy of yeast cells, expressing Pol30-tFT. Yeast cells, expressing *GAL1*-driven αSyn or S129A from 2 µm plasmid were induced for 6 h in galactose-containing medium prior to microscopy. Control cells are transformed with empty vector. Scale bar: 5 µm. (B) Quantification of the fluorescence signals in cells from A. The GFP and mCherry fluorescence was measured using SlideBook6 software. For each individual cell the ratio mCherry/GFP was calculated. The bars represent mean values ± SD. Significance of differences was calculated with *t*-test versus control cells (****p < 0.0001; n = 100). (C) Western blot analysis of Pol-tFT treated with cycloheximide. Cells expressing *GAL1*-driven αSyn or S129A or empty vector control from 2 µm plasmid were induced for 6 h in galactose-containing medium prior to treatment with 50 µg/mL cycloheximide to stop *de novo* protein synthesis. Immunoblotting analysis was performed at the indicated time points after addition of cycloheximide with GFP antibody. (E) Densitometric analysis of the immunodetection of the GFP signal from (C). The GFP signal was normalized to each individual signal at 0 h. The significance of the differences was calculated with *t*-test (***p < 0.001).

List of figures

List of tables

Abbreviations

%	percent
α	alpha
Δ	delta
2μ	(2 μm) 2 micrometer high-copy yeast expression vector
μg	microgram
μl	microliter
μm	micrometer
μM	micromolar
aa	amino acids
Ade (A)	adenine
Ala (A)	alanine
ALP	autophagy lysosomal pathway
Amp	ampicillin
ANOVA	analysis of variance
APS	ammonium persulfate
Arg (R)	arginine
AS	ammonium sulfate
Asn (N)	asparagine
Asp (D)	aspartic acid
αSyn	α-synuclein
ATP	adenosine triphosphate
ATP13A2	ATPase type 13A2
bg	background
BiFC	bimolecular fluorescence complementation
BLAST	basic local alignment search tool
bp	base pair(s)
BSA	bovine serum albumin
°C	degree Celsius
C. elegans	*Caenorhabditis elegans*
cDNA	complementary DNA
CEN/ARS	centromere/autonomously replicating sequence

CHX	cycloheximide chase
CKs	casein kinases
cm	centimeter
CMV	cytomegalovirus
CP	core particle
C-terminus	carboxy terminus
CYC1	*cytochrome C-1*
Cys (C)	cysteine
Da	Dalton
dH_2O	distilled water
D. melanogaster	*Drosophila melanogaster*
DMSO	dimethyl sulfoxide
DNA	deoxyribonucleic acid
DLB	dementia with Lewy bodies
dNTPs	deoxyribonucleoside triphosphates
Dox	doxycycline
DTT	dithiothreitol
DUB	deubiquitinase
ECL	enhanced chemiluminescence
E. coli	*Escherichia coli*
EDTA	ethylenediaminetetraacetic acid
EtOH	ethanol
EUROSCARF	European *Saccharomyces cerevisae* archive for functional analysis
EV	empty vector
FSC	forward scatter
g	gram
G418	geneticin
GABA	γ-aminobutyric acid
GAL	galactose
GAPDH	glyceraldehyde 3-phosphate dehydrogenase
GBD	global burden of disease
GFP	green fluorescent protein

Gln (Q)	glutamine
Glu (E)	glutamic acid
Gly (G)	glycine
GRKs	G protein-coupled receptor kinases
h	hour(s)
His (H)	histidine
HRP	horseradish peroxidase
IgG	immunoglobulin G
Ile (I)	isoleucine
kanMX4	kanamycin resistance
kb	kilobase pair(s)
kDa	kilodalton
l	liter
LB	lysogeny broth
LBs	Lewy bodies
Leu (L)	leucine
LiOAc	lithium acetate
log	decadic logarithm
LRRK2s	leucine-rich repeat kinases
Lys (K)	lysine
M	molar
MATa	mating type a
Met (M)	methionine
mg	milligram
MG132	N-benzyloxycarbonyl-L-leucyl-L-leucyl-L-leucinal
min	minutes
ml	milliliter
mm	millimeter
mM	millimolar
MSA	multiple system atrophy
n	number
NAC	non-amyloid-β component
ng	nanogram

nm	nanometer
nM	nanomolar
n.s.	not significant
N-terminus	amino terminus
OD_{600}	optical density measured at a wavelength of 600 nanometer
ori	origin of replication
PA	polyacrylamide
PABA	para-aminobenzoic acid
PAGE	polyacrylamide gel electrophoresis
PCR	polymerase chain reaction
PD	Parkinson´s disease
PEG	polyethylene glycol
Pfu	*Pyrococcus furiosus*
pH	*potentia hydrogenii*
Phe (F)	phenylalanine
PIM	protease inhibitor mix
PINK1	PTEN-induced putative kinase 1
PLKs	polo-like kinases
pmol	picomol
Pro (P)	proline
pS129	phosphorylated at serine 129
PTM	posttranslational modification
raff	raffinose
RNA	ribonucleic acid
RP	regulatory particle
rpm	revolutions per minute
s	seconds
S129	serine 129
SC	synthetic complete
S. cerevisiae	*Saccharomyces cerevisiae*
SDS	sodium dodecyl sulfate
SGA	synthetic genetic array
SNpc	*substantia nigra pars compacta*

Tet	tetracycline
tFT	tandem fluorescence timer
UPS	ubiquitin-proteasome system

Acknowledgments

Finally, I would love to express my appreciation to all, who have been along with me and supported me during this journey.

I would like to express my gratitude to Prof. Dr. Gerhard H. Braus for giving me the opportunity to join his research group and carry out my Ph.D. thesis under his supervision. I am grateful for his advisement, mentoring and patience.

My very special appreciation goes to Dr. Blagovesta Popova for her great support, help and encouragement during this time. I am very grateful for her kindness and endless patience. I am also thankful for proofreading my thesis.

I would like to thank my thesis committee members, Prof. Dr. Stefanie Pöggeler and Prof. Dr. Tiago Outeiro, for the cooperation, inspiring discussions and their feedback on my project during the years.

I am very grateful to Prof. Dr. Michael Knop for providing the tFT-library and high-throughput fluorescence measurements. I would like to thank Marie Niederleithinger for generation of tFT-library expressing αSyn or S129A encoding gene and high-throughput fluorescence measurements. Moreover, I would like to acknowledge Prof. Dr. Heike Krebber for help with gradient centrifugation.
I would like to thank all members of the Department of Molecular Microbiology and Genetics for a very pleasant atmosphere, scientific support and useful suggestions. I am also grateful to Ms. Heidi Northemann for her endless administrative support.

I am thankful to the bachelor students Jennifer Kluczny, Lea Trost, Pia Wilkening, Dilyana Zyapkova and the Master student Aybeg Nafiz Günenç, who contributed to my thesis with their experiments.

I would like to take the opportunity to thank to Göttingen Graduate School for Neurosciences, Biophysics, and Molecular Biosciences (GGNB) for providing seminars, workshops and retreats which gave me the opportunity for expanding my scientific knowledge as well as my soft skills. Moreover, I am grateful for granting me with travel fund and the bridging fund.

I would like to express my deepest gratitude to my parents for their endless support, love, patience and encouragement throughout the years. Without them, this would not

have been possible. I am also grateful to my friends, who have always been there for me and encouraged me. My special thanks go to Benjamin De Creus, who has been a constant source of emotional support, love and encouragement while working on my thesis. I am very grateful for his time spent proofreading the thesis.